LUBRICITY OF BIOMEDICAL CONDUITS

A THESIS SUBMITTED TO THE FACULTY OF
UNIVERSITY OF MINNESOTA
BY

THOMAS JAMES TURNER

IN PARTIAL FULFILLMENT OF THE REQUIREMENTS
FOR THE DEGREE OF
DOCTOR OF PHILOSOPHY

ADVISER: Dr. EPHRAIM M. SPARROW

DECEMBER 2013

Acknowledgements

I would like to acknowledge both my adviser Professor Ephraim M. Sparrow, and his wife Ruth May Sparrow for walking with me every step of the way (while not losing faith in me) during this doctoral journey. The Sparrows are not unlike archangels.

Additionally, I would like to thank my helpful colleagues, John M. Gorman, Jason L. Marrs, Michael N. Missaghi, Lance B. Lohstreter, and Brian R. Wollschalger for their many contributions to this document, and their patience with my many questions.

Dedication

This work is dedicated to my wife, Veasna Ann Turner.

Abstract

The research is motivated by the need to explore the inputs and mechanisms responsible for the creation of beneficial tribological coatings on medical grade silicone rubber tubing and how to quantify them. Despite the fact that biomedical conduits are routinely made lubricious by a host of different methods, there is an insufficiency in the present state of knowledge with regard to how to precisely quantify conduit bore lubricity. Test methods, newly invented, to characterize tubing bore lubricity are described in detail with greater emphasis on the extraction of coefficients of friction relative to historical testing methods.

A new invention for characterizing the lubricity of biomedical conduits makes use of a pressure cuff or air-bladder to compress a plasma-treated silicone tubing sample onto a friction element. The instrument setup is a metal sliding-friction-element/silicone-tubing system. The tubing is stationary while the friction element that has been inserted into the tubing bore is pulled. The tubing is held in place with a known and regulated pressure, which allows the normal force pressing on the sliding component to be known. The pull force (tangential force) is registered and recorded using a commercial pull-test frame. Knowing the normal and tangential forces means that the coefficient of friction for the system can be extracted using this instrument.

The running-in behavior observed during biomedical conduit friction assessment is quantified and a hypothesis regarding its source is set forth. The theme of the hypothesis is that material related to the constituents of silicone rubber is taken up by the friction element (coil, in this case) over several test cycles and thereby alters the system until it stabilizes. Subsequently, the coil becomes equilibrated with the chemical makeup of its environment, and this is why the resistance force stabilizes. The results of extensive experimentation showed that pristine coils displayed markedly more running-in phenomenon when compared to either an exercised coil or a stored-in-silicone tubing coil.

The outcome of the thesis is a thorough understanding of tubing bore lubricity quantification.

Table of Contents

List of Tables

Chapter 1

Chapter 2

Chapter 4

Chapter 5

List of Figures

Chapter 1

Chapter 2

Chapter 3

Chapter 4

Chapter 5

Chapter 1

INTRODUCTION

PROPOSED RESEARCH ACTIVITY

1 Goals of the research

The goals of the proposed research activity are to fundamentally understand the inputs and mechanisms responsible for the creation of a beneficial tribological coating system using medical grade silicone rubber tubing. The goals include the development of a tribometer that can be used to accurately assess the process output and the influence of the process inputs.

The formation of the investigated tribological coating system requires processing that renders silicone rubber tubing surfaces (both the external surface and the tube bore, also referred to as the "outer diameter" and the "inner lumen" surfaces respectively) lubricious. The friction reducing process and the tribological coating system need to be characterized, understood and controlled.

For the characterization, an effective measurement system must be available, and as such, part of the research activity will be to develop and optimize a tribometer that can be used to gauge whether or not the coating system meets the needs of downstream users. The downstream users are any persons that need to:

- Handle the tubing in post-treatment assembly operations
- Sterilize the tubing

- Package the tubing for surgical procedures
- Implant the tubing into a patient
- Have the tubing implanted in their body for medical therapy

2 Fundamentals of plasma coating - a proposed roadmap

The proposal is to investigate the pulsed plasma physical deposition process used to generate a tribological coating on medical silicone tubing. The tentative plan is to first improve the metrology (especially, the macroscale evaluation methods) and then investigate multiple hypotheses surrounding how inputs affect key coating outputs. The proposed research is shown in tabular form on the next two pages and then the proposal is elaborated upon later in this section.

Table 2.1: Part 1 - Proposed roadmap of experiments

Proposed Roadmap of Experiments - Part One				
Hypothesis	Experiment	Anticipated Outcome	Materials/ Methods	Analytical Tool Kit
Measurement of Tribological System Can be Improved	Measure Sliding Friction with Different Types of Tribometers and Map Tribological Output to Functional Requirements	Improved Tribological Characterization Tool	Construction and Analysis of New Tribometers	Lubricity testing, Gauge Repeatability and Reproducibility Studies, Handling Studies
Monomer Deprivation, Insufficient Feedstock	Permeation Study of Silicone Membranes with Various Species	Extraction of Diffusion Coefficient for various species, Extraction of Mass Flux, Mass Transport as a function of: Temperature, Pressure, Membrane Thickness	Permeation Cell, Various Silicone Gum Stocks, Various Membrane Thicknesses, Argon, Water Vapor, Monomer	Pressure Change Sensors, Volume Change Sensors, Residual Gas Analyzer
Monomer Leaving Inner Lumen Volume	Vary Pressure Gradient from Reactor Zone to Reactor Zone	Coating Characteristics as a Function of Differential Zone Pressures	Silicone Tubing, Physical Vapor Deposition Reactor, Designed Experiments Using Reactor Pressure as a Factor	Tribological Testing, Input Parameter Data Acquisition Files
Outer diameter surface treatment dependent on monomer concentration	Study Impact of Different Argon/Monomer Flow Ratios Utilized During Processing	Coating Characteristics as a function of Inert/Reactive Species Flow Ratios	Silicone Tubing, Physical Vapor Deposition Reactor, Designed Experiments Using Argon/Monomer Flow Ratio as a Factor	Lubricity testing, SEM, ZYGO, TOFSIMS, Laser Profilometry, XPS, RGA, OES, Ellipsometry, Nanoscratch Testing
Input power influences coating characteristics	Modify Input Power Settings During Processing - To Include the Peak Power, the Duty Cycle and the Frequency of Pulsed Power to the ID Electrode	Coating Characteristics as a function of Input Power Settings to the Electrodes	Silicone Tubing, Physical Vapor Deposition Reactor, Designed Experiments Using Input Powers as Factors	Lubricity testing, SEM, ZYGO, TOFSIMS, Laser Profilometry, XPS, RGA, OES, Ellipsometry, Nanoscratch Testing
Monomer Deprivation, Lack of Enviromental Control Leads to Unpredictable Outcomes	Step Reactor and Monomer Temperature to Various Equilibrium Settings	Film Lubricity/Morphology; Tubing Mechanical Properties, Monomer Vapor Pressure, [H2O], Coating Characteristics as a function of Process Temperature	Silicone Tubing, Physical Vapor Deposition Reactor, Designed Experiments Using Process Temperature as a Factor	Lubricity testing, SEM, ZYGO, TOFSIMS, Laser Profilometry, XPS, RGA, OES, Ellipsometry, Nanoscratch Testing

Table 2.1: Part 2 - Proposed roadmap of experiments

Proposed Roadmap of Experiments - Part Two				
Hypothesis	**Experiment**	**Anticipated Outcome**	**Materials/ Methods**	**Analytical Tool Kit**
Incoming Substrate Inconsistent	Analyze and Correlate Mechanical and Rheological Data from Silicone Rubber to Final Coating Characteristics	Better Understanding of the Relationship between Substrate Characteristics and Tribological Coating	Gum Stock Property Data, Silicone Tubing, Vendor Supplied Data, Internally Generated Coating Characteristic Data,	Statistical Software
Electrode Design Can be Improved by Controlling Electromagnetic Field Concentration	Design and Test Capactitive Electrode Utilized to Treat Tubing	Coating Characteristics as a function of Electromagnetic Field Profile	Silicone Tubing, Physical Vapor Deposition Reactor, Designed Experiments Using Different Electrode Designs as Attribute Inputs	Lubricity testing, SEM, ZYGO, TOFSIMS, Laser Profilometry, XPS, RGA, OES, Ellipsometry, Nanoscratch Testing, Langmuir Probe
Load on substrate impacts final dimensions	Compare Before and After Dimensions on Silicone Tubing after Suspending Various Loads on Tubing for Varying Amounts of Time	Determination of Plastic Deformation Limit on Substrate	Silicone Tubing of Varying Dimensions, Different Loads,	Tribological Testing, Input Parameter Data Acquisition Files
Plasma Ignition and Sustainability Impacted by Reactor Pressure	Step Reactor Absolute Pressure to Various Equilibrium Settings	Impact of Process Pressure on Plasma Characteristics	Silicone Tubing, Physical Vapor Deposition Reactor, Designed Experiments Using Absolute Process Pressure as a Factor	OES, Langmuir Probe, Input Parameter Data Acquisition Files
Tension During Process Influences Coating Characteristics	Vary Tension on Substrate During Processing	Coating Characteristics as a function of Tension on Substrate During Processing	Silicone Tubing, Physical Vapor Deposition Reactor, Designed Experiments Using Tension During Transport as a Factor	Lubricity testing, SEM, ZYGO, TOFSIMS, Laser Profilometry, XPS, RGA, OES, Ellipsometry, Nanoscratch Testing
Presence of Water Vapor Deleterious to Coating Properties	Vary Water Vapor Concentration within Lumen Volume	Impact of Water Vapor on Coating, Coating Characteristics as a function of Water Vapor Concentration	Silicone Tubing, Physical Vapor Deposition Reactor, Designed Experiments Using [Water Vapor] as a Factor	Lubricity testing, SEM, ZYGO, TOFSIMS, Laser Profilometry, XPS, RGA, OES, Ellipsometry, Nanoscratch Testing

3 Definition of appropriate metrics

3.1 Proposed improvements to tribological system evaluation

The goal of this exploration is to improve upon a currently in-use macroscale tribometer(s). Currently, pulling a known mass across a sample set of treated tubing samples is used to assess the exterior surface of plasma-treated tubing. The Gauge Repeatability and Reproducibility (GR&R) will be measured for this test method as a baseline. New methods will be explored using different test configurations and materials to reduce the gauge error. Controlled experiments will be performed and compared to the in-use methods.

In a current test methodology, an inserted tribo-partner or friction element into the tubing bore surface of plasma treated tubing is pulled and the extraction force is registered and recorded. The tribo-partner is threaded through the tubing lumen and then the assembly is arranged onto a fixture with tight bend radius. Jaws that are attached to a force transducer or load cell grip the free end of the tribo-partner. The friction element is withdrawn from the tubing while the instrument with the load cell records the resistive force needed to remove the tribo-partner at a set speed for a pre-determined length of time. The Gauge Repeatability and Reproducibility (GR&R) will be measured for this test method as a baseline. New methods to assess tubing bore lubricity will be explored using different test configurations and materials to reduce the gauge error. Controlled experiments will be performed and compared to the in-use method. The torque test method as described in Chapter 2 will be evaluated and compared to in-use inner diameter surface tribometers. The data from the inner diameter surface tribological testing will be used to infer “running-in” characteristics for the system(s) that have been chosen for the evaluations.

3.2 Monomer deprivation hypothesis - permeation investigation

As part of this research, the determination of the permeation and the amount of various species available to the process is of utmost importance. The inner lumen of the silicone tubing is coated with a film in a plasma polymerization process. The film is formed from fragments of molecules that are sourced from a monomer feedstock in the polymerizable vapor state. To enter the inner lumen volume, the polymerizable vapor must permeate the tubing wall. Additionally, there are inert gas atoms that are in the process environment that also permeate the tubing walls. The background, mathematics and methods for the proposed experiments follow.

The first observations on the transport of gases and vapors in polymeric membranes were apparently those of Thomas Graham in 1829. Graham observed that a wet pig bladder inflated to the bursting point when placed in an atmosphere of carbon dioxide [1]. As far back as 1831, it was known that rubber membranes are permeable to gases and that the permeation rates for different gases are not the same [2].

Note that the phenomenon of interest is permeation and should not be mistaken as purely a diffusion process. A distinction is drawn between these two phenomena, especially between the permeation constant and diffusion constant. Permeation is the over-all steady-state flow process from the gas phase on one side of the membrane or wall to the gas phase on the other side. Strictly speaking, the term diffusion in a solid applies to the internal process by which an atom is handed on or changed from one lattice position to another. In the case of gases going through solids, diffusion as a separate process is difficult to measure. The over-all process of permeation is experimentally much easier to study. Permeation involves several steps, as follows [3]:

1. Impact of the gas atoms or molecules on the surface.
2. Adsorption.

3. Possible dissociation upon adsorption.
4. Solution of the gas in the wall material at the incoming surface. The amount dissolved there depends on the solubility equilibrium.
5. Movement of the gas atoms from this saturated surface layer through the interior as atoms or ions, under a concentration gradient, to the outgoing surface. This constitutes diffusion proper. The concentration gradient is the driving force for diffusion and the process is given quantitative formulation in Fick's law.
6. Transfer of the dissolved gas to the outgoing surface layer and evaporation (recombination may occur).
7. Desorption of this gas and release on the low-pressure side of the membrane.

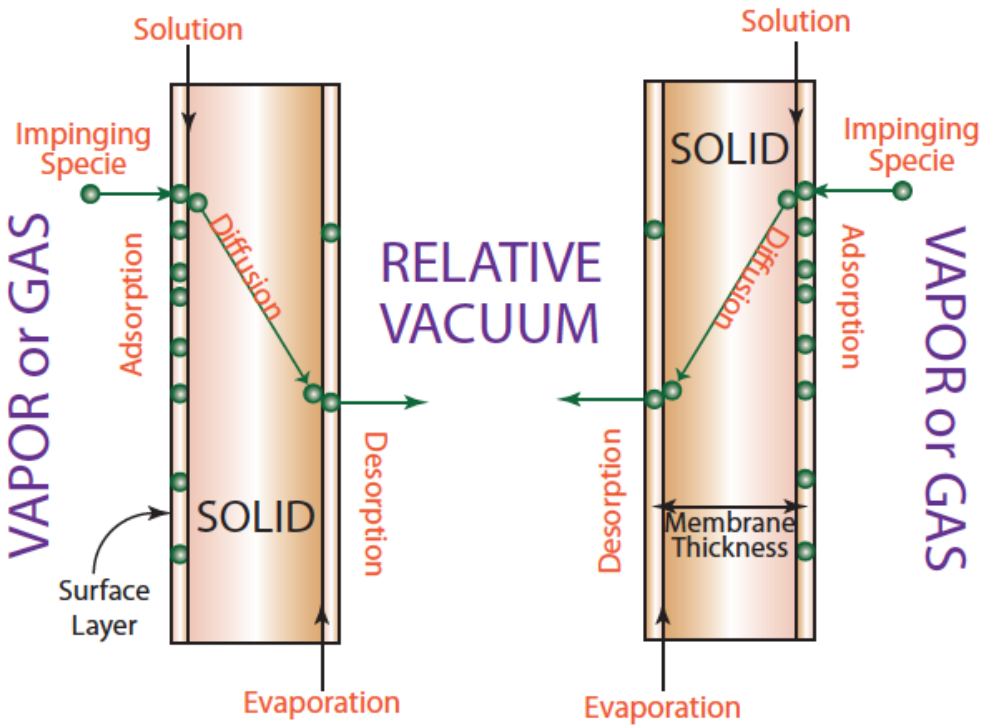

Figure 3.1: Permeation mechanisms in play as species permeates tubing walls

A depiction of an example permeating specie crossing the walls of tubing is shown in Figure 3.1. For rubber, it is an accepted fact that the quantity of dissolved gas in the rubber is proportional to the pressure, following Henry's law, while Fick's law

applies to the actual process of diffusion [2]. Henry's law dates back to 1803 and asserts that, at a constant temperature, the amount of a given gas that dissolves in a given type and volume of liquid is directly proportional to the partial pressure of that gas in equilibrium with that liquid.

$$p = k_H \cdot C \tag{1}$$

where

• p = The partial pressure of the gas/vapor surrounding the solution

• k_H = The Henry's Law constant for the solution

• C = The concentration of the dissolved gas in solution

Fick's first law (1855) is analogous to Fourier's law of heat conduction. Fick's first law relates the diffusive flux to a negative concentration gradient. In one dimension, Fick's first law can be expressed as shown in Equation 2.

$$J = -D \cdot \frac{\partial C}{\partial x} \tag{2}$$

where

• J = The "diffusion flux"; the amount of substance through a unit of area in a unit of time

• D = The diffusivity or diffusion coefficient

• C = The concentration of a species

• x = The position [length]

Exner in 1875 and Stefan in 1878 showed that the permeation of gases through soap films was proportional to the product of the solubility of the gas in water and the Fick's law diffusion coefficient. These results were extended and applied to rubber by

von Wroblewski in 1879. Wroblewski showed that the solution of gases in rubber followed Henry's law and also defined an absorption coefficient as the number of cm^3 of gas that dissolved in one cm^3 of rubber at one atmosphere of pressure. Combining this with Fick's law, Wroblewski showed that the steady state permeation rate through a membrane of thickness; l, is [1]:

$$P = \frac{(D \cdot S) \cdot \Delta p}{l} \tag{3}$$

In Equation (3), which is an equation that describes steady-state permeation:

• P = The "permeation flux" the amount of substance through a unit of area in a unit of time. NOTE that the "permeation flux" is the same as the "diffusion flux" and will be equated later.

• D = The diffusivity or diffusion coefficient

• S = The absorption coefficient

•Δp = The pressure difference across the membrane

• l = The membrane thickness

This is the basic transport equation used today, the product of the diffusion coefficient and the absorption coefficient D·S is known as the permeability coefficient. The permeability coefficient can also be defined as $\frac{P \cdot l}{\Delta p}$.

The kinetics of gas/vapor transport through a thin uniform film have been modeled and measurements of the transport can yield solubility, diffusivity and permeability in a single experiment. The steady-state flux of a gas/vapor in a system that obeys Henry's law can be expressed in equations that link the permeation rate, the diffusivity and the solubility. The equations that provide that linkage are Equations (2),

and (3). With the use of a permeation cell, one can record the rate of passage of gas/vapor through a membrane. The data can be plotted as a "material transmitted per unit area - time" curve, whose final slope allows the flux, J to be calculated. There is, however, an interval before the steady state can be approached due to the finite diffusion velocity of solute within the membrane (a transient).

For the transient or non-steady state model, use of Fick's second law is employed. In one dimension and with an assumed constant diffusion coefficient, Fick's second law can be expressed as shown in Equation (4),

$$\frac{\partial C}{\partial t} = D \frac{\partial^2 C}{\partial x^2} \tag{4}$$

where:

• C = The concentration of a species
• t = The time
• D = The assumed to be constant diffusion coefficient
• x = The position [length]

Defining a membrane wall of thickness, l and with focus on a single specie and one-dimensional permeation, a system might look like Figure 3.2.

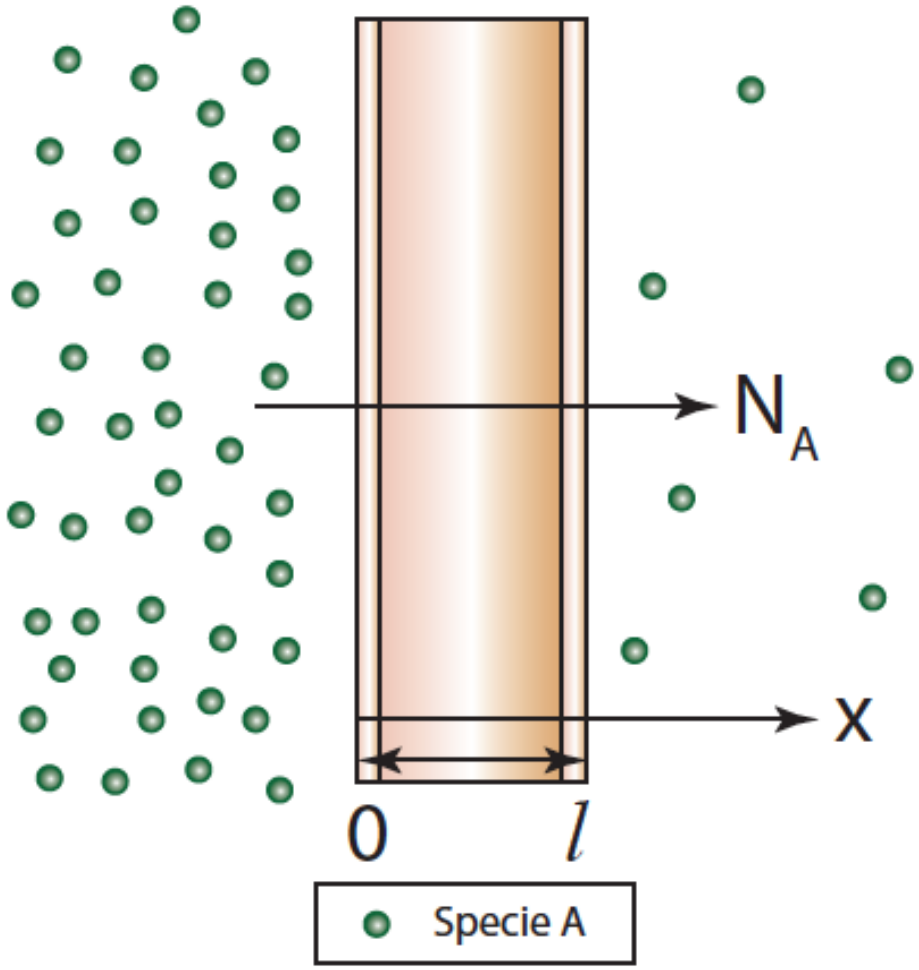

Figure 3.2: One-dimensional permeation of a single specie through a wall

The following derivation is taken in large part from Barrer and Rideal [4]. Now, if we assume that: Henry's Law is valid; that the gas diffusion coefficient is constant over the concentration range of interest, (usually valid for low-sorbing penetrants in rubbery polymers), and that the initial and boundary conditions are as follows:

$$\boldsymbol{C(0, t > 0) = C_1} \tag{5a}$$

$$\boldsymbol{C(l, t > 0) = C_2} \tag{5b}$$

$$\boldsymbol{C(x, t = 0) = C_0} \tag{5c}$$

The solution to Fick's Second Law, Equation (4) is:

$$\mathrm{C(x,t)} = C_1 + \frac{(C_2 - C_1)}{l} \cdot x + \frac{2}{\pi} \sum_{n=1}^{\infty} \frac{C_2 \mathrm{COS}(n\pi) - C_1}{n} \times$$

$$sin\left(\frac{n\pi \cdot x}{l}\right) exp\left\{-\frac{Dn^2\pi^2 t}{l^2}\right\} + \frac{4C_0}{\pi} \sum_{m=0}^{\infty} \left(\frac{1}{2m+1}\right) sin\left\{\frac{(2m+1)\pi \cdot x}{l}\right\} \times$$

$$exp\left\{-\frac{\left(D(2m+1)^2\pi^2 t\right)}{l^2}\right\} \tag{6}$$

Differentiating Eq. 6 with respect to x and setting x = 0 leads to:

$$\{\partial C/\partial x\}_{x=0} =$$

$$\frac{(C_2 - C_1)}{l} \cdot \frac{2}{l} \sum_{n=1}^{\infty} \left(\frac{C_2 \cos(n\pi) - C_1}{n}\right) exp\left\{-\frac{\left(D(n)^2\pi^2 t\right)}{l^2}\right\} +$$

$$\frac{4C_0}{l} \sum_{m=0}^{\infty} exp\left\{-\frac{D(2m+1)^2\pi^2 t}{l^2}\right\} \tag{7}$$

But, given that the gas/vapor flows through the membrane into a known volume; V, the flow rate of the gas/vapor per unit area is given by:

$$V \cdot \frac{dC_g}{dt} = D\left(\frac{\partial C}{\partial x}\right)_{x=0} \tag{8}$$

Substituting Eq. 8 into Eq. 7 and integrating it from t = 0 to t = t, then we obtain and expression for Cg.

$$C_g = \left[\frac{D(C_2 - C_1)}{l \cdot V}\right] \cdot t + \frac{2l}{\pi^2 V}\sum_{n=1}^{\infty}\left[\frac{C_2\cos(n\pi)}{n^2} - \frac{C_1}{n^2}\right]\left[1 - exp\left\{-\frac{Dn^2\pi^2 t}{l^2}\right\}\right] +$$

$$\frac{4lC_0}{\pi^2 V}\sum_{m=0}^{\infty}\left[\frac{1}{(2m+1)^2}\right]\left[1 - exp\left\{-\frac{D(2m+1)^2\pi^2 t}{l^2}\right\}\right] \tag{9}$$

As $t \to \infty$, Eq. 9 approaches the line:

$$C_g \to \frac{D}{lV}\left\{[C_2 - C_1] \cdot t - \frac{C_2 l^2}{6D} - \frac{C_1 l^2}{3D} + \frac{C_0 l^2}{2D}\right\} \tag{10}$$

Equation 10 arises as the infinite series collapse to the finite values as shown.

$$\sum_{n=1}^{\infty}\frac{\cos n\pi}{n^2} = -\frac{\pi^2}{12}$$

$$\sum_{n=1}^{\infty}\frac{1}{n^2} = \frac{\pi^2}{6}$$

$$\sum_{m=0}^{\infty}\frac{1}{(2m+1)^2} = \frac{\pi^2}{8}$$

After setting C_0 and C_1 to zero, Eq. 10 becomes:

$$C_g = \left\{\frac{DC_2}{lV}\right\}\left\{t - \frac{l^2}{6D}\right\} \tag{11}$$

A term "time lag" has been coined [4] and can be written as

$$\Theta = \frac{l^2}{D}\left[\frac{1}{C_2 - C_1}\right]\left[\frac{C_2}{6} + \frac{C_1}{3} - \frac{C_0}{2}\right] \tag{12}$$

After setting C_0 and C_1 to zero, Eq. 12 becomes:

$$\Theta = \frac{l^2}{6D} \tag{13}$$

Now, with the aid of Eq. 13, a simple method of measuring the diffusion coefficient is available. If a plot of the amount of gas/vapor collected after passing through a rubber membrane as a function of time per unit area is generated, then the extrapolated x-intercept will be Θ, the time lag. Typical plots found in the literature look similar to the one shown in Figure 3.3. This figure identifies: the time lag as the x-intercept of an extrapolated line from the point where the flux has attained steady-state; the slope of the steady-state line as the permeability; and, the portion of the data collection that pertains to diffusion through the membrane.

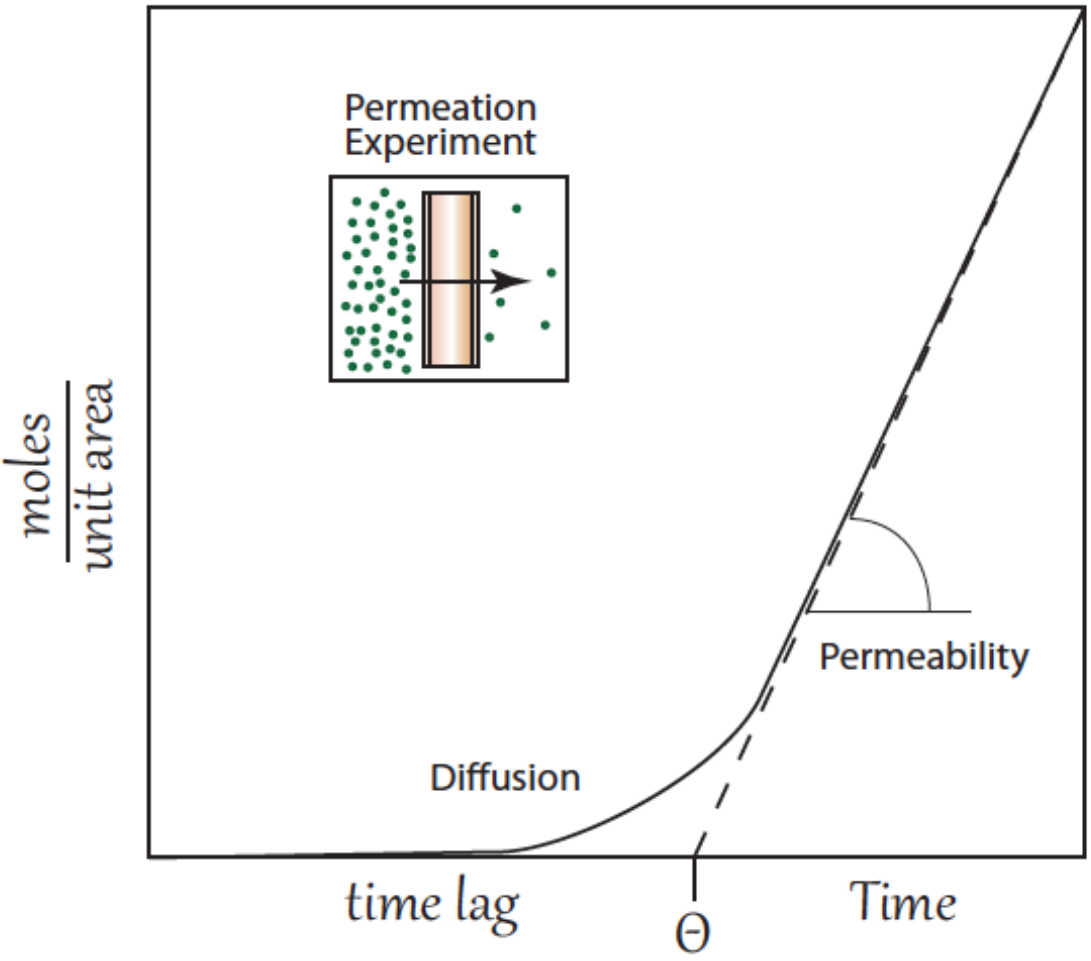

Figure 3.3: Typical plot of permeation experiment showing time lag

The flux of gas/vapor moving through a polymer is typically measured using a permeation cell. Three common types of permeation cells are used to measure the flux and they are:

1. Variable-Volume Constant-Pressure Method - measure Δvolume with Δtime at constant pressure

2. Variable-Pressure Constant-Volume Method - measure Δpressure with Δtime at constant Volume

3. Continuous-Flow Method - Sweep permeating gas with an inert gas stream, measure Δconcentration with Δtime

A permeation cell is used to measure transport properties. In essence, a permeation cell has two zones, and provides a mount for the membrane under test; support for the membrane if needed, an inlet for the penetrant gas/vapor; sealing mechanisms to ensure gas/vapor must cross only the membrane; and instrumentation to detect changes to the system over time.

Schematics of the three listed permeation cells [5] that might be used in an experiment designed to measure gas/vapor flux are shown below in Figure 3.4. Figure 3.4(a) shows a variable-volume constant-pressure permeation cell where the volume change would be measured; figure 3.4(b) shows a variable-pressure constant volume permeation cell where the pressure change would be measured; and finally, figure 3.4(c) shows a continuous flow permeation cell where the swept out species would be measured in an instrument such as a gas chromatograph or an inductively coupled plasma mass-spectrometer.

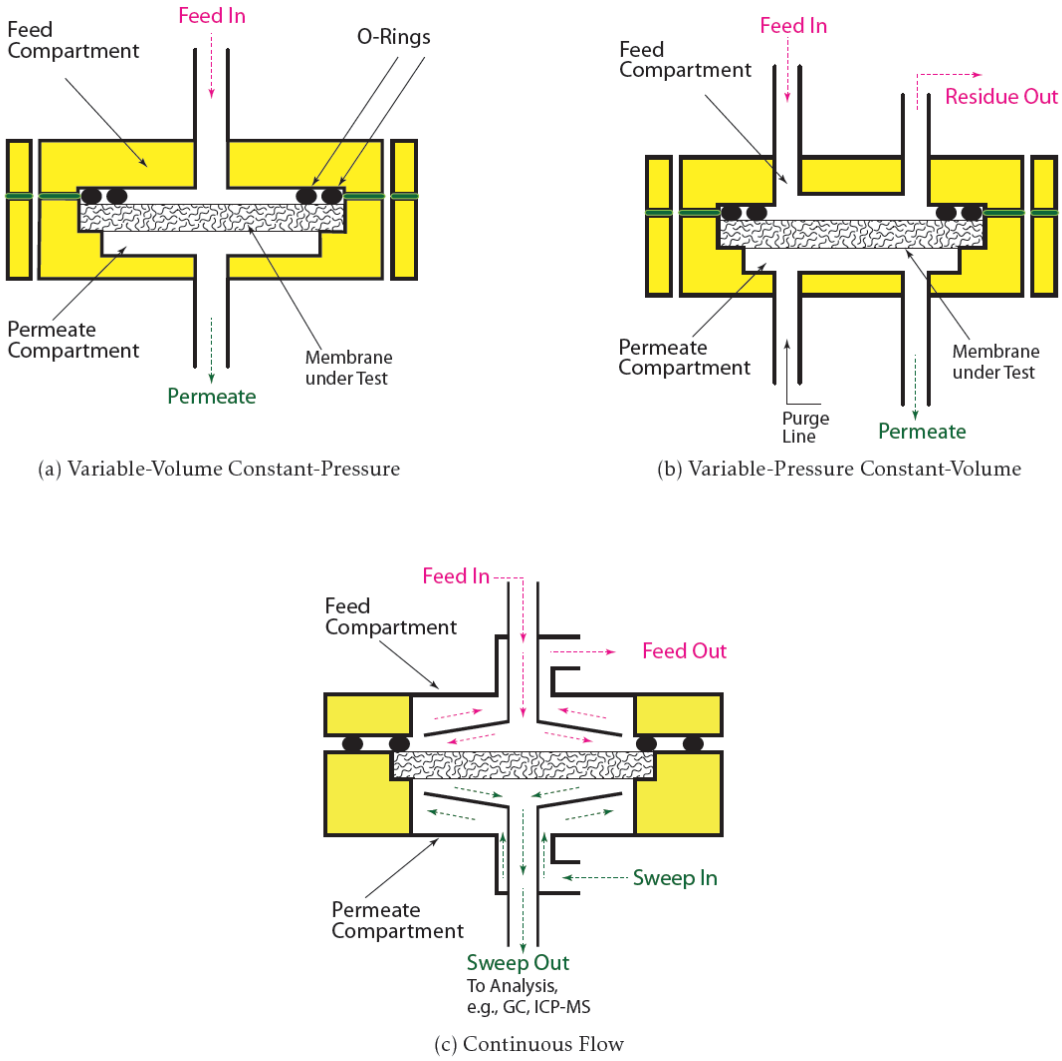

Figure 3.4: Permeation cells: (a) variable-volume constant-pressure; (b) variable-pressure constant-volume; and, (c) continuous flow

Figure 3.4(a) shows a variable-volume constant-pressure permeation cell where permeate side would be ported to a bubble flow meter to measure ΔV as a function of time; figure 3.4(b) shows a variable-pressure constant-volume permeation cell where the permeate side of the membrane would be measured with a pressure transducer to capture Δp as a function of time; and finally, figure 3.4(c) shows a continuous flow permeation cell where the swept out species and carrier gas from the permeate side of the membrane

would be measured in an instrument such as a gas chromatograph (GC) to capture **Δ**C as a function of time. Figure 3.5 shows the required inputs and outputs for different styles of permeation cells.

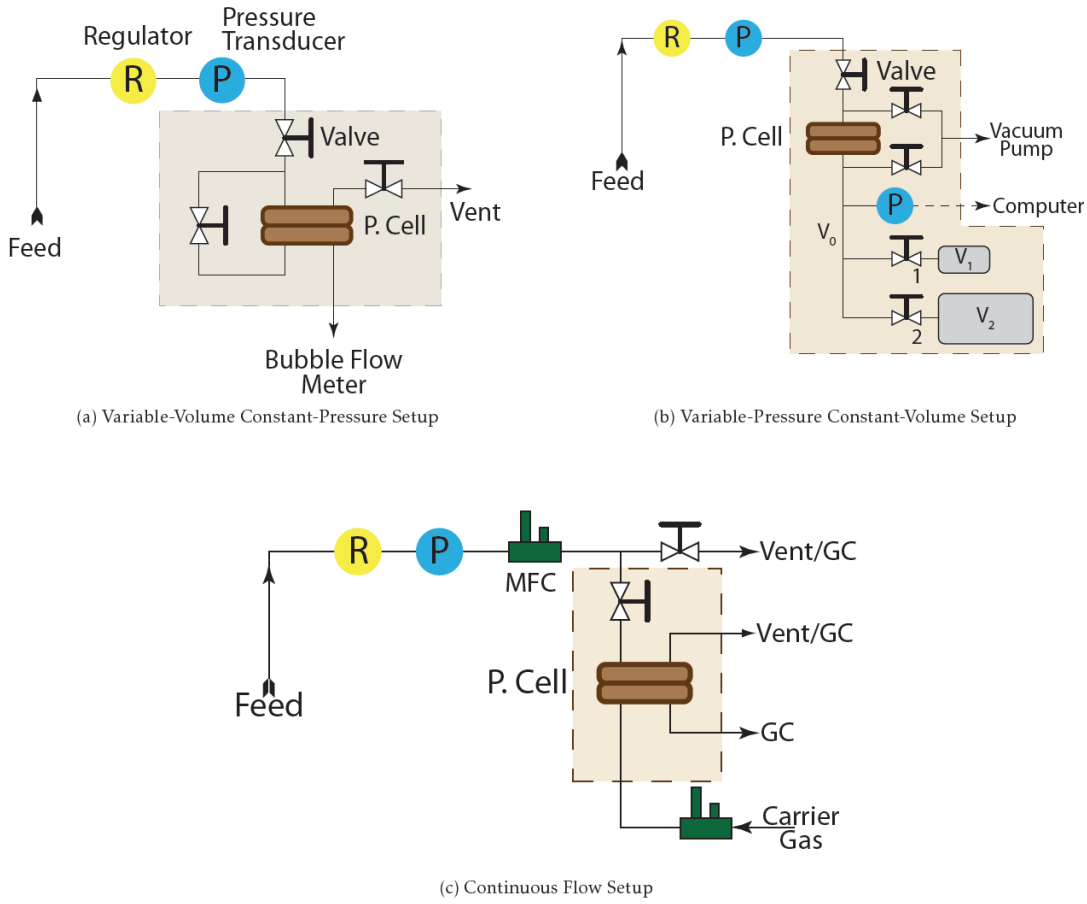

Figure 3.5: Permeation cells with inputs/outputs identified: (a) variable-volume constant-pressure; (b) variable-pressure constant-volume; and, (c) continuous flow

A different method of measuring the kinetic transport character of a penetrant and membrane system is known as the sorption or desorption method. In this method, the migration of a gas/vapor into or out of a film or membrane is monitored by recording the change in weight of the film/penetrant system as it undergoes either a sorption or a desorption process. If a film or membrane is suddenly immersed in a penetrant at t = 0 and the concentration of the penetrant is everywhere C_1, then the solution to Fick's

Second Law, Eq. 4 is:

$$\frac{C(x,t)}{C_1} = 1 - \frac{4}{\pi}\sum_{n=0}^{\infty}\frac{(-1)^n}{(2n+1)}\left\{exp\left(-\left(\frac{D(2n+1)^2\pi^2 t}{l^2}\right)\right)\right\}\left\{cos\left(\frac{(2n+1)\cdot\pi\cdot x}{2l}\right)\right\} \tag{14}$$

In this solution, the film thickness is equal to $2l$, and C_1, the gas concentration in contact with the faces of the film is considered as immediately established. Note that this equation does not take into account the diffusion towards the edges of the membrane, as this is considered a unidirectional transport.

The concentration equation given above can be integrated to obtain the mass of penetrant $M(t)$, absorbed by the sample at any given time $\boldsymbol{t}$ with the assumptions that the temperature and pressure is held constant to yield the following "Mass Ratio" equation:

$$\frac{M(t)}{M_\infty} = 1 - \sum_{n=0}^{\infty}\frac{8}{(2n+1)^2\pi^2}\left\{exp\left(-\left(\frac{D(2n+1)^2\pi^2 t}{l^2}\right)\right)\right\} \tag{15}$$

In the above equation, M_∞ is the mass of the specie that will be absorbed by the film or membrane at equilibrium, Of course, the volume of the gas absorbed at equilibrium V_∞ in cm^3 (Standard Temperature Pressure) can be determined using:

$$V_\infty = \frac{M_\infty - M_i}{(Molecular\ Weight)_{gas/vapor}}\cdot 22{,}400 \tag{16}$$

This relationship uses the constant 22,400 that corresponds to the volume in cm^3 (Standard Temperature Pressure) occupied by a mole of gas/vapor at standard conditions of pressure and temperature (1 atmosphere and 273.15K). M_i is the initial mass of the

sample and $(Molecular\ Weight)_{gas/vapor}$ is the molar mass of the gas/vapor under investigation.

With V_∞ determined, the solubility coefficient $\left\{in\ \frac{cm^3(STP)}{cm^3 \cdot MPa}\right\}$, is obtained using

$$S = \frac{V_\infty}{p \cdot V_{membrane}} \tag{17}$$

where,

p is the applied gas pressure and *Vmembrane* is the volume of the polymer membrane.

According to the "Mass Ratio" equation, the value of $\frac{t}{l^2}$ for which the mass ratio $\frac{M(t)}{M_\infty}$ is equal to $\frac{1}{2}$ occurs when:

$$\left[\frac{t}{l^2}\right]_{\frac{1}{2}} = \frac{1}{D}\left[\frac{-1}{\pi^2}\right] \cdot ln\left[\frac{\pi^2}{16} - \frac{1}{9}\left(\frac{\pi^2}{16}\right)^9\right] \tag{18}$$

Eq. 18 can be converted to:

$$D = \frac{0.04919}{\left[\frac{t}{l^2}\right]_{\frac{1}{2}}} \tag{19}$$

During a sorption experiment (see Figure 3.6), the change is weight is measured either directly or indirectly. The sorption measurement allows the experimentalist to directly obtain the solubility coefficient and to calculate, assuming some hypotheses, an apparent diffusion coefficient.

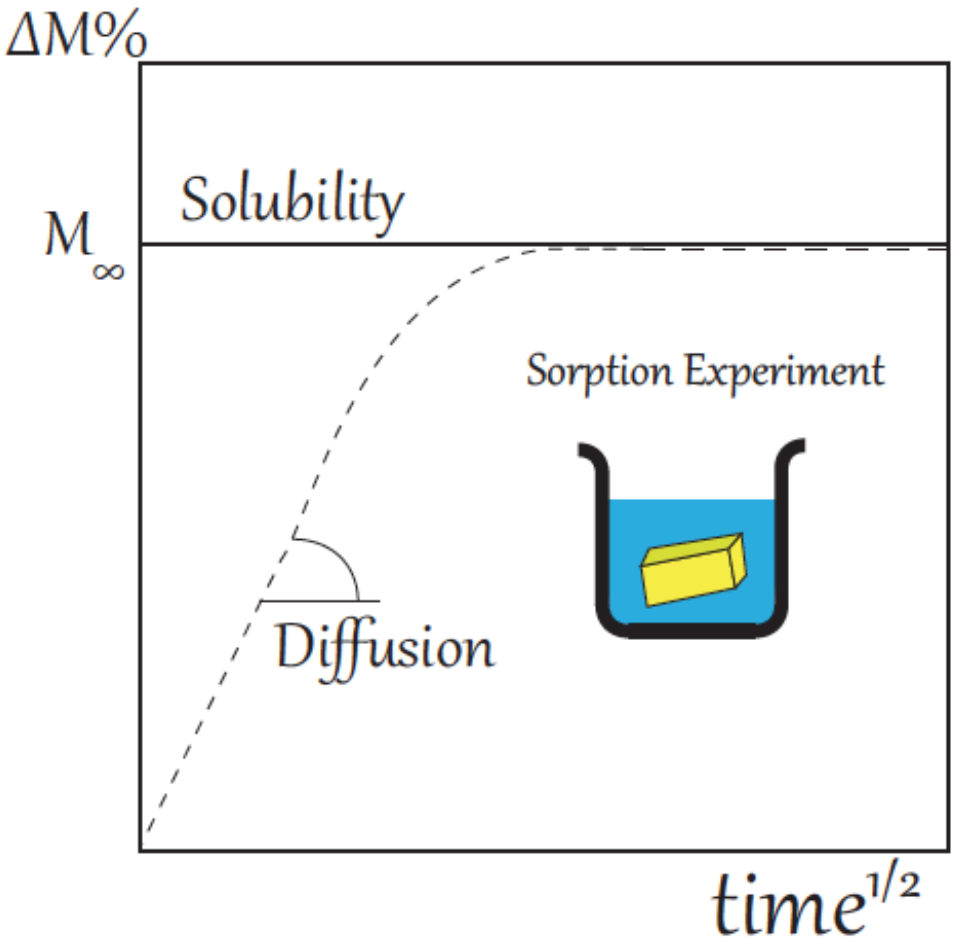

Figure 3.6: Typical sorption experimental setup

These techniques must be very sensitive, because the absorbed quantities are often very small [6]. The literature indicates various techniques to monitor the weight change. One technique is known as the gravimetric method that might use an electromagnetic coupling to transmit the sample weight to an external balance, and is known as a "magnetic suspension balance". One of the advantages of this device is the separation of the saturation system from the balance, avoiding a deterioration of the balance by aggressive/corrosive gases or vapors. A second approach is based on oscillation techniques. This kind of method is called indirect because the sample weight is deduced from the resonance characteristics of a support. The main method is the quartz crystal microbalance. A polymer film is deposited on a piezoelectric crystal. Under the influence

of an alternating current, this crystal undergoes a deformation that becomes maximal at the frequency of resonance. This frequency depends on the mass of the support: an increase of the polymer mass entails a reduction of the crystal resonance frequency.

3.3 Partial and absolute pressure gradient studies

In this study, the influence of partial and absolute pressure on the tribological characteristics of plasma treated medical silicone tubing will be investigated. The governing hypothesis is that the monomer feedstock is permeating out of the lumen volume as the tubing is being transported to the capacitive coupled so-called ID electrode. A plasma reactor used to treat silicone rubber tubing may resemble the following schematic and image shown in Figure 3.7.

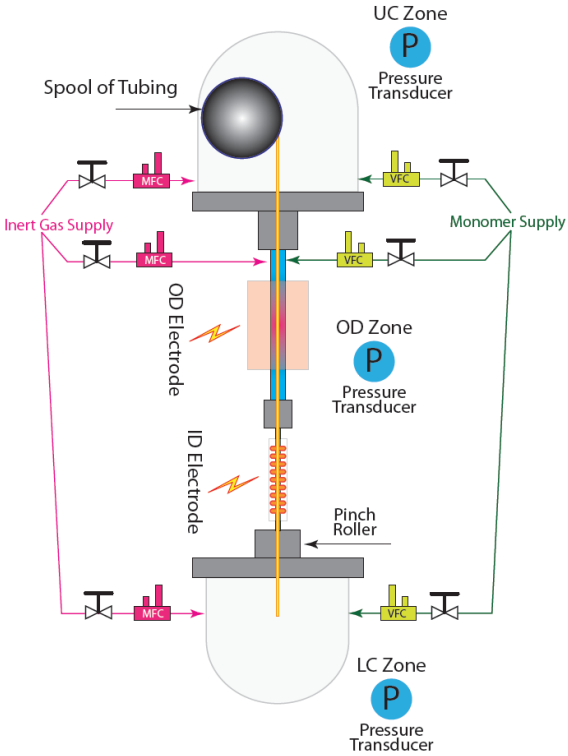

(a) Schematic of Plasma Reactor

(b) Plasma Reactor Treating Tubing

Figure 3.7: Reactor setup for plasma polymerization processing: (a) depiction of reactor w/ key hardware; (b) reactor treating tubing

Figure 3.7 is intended to show three distinct zones:

• UC Zone: The Upper Chamber Zone where a spool of tubing is loaded and can be saturated with monomer

• OD Zone: The Outside Diameter Treatment zone where continuous wave plasma treats the outside diameter surface

• LC Zone: The Lower Collection Zone where the treated tubing is collecting post treatment

Each zone is independently controlled with regard to pressure, the mass of inert gas flowing to that zone, and the volume of monomer feedstock entering that zone. The mass of inert gas is metered out with mass flow controllers (MFC's) and the volume of monomer feedstock is metered out with vapor flow controllers (VFC's). Prior to initiating the plasma polymerization process, the reactor is evacuated to a low pressure and then undergoes a leak integrity check to ensure that no gross vacuum leaks exist.

Then, the tubing dwells In the Upper Chamber Zone during what is referred to as a Saturation phase. It is in this phase that monomer feedstock flows into the UC Zone and is allowed to permeate and equilibrate with the batch of tubing that is loaded onto the spool.

Following the saturation phase, the tubing is transported through the reactor using a "pinch roller" that literally pinches and pulls the tubing through the reactor at a rate (AKA, "Line Speed") determined by the process designer.

On the way down through the reactor, the tubing passes through the Outside Diameter (OD) Treatment Zone. In this zone, inductively coupled continuous wave Radio Frequency plasma bathes the OD surface. The plasma species in the OD Zone can be sourced from an inert gas supply, a monomer supply (hexamethyldisiloxane); or can be a combination of the both of these species. This portion of the process then either treats (if using a pure inert gas) or coats (if using a pure monomer vapor) or simultaneously treats and coats (if using a combination of inert gas and monomer vapor) the OD surface to

impart lubricity to that surface.

As the tubing is pulled down and through the reactor, it passes through a tightly toleranced Inner Diameter (ID) glass tube that is encased inside of an Inner Diameter (ID) Electrode. In this area of the reactor, the ID Electrode and input ID Radio Frequency (RF) pulsed power with a prescribed duty cycle and frequency form capacitively coupled RF plasma. The plasma is confined to the inside of the tubing lumen. It is this portion of the process that lays down the tribological coating on the inside diameter surfaces to render those surfaces lubricious. The plasma polymerization process sequencing then follows the timeline shown in Figure 3.8:

Figure 3.8: The plasma polymerization process sequencing

The process is designed to treat, coat or treat and coat the outer diameter and inner diameter surfaces with a film as the tubing is conveyed through the reactor. With regard

to the inner diameter surface, the process relies on there being sufficient feedstock monomer in the lumen volume to feed the plasma and subsequently be shattered into molecular fragments that are the building blocks of a tribological film.

Partial pressure studies will be to perform designed experiments using a reactor similar to the one shown in Figure 3.7. The experimental plans are the result of discussions surrounding a question regarding poor and/or erratic inner diameter surface lubricity output from treated multi-lumen silicone tubing. The question is: "Is the process monomer starved by the time the inner lumen plasma is lit"? The experimental setup will be to flow pure monomer vapor to the reactor, set up a zero monomer concentration gradient condition and process tubing at different constant absolute pressures. Note that the reactor has three independently controlled zones with regard to pressure and monomer or inert gas volumetric flow inputs. Each independently controlled zone has an entrant port that allows for the introduction of feedstock monomer and/or other gasses (e.g., an inert gas). The zones can be termed: the Upper Chamber Zone; the Outside Diameter (OD) Treatment Zone; and the Lower Collection Zone. The monomer vapor flows will be set to flow to each and every zone and the only specie allowed to flow into the three zones will be the monomer. The pressure will be allowed to equilibrate to result in a zero concentration gradient condition with regard to the feedstock monomer. Thus, there will be no concentration driving force for the monomer to permeate into or out of the inner lumens of the multi-lumen silicone tubing. The first set of experiments will involve processing multi-lumen silicone tubing at the following constant pressures (in millitorr) in all three independently controlled zones: 100; 250; 500; 750; 1000; 1500; 2000; and 4000 for both saturation (a pre-treatment equilibration phase wherein the monomer is allowed to permeate through the tubing walls) and plasma treatment.

Absolute pressure gradient studies will explore the impact of a mechanical pressure driving force with the maximum concentration driving forces in place. The reactor will be configured to flow pure monomer in the Upper Chamber zone and pure argon to both the Outside Diameter Treatment Zone and the Lower Collection Zone. This

configuration will set up the maximum concentration driving force between the inner lumen and the outside surface. The reasoning behind this experiment is that it might be desirable to selectively target regions of the tubing to the type of modification employed. For example, if a tribological coating serves to reduce friction, it may impact adhesion later on in processing. Surface treatment not involving the breaking or formation of chemical bonds could be employed on the outside diameter surface, provide the needed friction reduction and not impact the adhesion characteristics of the silicone rubber. This experiment will input volumetric flow rates of the inert gas, argon and vary absolute pressure. Again, the tribological characteristics of the processed silicone tubing will be assessed using the tubing surface tribometers that have been refined by previous work.

3.4 Degree of surface coating/surface treatment

This part of the proposed research will study the differences between surface treatment and surface coating on the outside diameter tubing surfaces. The research is motivated by the desire to selectively treat certain surfaces with a chemical treatment (i.e., a tribological coating is to be generated) and yet other surfaces with an inert treatment that does not involve the breaking or formation of chemical bonds.

The reasoning behind wanting to selectively target certain surfaces is that; downstream of plasma polymerization, the next user of the tubing may want to bond the outer diameter surface to another material. There is some evidence that a coating on the outer diameter surface that is not tenacious enough or if the surface is different chemically than a silicone tubing that has not been subjected to a plasma polymerization process may not bond to other materials as strongly as wished for.

For this effort, varying ratios of the inert gas to monomer vapor will be the process inputs. Tubing will be processed and then the tribological characteristics of the processed silicone tubing will be assessed using macroscale and nanoscale tribological analyses.

3.5 Impact of input power settings

The reactor has two RF generators in place. One RF generator is used to power the OD Electrode and the other RF generator is used to power the ID Electrode. The generators allow the user to vary: the peak power in Watts, the frequency in Hertz (for example, when using a pulsed power), and the duty cycle in percentage.

This research will explore the influence of the peak power, the power frequency and the power duty cycle on the tubing surface character. Varying power settings will be input; the tubing will be processed and then evaluated with macroscale and nanoscale tribological methods.

3.6 Influence of reactor temperature

Currently, the process occurs without any elaborate environmental controls in place. This means that there may be relatively wide swings in ambient temperature, in the relative humidity and in the general processing cleanliness. Note that the source of the monomer feedstock (hexamethyldisiloxane or HMDSO for short) is a liquid at room temperature, and it is the polymerizable vapor that is pulled into the reactor through a vapor flow controller. It is well known that vapor pressure and temperature are related to each other in a very non-linear fashion. Note that a plot (see Figure 3.9) of the natural log of the vapor pressure, $ln(p_{vap})$, as a function of $\frac{1}{T}$, (T is absolute temperature here) is a straight line with a slope equal to that of $-\frac{\Delta H_{vap}}{R}$. We can use this fact to derive a simple equation that relates the vapor pressure at certain temperatures to the heat of vaporization. This derivation leads to the Clausius-Clapeyron Equation,

$$ln\left(\frac{p_2}{p_1}\right) = -\frac{\Delta H_{vap}}{R} \cdot \left(\frac{1}{T_2} - \frac{1}{T_1}\right) \tag{20}$$

where

- p_1 and p_2 are the vapor pressures at two distinct temperatures
- ΔH_{vap} is the heat of vaporization
- R is the universal gas constant
- T_1 and T_2 are the two distinct temperatures

Equation 20 allows the determination of the vapor pressure of a liquid at any temperature given the heat of vaporization, or the heat of vaporization given the vapor pressure at two different temperatures.

Vapor pressure data for the monomer used (hexamethyldisiloxane) has recently been fit to a "PC-SAFT" equation with a deviation of no more than 0.7 % between the model [7] and the empirical data [8]. The HMDSO vapor pressure as a function of temperature data provided by Scott [8] show the expected linear relationship between the natural log of the vapor pressure, $\ln(p_{vap})$ and the inverse absolute temperature, $\frac{1}{T}$.

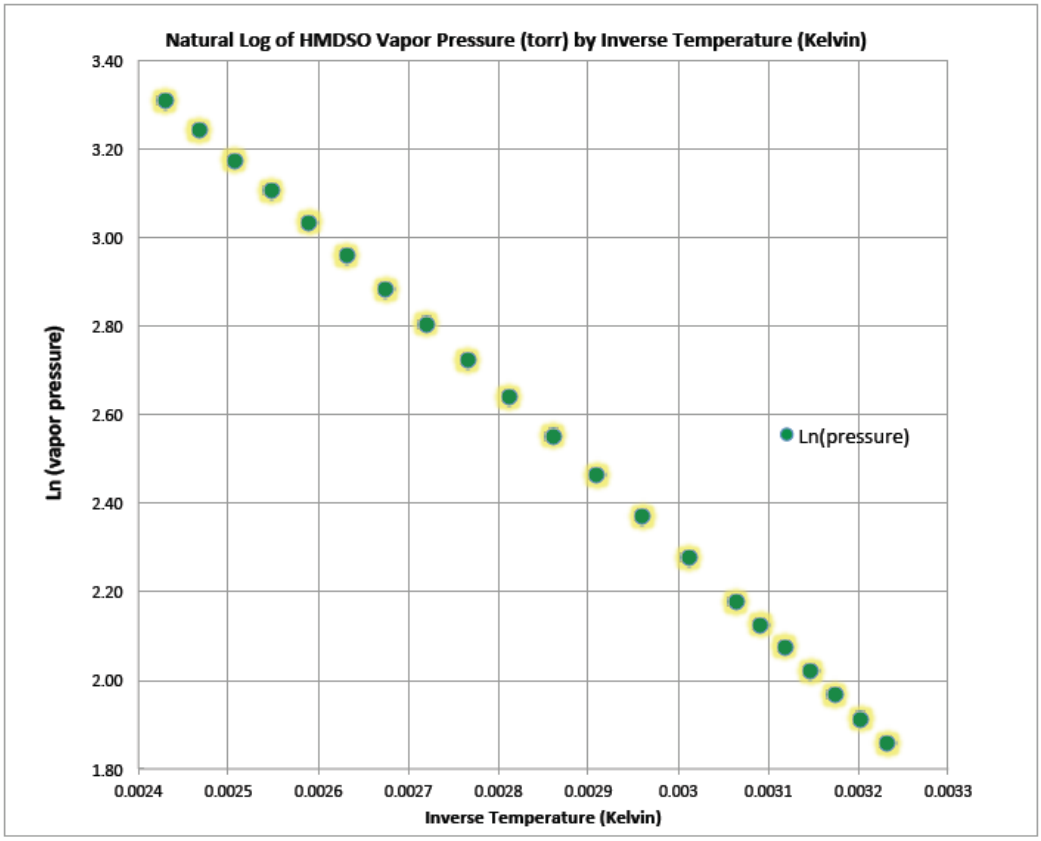

Figure 3.9: Natural log of the vapor pressure, as a function of inverse absolute temperature for HMDSO, pressure in torr and temperature in Kelvin

Given the profound sensitivity of the monomer feedstock vapor pressure to ambient temperature, the effort here is directed toward: controlling the ambient temperature during processing; controlling the monomer feedstock temperature (and thereby, its vapor pressure); controlling the input polymerizable vapor lines to the reactor; and controlling the reactor temperature itself. It is desired to maintain the vapor delivery lines and the reactor at temperatures in excess of the liquid monomer temperature to prevent condensation.

An additional perceived benefit of temperature control is that undesirable water tied up with the tubing substrate will be more readily driven off of the tubing and removed from the process environment.

3.7 Incoming substrate variability

For many processes that are not completely vertically integrated, there is much reliance on the consistency and quality of the raw materials. If there is variability inherent in the incoming material, then there is a strong likelihood that the outgoing processed material will have associated variability. This will stand unless the process can "swamp" or "mute" that variability, or if the variability is favorable to the desired processing outcome.

Because the personnel may not know what incoming material characteristics are needed or desired, there might be uncontrolled "noise" variables that can be detrimental to the outcome. The effort for this part of the research is directed at determining what material characteristics influence the output and the outputs' sensitivity level to those material characteristics. Once the significant incoming material characteristics are identified, then the goal will be to work with the supplier to control those parameters and/or characteristics.

3.8 Characterize new inner diameter electrode

The inner diameter electrode evolved on a positive selection approach basis. Here the meaning of a positive selection approach basis means that, an electrode would be tried, and if it worked, it was put into use. This approach is dangerous as it can result in the rejection of a potentially better solution out of hand. A much more worthwhile approach would be to progressively eliminate all feasible solutions; i.e., explore all possible solutions for a new ID electrode design. This approach, albeit more time-consuming, encourages the acquisition of knowledge, rather than assumes it. A progressive elimination approach will also bolsters the fundamental knowledge base.

The task ahead is to redesign the most commonly used ID electrode such that the electromagnetic force lines are forced to the centerline of the tubing. The redesigned ID electrode will be put into place and tested by running the process and using comparative

macroscale and nanoscale tribological outputs. In addition to merely testing a prototypical electrode, mathematical models of the electromagnetic field generated by and surrounding the ID electrode will be developed. This method will enable us to investigate alternative designs without having to bother with prototyping them if they showed to be non-worthwhile. Once a viable mathematical model is built, new configurations of an ID electrode can be tried at minimal cost.

3.9 Permanent deformation of viscoelastic tubing

In an ideal thin-walled cylinder subjected to increasing axial load and internal pressure plastic instability occurs when equilibrium can no longer be maintained in an element of the cylinder. At this point the material behavior is insufficient to compensate for the changes in dimensions of the element [9]. The experimental task is to determine at what point the strains become non-uniform and how much the dimensions are altered. The point of interest is a point beyond the elastic limit.

An interesting passage regarding this limit is found in an article entitled, “ELASTICITY BEYOND THE ELASTIC LIMIT”. This paper [10], presents the following ideas regarding the elastic limit:

“Theories of elasticity have so far presupposed the existence of what Love [11] called a “state of ease ” of “perfect elasticity” in which “a body can be strained without taking any set”; that state ranging between an “initial”, “unstressed” and “unstrained” state on one hand and the “elastic limit” on the other. Recent technological progress has gradually reduced, absolutely and, still more, relatively, the field in which this assumption holds good. Not only has increased accuracy of measurements of permanent sets lowered the elastic limit until in many cases as, for instance, annealed copper, it has nearly disappeared. More important, in materials which do show a definite elastic limit as, for instance, mild steel, deformations in most practical applications go beyond that limit. In addition, one has to consider elastic materials such as bitumen or cement stone

showing creep: their elastic potential gradually disappears through relaxation. Finally, there are such materials as rubber which can be caused to undergo very large deformations, a certain part of which will always be non-recoverable. It therefore becomes necessary to consider elasticity beyond the elastic limit. If we define elasticity with Love as "the property of recovery of an original size and shape"' there would in all these cases be no question of elasticity because the original size and shape is not recovered. However, some of the deformation is always recovered: but which part of it is recoverable, becomes apparent only when all external forces, gravity included, have been removed. We may denote as the ground-position that position of the body which is then reached. To every deformation there corresponds a ground position of its own, which generally will not be the initial position from which the deformation started. Let us denote by deformation a change of size and of shape in general, whether recoverable or not, and by strain that part of it which is recovered when all external forces have been removed. Generally, the strain will differ from the deformation not only in magnitude, but also in the orientation of the principal axes."

Here, the intent is to study permanent deformation of medical grade silicone rubber tubing. This will be achieved by generating stress-strain curves using variously dimensioned silicone tubing to determine at what point does plastic deformation begin. The motivation behind studying deformation on the silicone tubing is driven by the fact that, when stringing a conductor through tubing, the dimensionality of both the tubing and the conductor come into play. During processing, there is a certain amount of tension on the tubing, which is not well controlled. The tension imparts a strain on the tubing and may lead to a change in the tubing dimensions that are not recoverable. The processed tubing ranges greatly in size and the smaller the tubing outside diameter the greater the likelihood of permanent plastic deformation becomes. Mathematical modeling of the viscoelastic behavior will be performed and compared to empirical findings. These models can be used if and when new silicone gumstock resins are developed.

3.10 Reactor pressure and plasma character

This part of the proposed research will explore the relationship between the absolute pressure in the plasma volume and the plasma characteristics. A Langmuir probe will be used to gather data that will be analyzed in order to determine the plasma density, temperature, and potential as functions of pressure, gas flow, and input RF power. Note that both reaction and deposition rates are dependent on temperature, pressure, gas flow and plasma density making this study valuable in adding to the fundamental knowledge base.

3.11 Significance of tension on output

To plasma treat tubing that tubing needs to be transported through the plasma reactor. The tubing is pulled through the reactor using a pinch/pull apparatus and on the current embodiment of the process; the tension is not as well controlled as desired. This is because the spooling of the tubing is done in a relatively manual fashion and can lead to varying degrees of tension on the spooled tubing. Also, the reactors in use are not all identical and there are varying levels of tension control between the reactors available. Newer reactors employ master-slave motors that can use tension as a feedback to motor spin rates and as such, the tension control is superior to the older style reactors. Note that there is discussion in the literature regarding the impact of tension and line speed on the textured nature (and therefore the tribological nature) of the coating [12] as follows.

"For example, elastomeric material can be subjected to a tension so as to stretch it prior to deposition of the surface texture; that is, plasma is deposited onto the prestretched substrate under tension to achieve surface texture. In the case of elongate material such as tubing or ribbon, the tension is preferably constant and is applied so as to stretch the tubing or ribbon longitudinally. The prestretched tubing is moved through the plasma deposition chamber in a continuous process under constant tension at a defined line speed, and raised ridges are formed that are typically roughly perpendicular to the longitudinal axis of the elastomeric material."

The purpose of this tension study is to better control the tension imparted to the tubing during spooling and subsequent processing. Tubing with controlled tension levels will be processed for comparative evaluations. The macroscale and nanoscale tribological characteristics of the processed silicone tubing will be assessed using the methods that have been refined by previous work.

3.12 Influence of water partial pressure in the reactor

The focus of this section is to test the hypothesis that water vapor is deleterious to the tribological coating. In this study, hydrated tubing will be generated using an environmental chamber and processed through the reactor. The counterpart to this experiment will be to generate desiccated tubing using a heated vacuum oven and then process that tubing through the reactor. The two "flavors" of tubing will be compared and contrasted using both macroscale and nanoscale tribological evaluation techniques.

CHARACTERIZATION OF COATINGS

4 Key characteristics of coatings

4.1 Essential design outputs

After a coating has been generated, many things need to be understood regarding the nature of the coating system in order to ascertain what has been produced, its properties and its performance. If a coating has been produced for a long period of time in full production mode, then the level of characterization and/or evaluation is likely much different than a coating at the research or development phase of its life cycle. Full-scale production coating systems are usually characterized or evaluated to ensure quality control and for process repeatability assessment. Coatings in the research and development phase need to be evaluated for their specific properties and to understand the influence of input process parameters on those properties. Often, coatings that have been optimized need routine adhesion and thickness assessment. On the other hand, coatings under development might need friction, wear and composition evaluation. Obviously, sound and well-defined specifications need to be in place, since only with delineated standards can the design engineer or others clearly communicate what is required. Some companies refer to specifying these requirements as EDOs, an abbreviation for Essential Design Outputs. Some of the fundamental and critical characteristics for a coating are displayed in Figure 4.1.

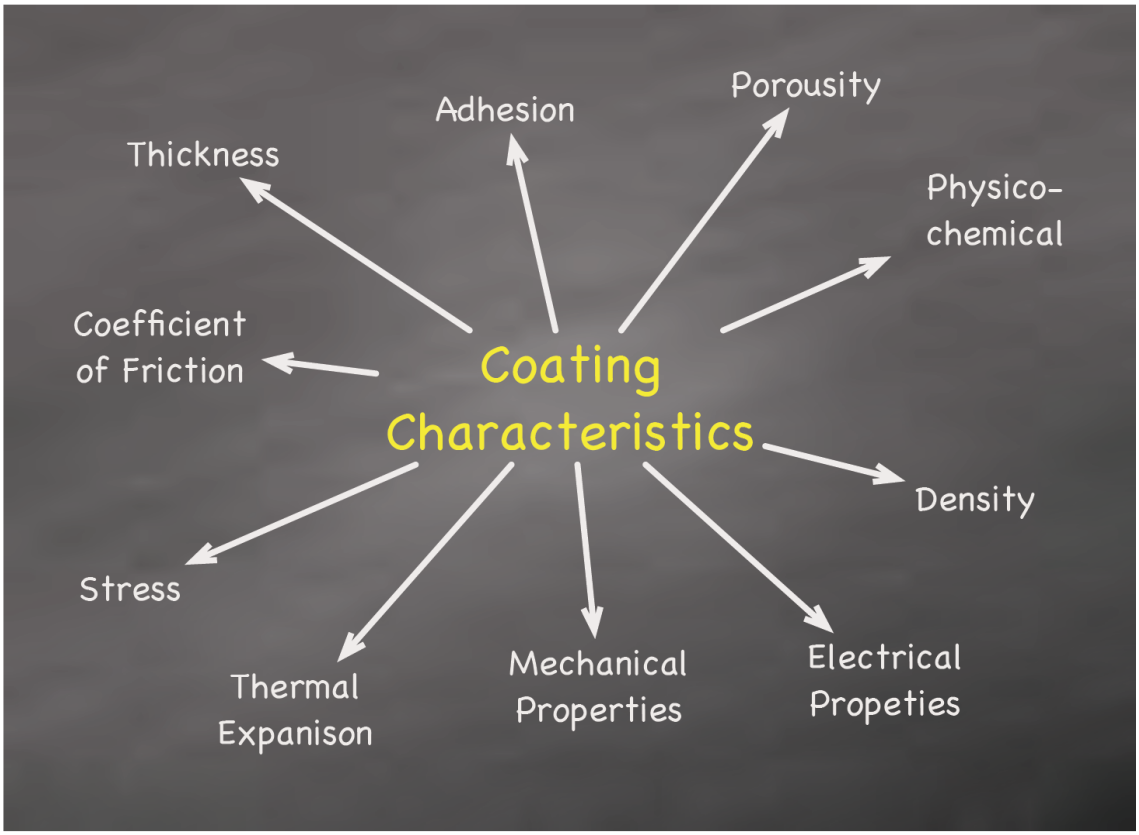

Figure 4.1: Fundamental and critical coating characteristics

4.2 Methods of characterization

Intrinsic coating properties need to be measured for comparative purposes, as more and more computer databases exist with coating properties. Knowing the fundamental coating properties can aid in selection, modeling and prediction of a coating system. The goal of coating evaluation and characterization should be effective, precise, and repeatable property measurements that are independent of the evaluator; easy to acquire and perhaps, recorded in real time during the processing steps.

Evaluation of coating characteristics includes but is not limited to: assessing the roughness, thickness, mechanical properties, physic-chemical properties, and tribological properties. Also, it would be desirable to have accelerated testing methods. Finally, the

ultimate characterization tools include industrial field-testing and utilize standardized test methods.

This research is focused on the tribological characteristics of a coating system using medical silicone rubber tubing as the substrate. Of paramount interest is the degree of friction reduction on the exterior and interior tubing wall surfaces. The need to assess the degree of friction reduction on silicone tubing comes from wanting to know if the process works as intended and if downstream assembly operations will be successful or not. Furthermore, the degree of "process goodness" will need to be assessed for process improvements and routine quality controls. A well-designed test method can be used to infer the lubricious nature of the entire tribological system on a macroscopic level. Additionally, a well-designed test can be used to direct the researcher to better processing techniques as it can provide a feedback loop when executing designed experiments. Once a process is deployed, a well-designed test method will afford process monitoring and can signal when a process is going out of control prior to catastrophic losses. It is a well-known adage that, "You cannot improve that which you cannot measure". There are a multitude of other important characteristics to be evaluated when developing and deploying a coating system. Table 4.2 shows coating characterization and evaluation methods.

Table 4.1: Part 1 - Fundamental and critical coating characterization

Coating Characterization & Evaluation							
Characteristic	Roughness	Thickness	Mechanical Evaluation				
			Hardness	Elastic Modulus	Fracture Toughess	Residual Stress	Adhesion
Test Method	Profilometry: • Stylus • Laser White Light Interferometry Scanning Tunnelling Microscopy Atomic Force Microscopy	Optical Methods • SEM • Holography • Ellipsometry • Metallography Removal Methods • Ball Cratering • Feeler Gauge • Coulometric • Stylus Profilometer E-Mag Methods • Mag Flux • Eddy Current • Capacity Scattering Methods • Beta Back Scattering • Ultrasonic Excitation Methods • X-ray Flourescence	Indentation • Vickers • Knoop Nano-indentation	Analysis of the Un-loading Curve Post Nano-indendation Cantilever & Beam	Qualitative • Indentation • Scratch Quantitative • Bending • Buckling • Indentation • Scratching • Tensile Testing	Curvature Measu-ments of Thin Plates Pre- & Post- Coating Generation X-ray Diffraction $\sin^2 \Psi$ • Measures bi-axial stress states • Relates Strain and Stress in Coatings	Pull-Off Tests Indentation Tests Scratch Test Laser Techniques Body-force Methods Acoustic Imaging

Table 4.1: Part 2 - Fundamental and critical coating characterization

Coating Characterization & Evaluation								
Characteristic	Physico-chemical	Tribological Evaluation				Accelerated Testing		
		Friction & Wear Tests	Abrasion Testing	Rolling Contact Fatigue Tests	Simulation Tests	Wear & Lubrication Maps	Test Parameter Monitoring	Wear Track Analysis
Test Method	Interactions between photons, X-rays, ions and electrons. Output is elemental and/or compound analyses. The output may be quantitative. First there is an excitation and interaction, then there is some type of dispersion which is then detected and a spectrogram is created. Popular methods include: SEM, TEM, XRD, AES, XPS, RBS and SIMS,	Pin-on-Disk; Pin-on-Flat; Pin-on-Cylinder; Thrust Washers; Pin into Bushing; Block-on-Ring; Crossed Cylinders	Dry Abrasion Test; Rubber Wheel Test; Ball Cratering	Twin-disk Machine	Multi-stroke plane - strain compression test; Bending-under-Tension	Maps that show the regimes of different wear mechanisms depending on two parameters along the coordinate axes. The wear mechanisms might be: Adhesion; Abrasion; Fatigue and Chemical Wear mapped into Seizure; Melt Wear; Severe or Mild Oxidation Wear; Delamination Wear and Ultra-mild Wear	Inference of dominate lubrication or wear mechanisms by monitoring test parameters such as: friction; lubricant film thickness; temperature; wear and surface roughness	Analysis of marks or depressions left on sliding surfaces after interaction. Each wear mechanism leaves its own features and the mechanism can often be identified by these marks. Comparison of wear scars from labratory testing to wear scars from real components taken from the field. Post mortem analysis of field tested components.

4.3 Macroscale coating friction characterization

The purpose of performing a plasma polymerization process on medical silicone rubber tubing is to reduce friction. For the selected proposed research, there is enormous interest in determining if the outer and inner diameter surfaces have reduced friction both prior to and after processing.

Tubing exterior (outer diameter) surface friction reduction characterization

It is a relatively simple exercise to measure the change in the tactile nature or friction reduction of the outer diameter (OD) tubing surface via so-called "sled testing". Currently, silicone rubber tube sled testing to characterize the friction reduction on the exterior tubing surface is performed as follows:

1. Insert rods down the bore of two sample lengths of tubing
2. Place rod/tubing assemblies in grooves created in a fixture
3. Clamp the ends of the rod/tubing assemblies to fix them in their grooves
4. Place a sled of known weight on top of the two-rod/tubing assemblies
5. Using a commercial sled-type testing device, pull the sled for a pre-determined time and at a pre-determined speed all the while recording the force require to pull the sled

The sled testing method and many others commonly used friction and wear evaluation methods [13, 14] are illustrated below in Figure 4.2.

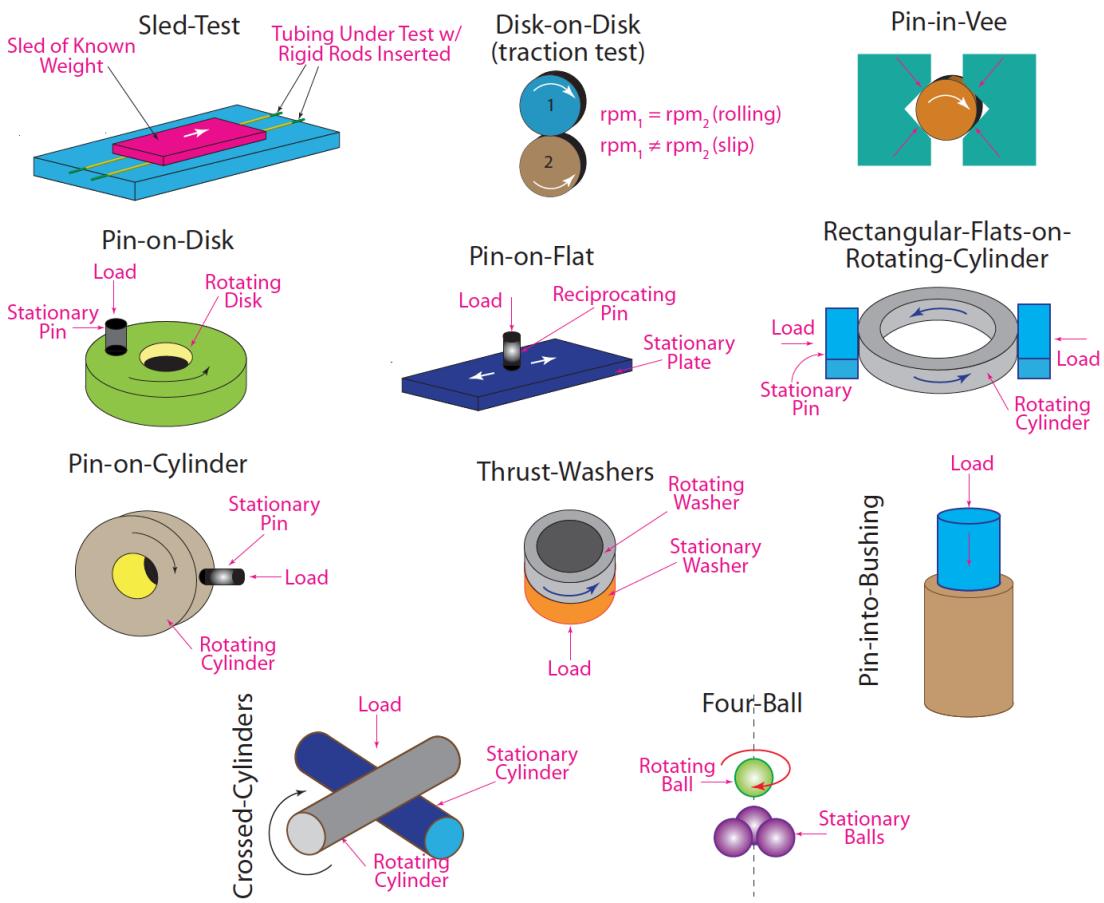

Figure 4.2: Commonly used friction and wear characterization methods

Other tribometer configurations to measure the outside diameter surface friction of tubing can be found in the open literature. One example test method places a sample of the tubing on the face of a reciprocating block of known mass. This test setup is shown in Figure 4.3.

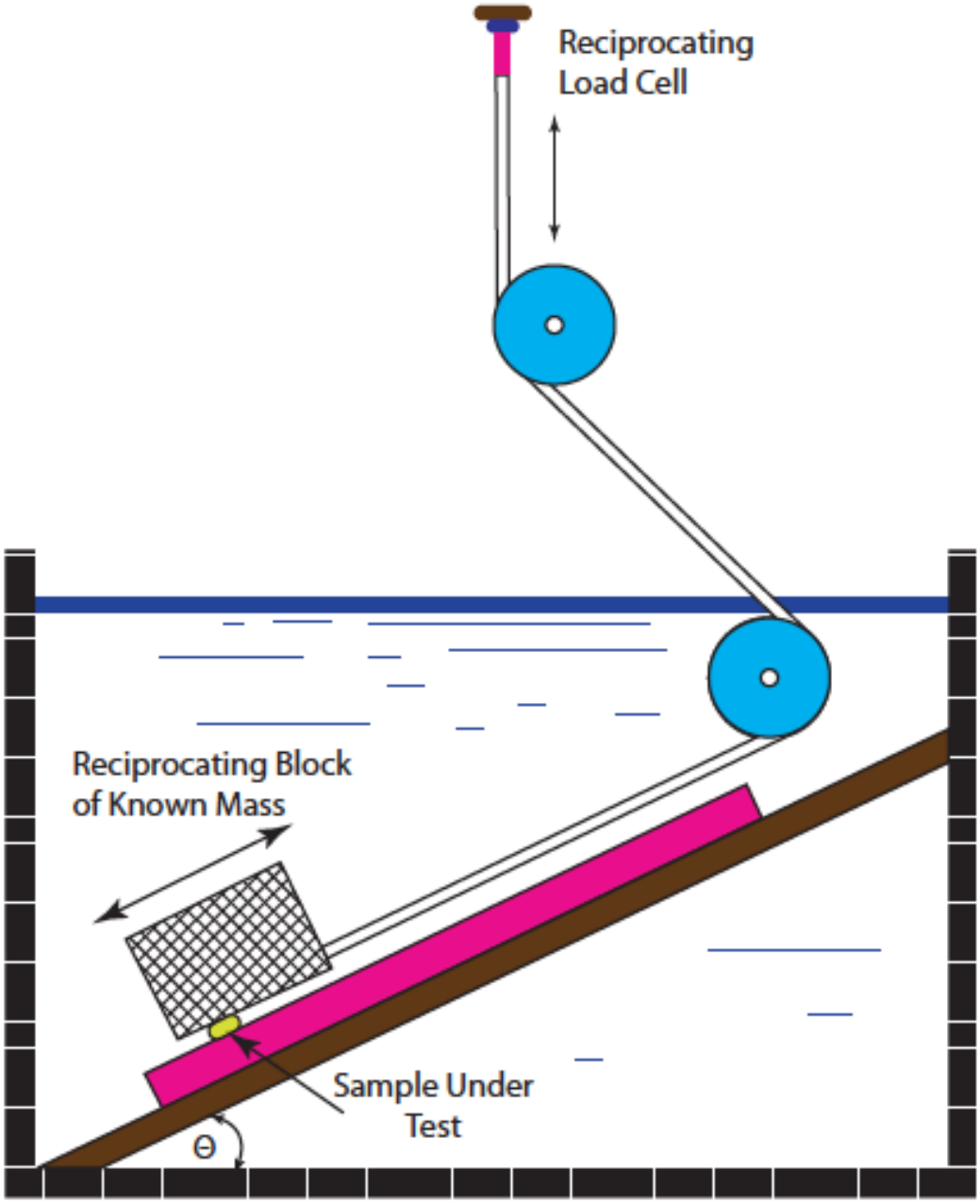

Figure 4.3: Outside diameter (OD) surface tribometer [15]

The treated sample is slid back and forth against a chosen surface (or "counterface") using a reciprocating motion while the force is recorded by a force transducer (or load cell). Both the sample and the counterface are on an inclined plane of known angle. The test can be employed to extract both friction and wear characteristics

of the sample/counterface system. This test can be performed in a submerged state (e.g., submerged in a physiological saline solution) to better emulate end-use conditions [15].

Tubing bore (inner diameter) surface friction reduction characterization

In practice, it has proven to be a rather difficult task to measure the tribological nature of the inner diameter (ID) surfaces. Some practitioners use a "wire-within-a- tube" system to characterize the macroscopic scale tribology of the inner tubing wall surface friction reduction. A literature survey will indicate that the biomedical industry normally measures some resistive force or torque involved with the insertion, extraction or rotation of a friction element or "tribo-partner" within a tube.

Ideally, the evaluation method to characterize the inner lumen lubricity will have certain key characteristics, namely:

1. The test shall **Represent End-Use Conditions**.
2. The test shall be **Quantitative**.
3. The test shall **Generate Continuous Variables Data**.
4. The test shall be **Repeatable**.
5. The test shall be **Rapid**.
6. The test shall be **Easily Executed**.
7. The test shall deliver **Easily Accessed Data**.

One example of an inner diameter (ID) lubricity test uses a "wire-within-a-tube" system which measures the extraction force required to withdraw a medical guide wire or similar tribo-partner using a tensile force tester (Lloyd Instruments LRX test system) at a set rate. This test method is described by McLaughlin [16] and is depicted below in Figure 4.4.

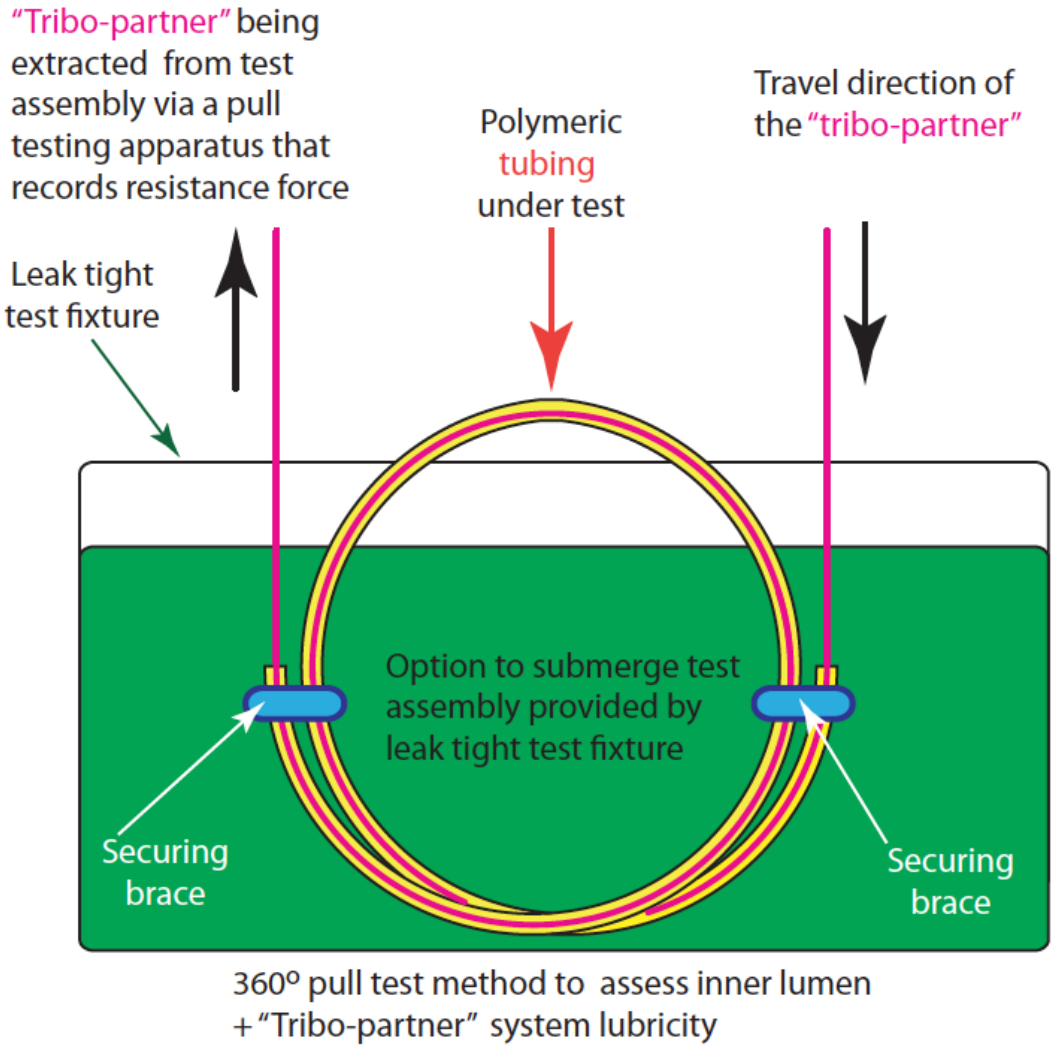

Figure 4.4: Macroscale extraction force tribology test layout for comparative inner diameter (ID) lubricity measurements [16]

In the test method displayed in Figure 4.4, a guidewire that is coated with a plasma-enhanced chemical polymerizable vapor deposition of diamond-like carbon film is being evaluated. The guidewire was made from medical grade stainless steel and subsequently coated. This test requires the pulling of the guidewire under test at a constant velocity after being strung through a low-density polyethylene tube. The wire-within-a-tubing assembly is placed into a fixture on a test frame and then the extraction force is recorded with a force transducer during the test. The setup includes a completely circular 360° coil assembly which could be immersed in a liquid to better simulate the

end use conditions.

As another example, there are patents in the open literature on torque testing of treated silicone tubing [17]. A schematic of the general test fixturing for comparative inner diameter (ID) lubricity testing is shown in Figure 4.5.

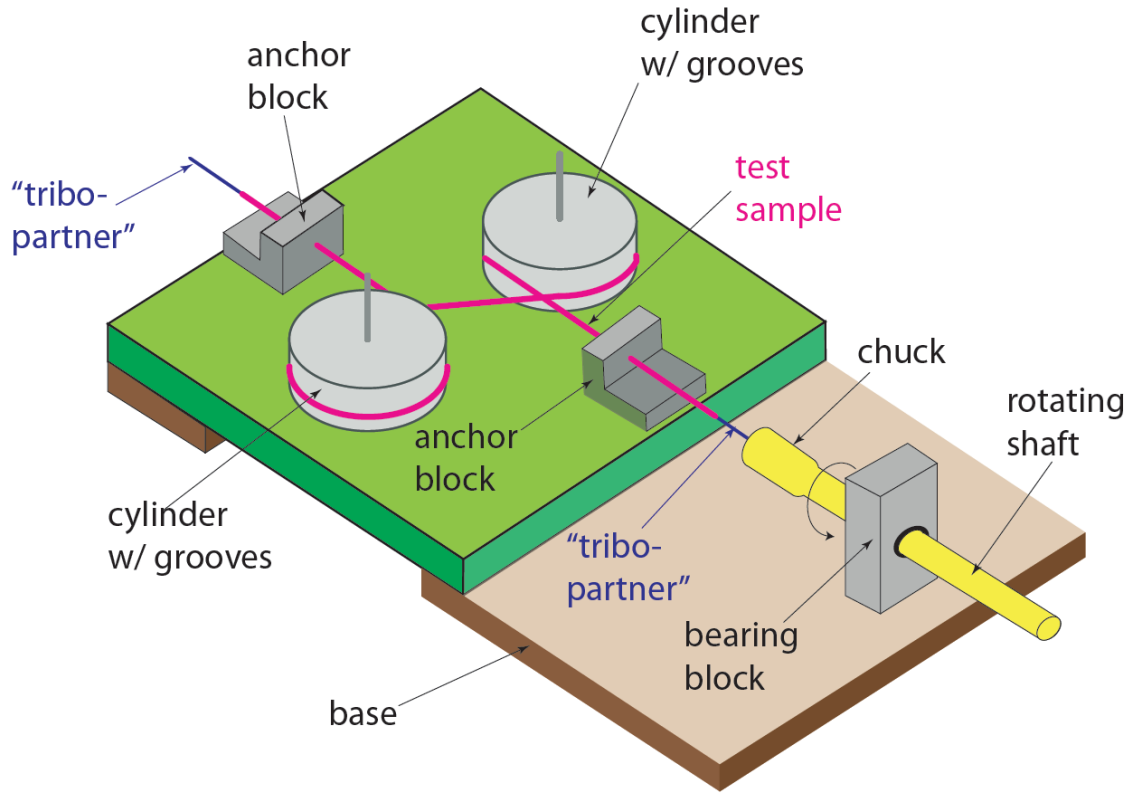

Figure 4.5: Macroscale torque tribology test layout for comparative inner diameter (ID) lubricity measurements [17]

Excerpts from the cited patent describe the torque test method as follows, " . . . shows a fixture for performing comparative torque tests on rotatable pin, screw-in type lead assemblies. The fixture includes a base having mounted adjacent one end thereof a low friction-bearing block. A shaft, rotatably carried by the bearing block, has an outer end portion and an inner end portion. . . . the outer end portion of the shaft . . . is . . . coupled to a device . . . for measuring the force required to rotate the shaft. The inner end portion of the shaft carries a clamp to which is secured one end of a conductor coil of a

selected length of test lead. The test lead, which includes outer insulative tubing, is held in place by anchoring blocks mounted on the base. The free end of the lead projects from the block. The portion of the lead between the blocks is wound around a pair of space apart cylinders mounted on the base so as to introduce resistance to the rotation of the conductor coil within the insulative tubing".

In a final example of an inner diameter (ID) lubricity test, Onishi *et al*. [15] describe an inner diameter surface test that uses a reciprocating inflatable catheter balloon. Their test setup is shown below in Figure 4.6.

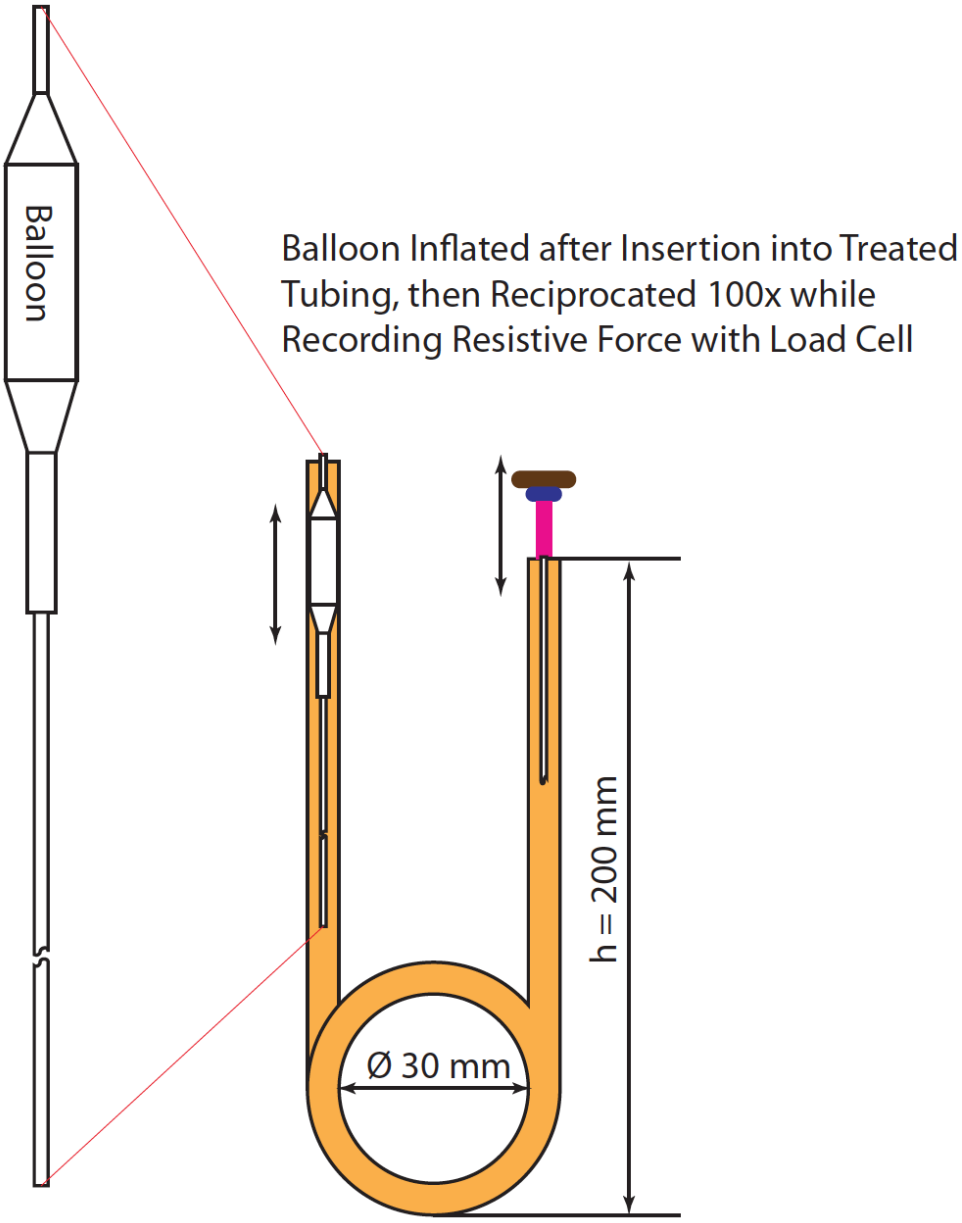

Figure 4.6: Reciprocating balloon test method for ID surface evaluation [15]

The cited patent describes the ID surface test method using the following excerpted passages, "The separately prepared balloon 5 was bonded to the tip of the shaft, thereby fabricating a catheter. Then, a pipe having an inside diameter of 3 mm and an outside diameter of 5 mm was wound in one turn (i.d. 30 mm) and a half and this loop portion of the pipe was filled with water to form a channel (h = 200 mm) that simulated a

blood vessel system in the living body. With the balloon folded back, [the] catheter was inserted into the channel and set up in such a way that the tip of the balloon was located at the terminal end of the loop. The end of the shaft was set in the load cell of an autograph (Model AGS-100A of Shimadzu Corp.), and the balloon was reciprocated 100 times over a stroke of 10 mm in the pipe. The value of resistance as measured right after the end of 100 strokes was taken as the final frictional resistance (gf)."

The patent further describes the test setup (note: the authors values and units are quoted verbatim) as using a load cell with a 5 kg_f capacity, a stroke length of 10 mm, a stroke speed of 100 mm min: and the stroke count set to 100 times. Apparently, the balloon was inflated to a pressure of 8kg/cm^2 after insertion into the "pipe". The patent also shows and describes a similar inner diameter surface test setup using a smaller pipe and same balloon system set up in the vertical plane with no coiling involved. Either method could be used to measure comparative lubricity and wear. The inner diameter (ID) lubricity test methods described have the advantages of being easy to set up and all use instruments to either rotate or withdraw the tribo-partners. The reciprocating balloon method has an advantage over the others in that the inflated balloon would necessarily contact the inner lumen walls in a 360° fashion. The full coil method and the torque test method afford the opportunity to use tribo-partners that may better represent end-use conditions for lead body assembly functional needs.

4.4 Nanoscale coating characterization

For nanoscale tribological assessments, the proposed research will use one or more of the following evaluation methods:

- SEM: Scanning Electron Microscopy for morphological comparative studies
- FTIR: Fourier Transform Infrared spectroscopy to look for different chemical species
- XPS: X-ray Photon Spectroscopy to look for different chemical species/bonding
- TOF-SIMS: Time of Flight - Secondary Ion Mass Spectroscopy for chemical species

evaluations

• PUPS: PUpil-Plane Scanning White-Light Interference (SWLI) microscopy for morphological/roughness comparative studies

4.5 Validation of coating characterization

The validation of the coating characterization will rest in the ability to predict whether or not the treated silicone tubing can be easily strung or is useable at downstream assembly and implant operations. If the evaluations have merit, then the output of the measurement systems will be able to distinguish between at least three degrees of processing "goodness" as follows:

- Tubing is not useable by assemblers and/or other downstream users
- Tubing can be used by assemblers and/or other downstream users only with great difficulty
- Tubing can be used by assemblers and/or other downstream users with no caveats

One way to gather meaningful information about the usability of the treated tubing in downstream assembly operations is to conduct surveys that map the characterization output to the qualitative opinions of the assemblers. A survey will need to be designed that does not bias the respondent and provides honest appraisals. Additionally, the inputs from implanting physicians can be valuable regarding the quality of the biomedical conduits.

Of course, gauge repeatability and reproducibility (GR&R) studies would show low gauge error relative to currently employed measurement methods to validate any improvements gained. Additionally, it is necessary that the data generated show correspondence to the required functionality at every subsequent step along the component's life cycle. This is especially important for the ease of stringability at

downstream assembly operations, but can be important during device implantation, too.

Chapter 2

METHODS OF CHARACTERIZING LUBRICTY OF BIOMEDICAL CONDUITS

1 Introduction

A critical requirement for the silicone tubing used in biomedical devices is that it has to have lubricious surfaces. Lubricious surfaces are required in order to assemble lead bodies, to prevent conductive coils from binding or seizing inside of insulative tubing, and to facilitate placement during the implant procedure,

Plasma-treated monolumen silicone tubing is utilized as inner insulation for the electrical conductors. The location of the inner insulator inside of a lead body is shown in cross-sectional view of a lead body in Figure 1.1 (here, the white areas indicate the spacing distance between the elements of the lead body).

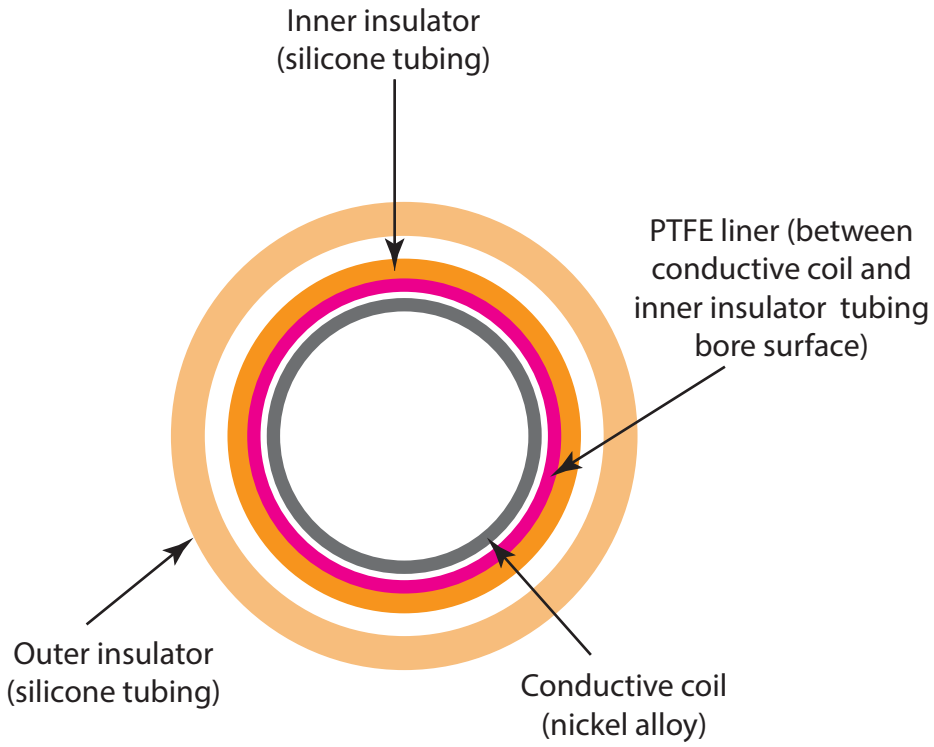

Figure 1.1: Cross-sectional view of a lead body showing inner insulator location

Additionally, the outer layer in various medical device lead-body assemblies incorporates plasma-treated silicone tubing. As an example application for plasma-treated silicone tubing, a representative lead-body assembly will be used. This example is known as a "screw-in lead model" and is shown in composite fashion as Figure 1.2.

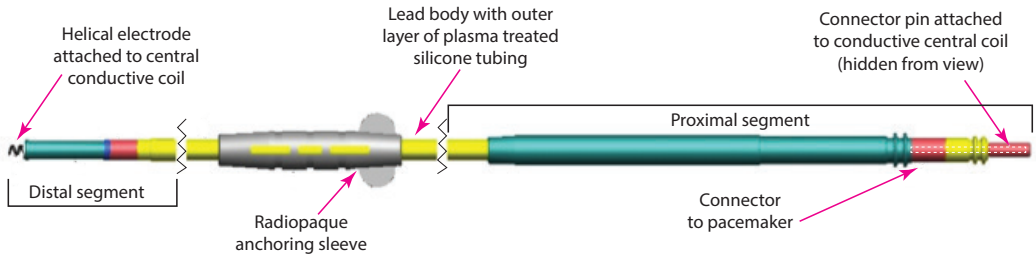

Figure 1.2: An example screw-in lead body assembly

Figure 1.2 shows what is known as a helical electrode that resembles a corkscrew. This helical electrode is an electrically active titanium-nitride-coated component. The

electrode is made out of a platinum alloy and is attached to the myocardial heart tissue by the implanting physician. The physician grips the proximally located connector pin that is attached to a central conducting coil that, in turn, is attached to the helical electrode and then rotates the helical electrode into the heart tissue, [This suggests that the proximal end is connected to the heart.]

A longitudinal-sectional view of the distal segment in Figure 1.3 shows the locations of both the inner insulating silicone tubing and the outer layer of silicone tubing within the lead-body assembly.

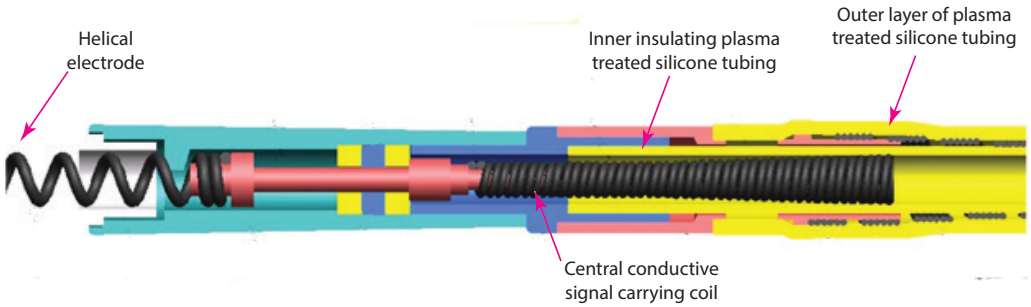

Figure 1.3: A longitudinal-section of the distal segment showing silicone tubing locations

The distal segment of the lead-body assembly is the portion of the assembly that is situated inside the heart. In this part of the assembly, there is intimate contact between the central conductive coil and the inner insulating plasma-treated silicone tubing bore. These contacting surfaces benefit from low friction during implantation and during the life of the assembly. During implantation, the fixation of the helical coil is facilitated due to better torque transfer when there is less friction between the rotating coil and the tubing bore surface. Furthermore, the ability to stress relieve interactions between the central conductive coil and the inner insulating tubing-bore surface during normal movements of that area, e.g., heart beating, is improved with lower friction contacts.

The longitudinal-sectional view of the proximal segment (Figure 1.4) further illustrates and reinforces the location of the tubing layers.

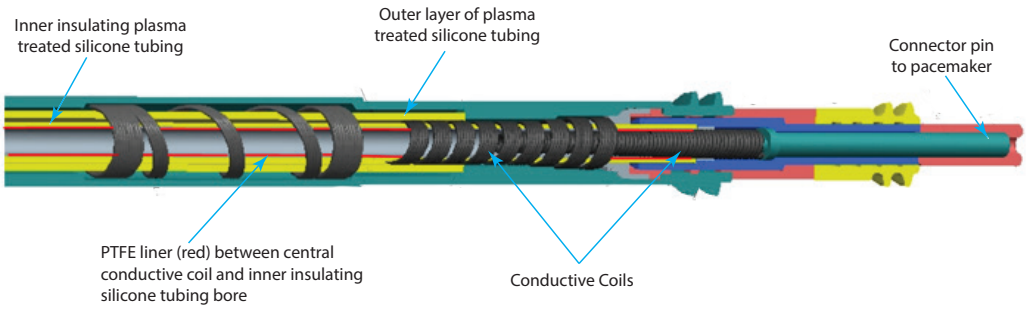

Figure 1.4: A longitudinal-section of the proximal segment showing silicone tubing locations

Figure 1.4 shows a PTFE liner that serves as a lubricious interface between the central conductive coil and the tubing bore surface of the inner insulating plasma-treated tubing. This liner is not present in the distal segment of the lead-body assembly because its presence would increase the electrode tip pressure and also increase the likelihood of the electrode perforating the heart tissue.

Note that the inner insulating silicone tubing is plasma treated to render both the tubing bore and the tubing exterior surfaces lubricious. On the other hand, the outer layer of silicone tubing is plasma-treated to exclusively make the tubing exterior surface lubricious, The inner insulating tubing is treated on the tubing bore surface to facilitate the stringing of the signal-carrying conduits during lead body assembly, to make for more efficient torque transfer during implantation, and to increase the reliability of the final lead body. The outer layer of silicone tubing is treated on its exterior surface as a means to facilitate placement during the implantation operation. A more global illustration of a typical pacemaker with its lead-body assembly is shown in Figure 1.5.

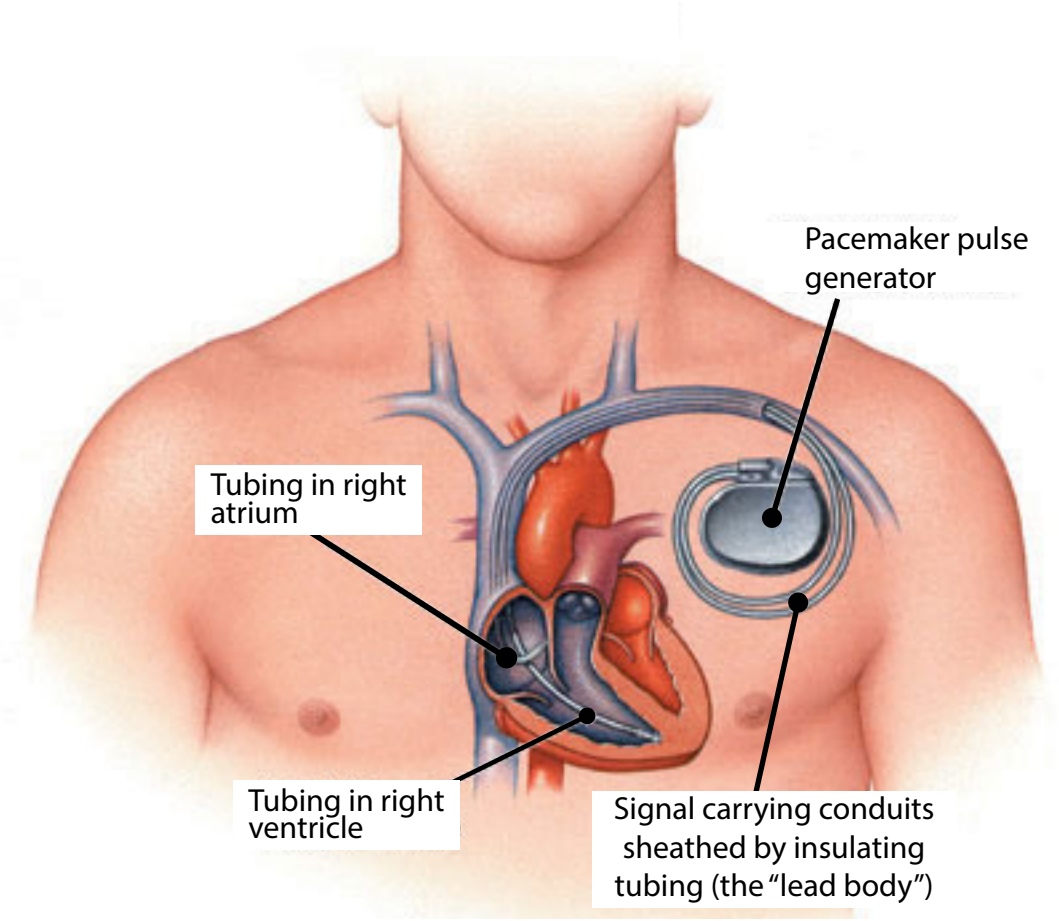

Figure 1.5: A pacemaker pulse generator and its signal-carrying lead body

2 An historical method to assess biomedical conduit lubricity

In practice, very long lengths (up to 2500 feet) of the inner insulating tubing are plasma treated in a batch-mode fashion to reduce friction. After plasma treatment, batch representative destructive-sample testing is performed to determine if the tubing bore and the tubing exterior have been treated well enough to meet the design requirements.

The tubing bore lubricity test method was historically implemented by pulling the electrical conductor (a coil in this case) through a fixtured stationary plasma-treated tubing test sample in a "U-bend" fixture with a ½-inch radius of curvature while

registering and recording the resistance force. The apparatus for this test is shown in Figure 2.1.

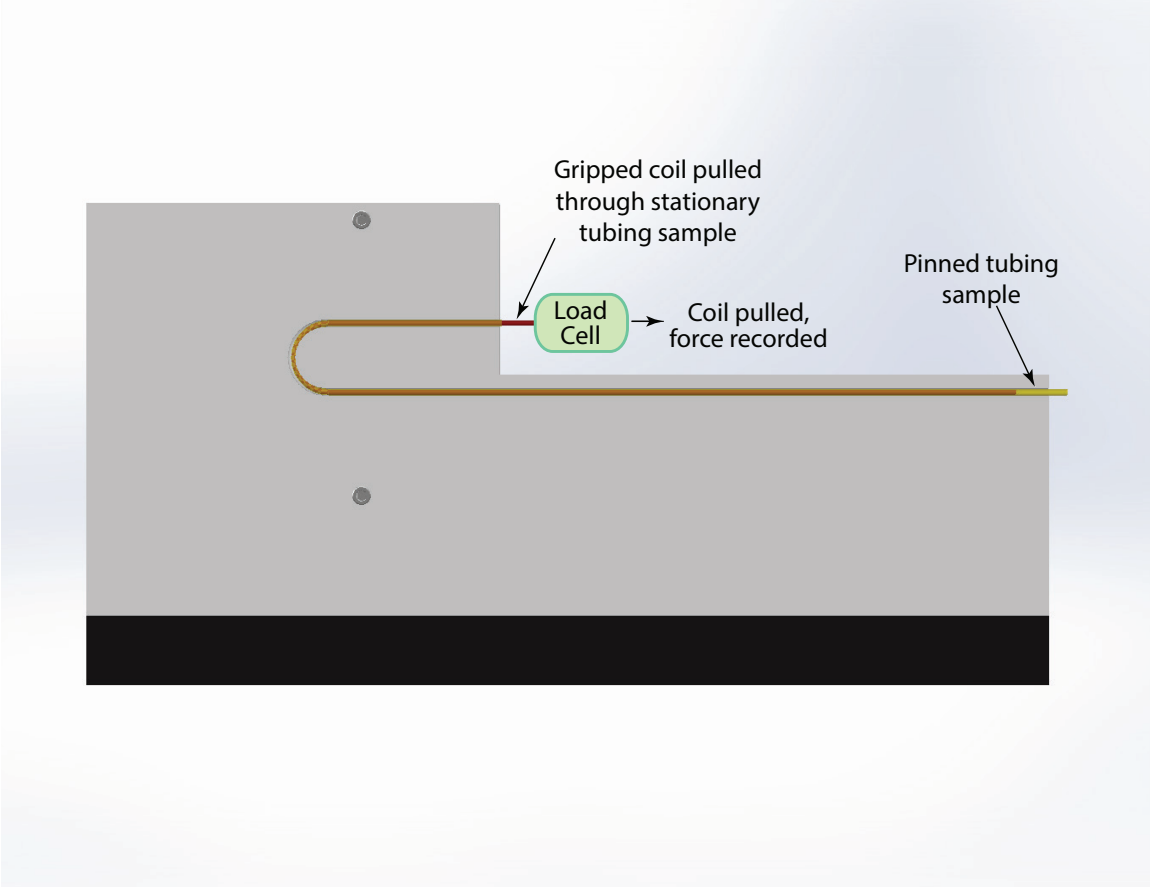

Figure 2.1: Top view of a U-bend test fixture

Figure 2.1 shows the location where the tubing sample is pinned and held stationary during the test. Also depicted is the site where the coil is gripped by a clamp (not shown) that is connected to a load cell. After the coil gripped, the test cycle is started which consists of pulling the coil for a programmed distance at a set speed. During the pull, the force is registered and recorded after a few seconds of what is known as "pre-w". The pre-peel is programmed into the test recipe to discount or ignore the force needed to overcome static friction. The final test result is the average pull force. The test is based on the fact that the lower the force required to pull the coil, the more lubricious the tubing bore is. A perspective view of the U-bend test fixture is shown in Figure 2.2.

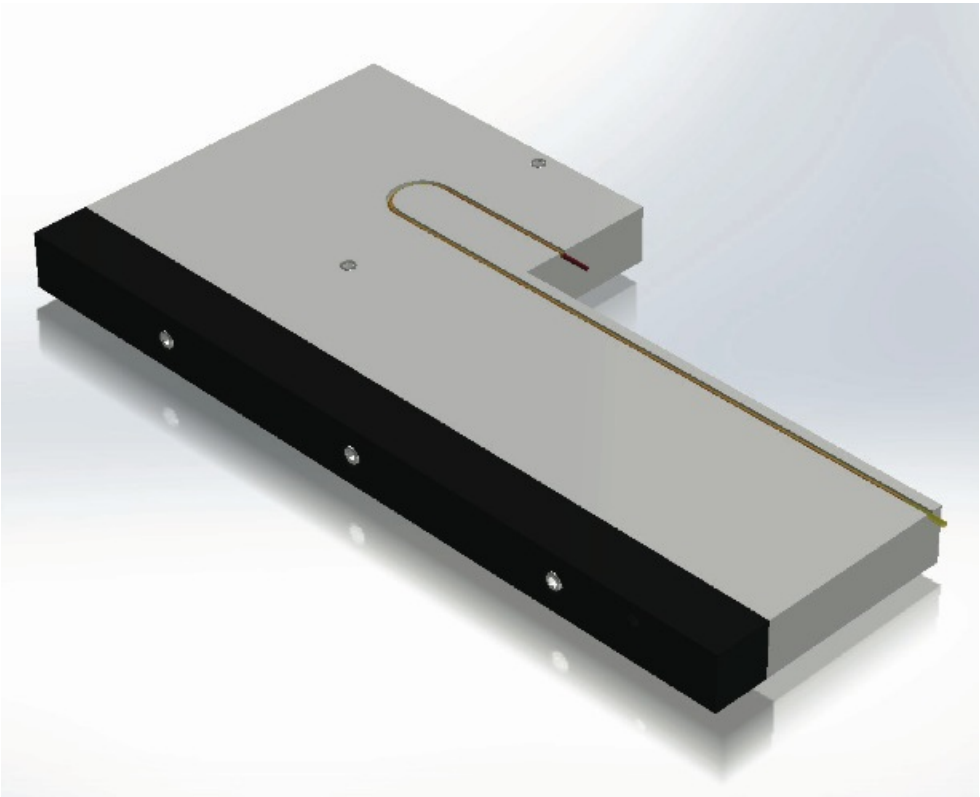

Figure 2.2: Perspective view of a U-bend test fixture

This apparatus is a traditional instrument and is heavily dependent on the skills of an operator. Those skills are, in principle, certified but the certification process is loose. The equipment may either be purchased commercially or manufactured in-house. The manufacturing process is implemented by the use of a rotating ball end mill that translates in the groove direction. The surface finish of the groove is not a prescribed quantity. The medium that is being characterized consists of a stationary plasma-treated silicone tubing sample with a moving nickel alloy coil in relative motion to the tubing sample. An example illustration of the nickel alloy-coil used in the U-bend test method is shown in Figure 2.3.

Figure 2.3: Coil construction of the moving element used in the U-bend test method

The mode of operation is specified as the speed by which the coil travels and the time of travel. The result is an averaged force. No attempt has been made to extract the coefficient of friction (COF) since the actual normal forces between the coil and the tubing are not well understood. The instrument uses a Thwing-Albert friction peel tester [West Berlin, New Jersey] that can be commercially acquired. The instrument is set up in a tensile tester mode such that the linear resistance force is recorded while the coil is being withdrawn from the tubing sample.

The historical test method shows poor gauge reproducibility and repeatability. A gauge study typically involves the use of multiple parts involving multiple operators with random replications of the test (with regard to both the operator and sample). A gauge study was performed employing three certified test operators on the U-bend test method and is summarized in Figure 2.4.

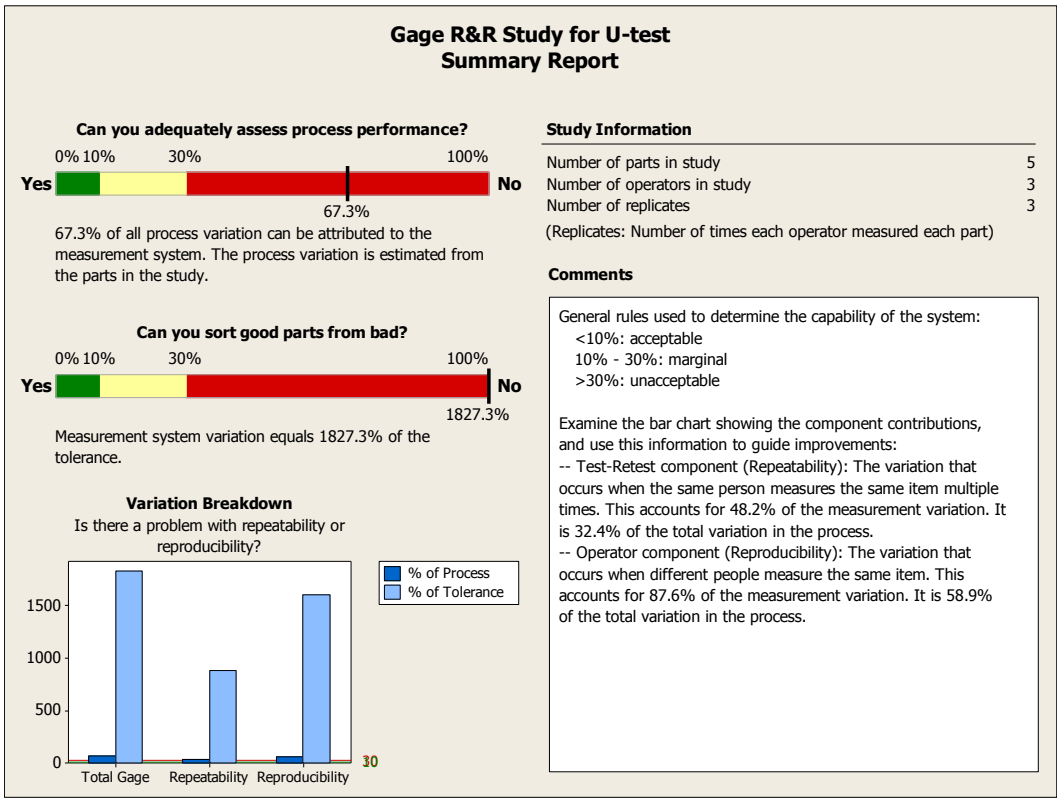

Figure 2.4: Summarized output from a U-bend test gauge study

The summarized gauge study for the U-bend test method indicates that 32.4% of the total variation in the process lies with non-repeatability and that 58.9% of the total variation in the process lies with non-reproducibility, The gauge study shows that this test measurement method cannot distinguish good product from bad product. In other words, the gauge is poor for this test method.

This historical test method does not mimic the use condition for the screw-in lead models for the implantation procedure. The implant use condition is better tested using a method that registers and records the resistance or torque that a rotating coil generates inside stationary plasma-treated tubing samples. This "torque test" method is developed here and will now be described.

3 Straight groove torque methodology

The apparatus for torque testing uses a torque transducer that is mechanically coupled to a gripper as shown in Figure 3.1.

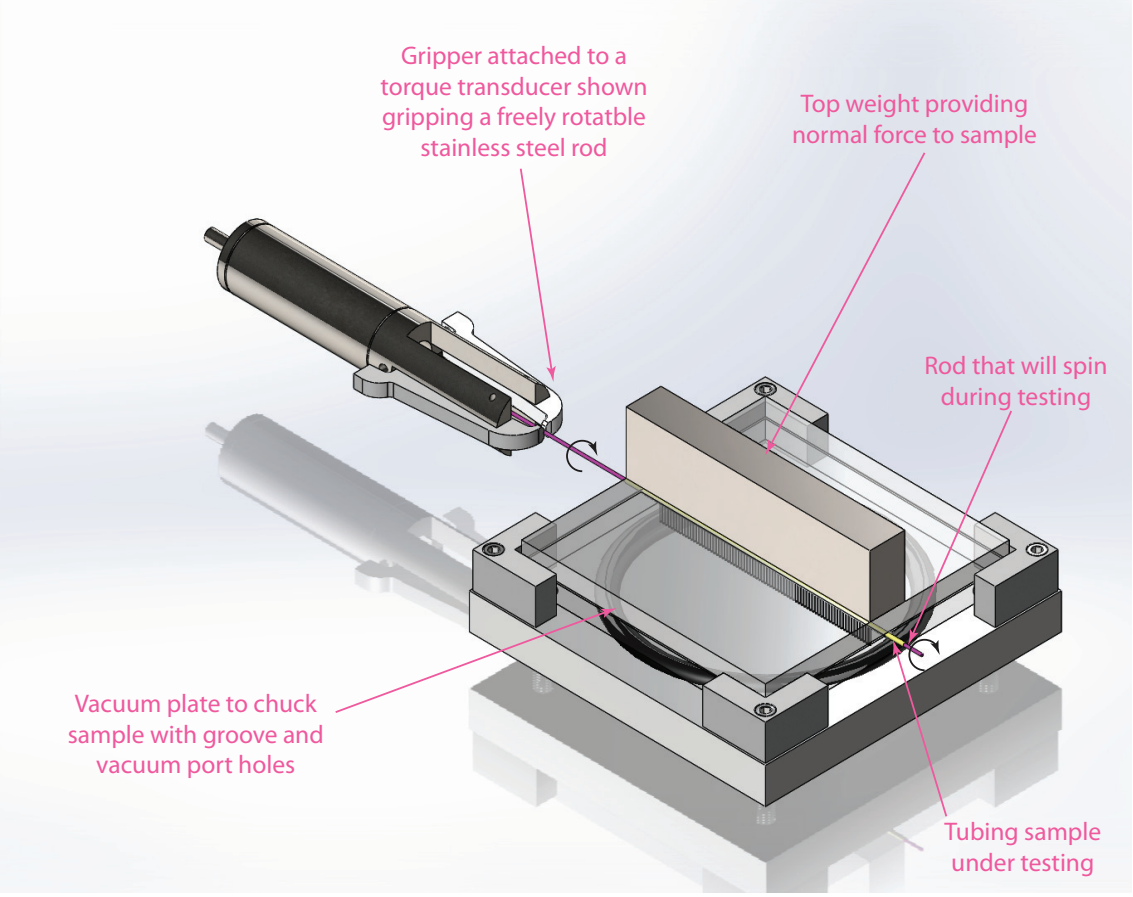

Figure 3.1: Top view of the torque test fixture

The torque measurement is motivated by the desire to better mimic the actual use condition wherein an implanting physician torques the helical electrode into the heart muscle. This instrument was specifically developed for this research is not heavily dependent on the skills of an operator. Nevertheless, the skills are certified, and the certification process is more stringent than that for the traditional U-bend test method. The equipment is custom and cannot be purchased off-the-shelf.

The medium that is being characterized consists of a stationary plasma-treated silicone tubing sample with a rotating stainless steel rod in relative motion to the tubing sample. The mode of operation is specified by the rotational speed by which the rod is turned and the number of revolutions. The result is an averaged torque value.

The specific critical parts of the torque-characterizing device are shown in Figure 3.2 and will now be described.

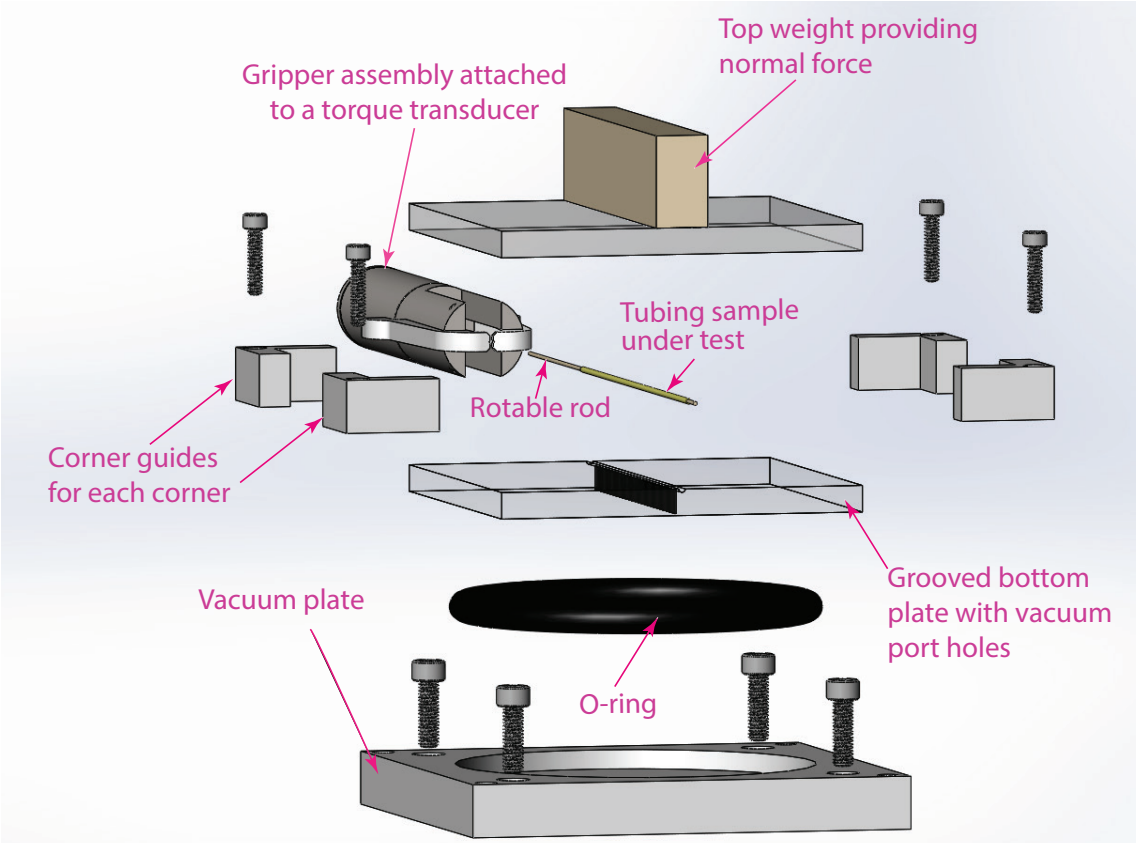

Figure 3.2: Exploded view of the torque characterization device

The vacuum plate is securely fixed to table that is in front of the grippers, and it is aligned to the axis of rotation. The plate has a cylindrical chamber that is under vacuum during the test. The vacuum serves to fixate the tubing sample/rod test assembly that is

placed in the grooved bottom plate. There are corner guides on each of the four corners of the fixture. These guides aid the device in placing the weighted top plate (that provides for a known normal force) in the sample position for every test. The grippers serve to clamp down on the rotatable rod and are physically coupled to the torque transducer. During the test, the grippers are used to securely grip the rod and rotate for a set amount of rotations.

The torque characterization method shows much improved gauge reproducibility and repeatability relative to the traditional U-bend test method. A gauge study was performed employing three trained test operators for the torque test method and is summarized in the Figure 3.3.

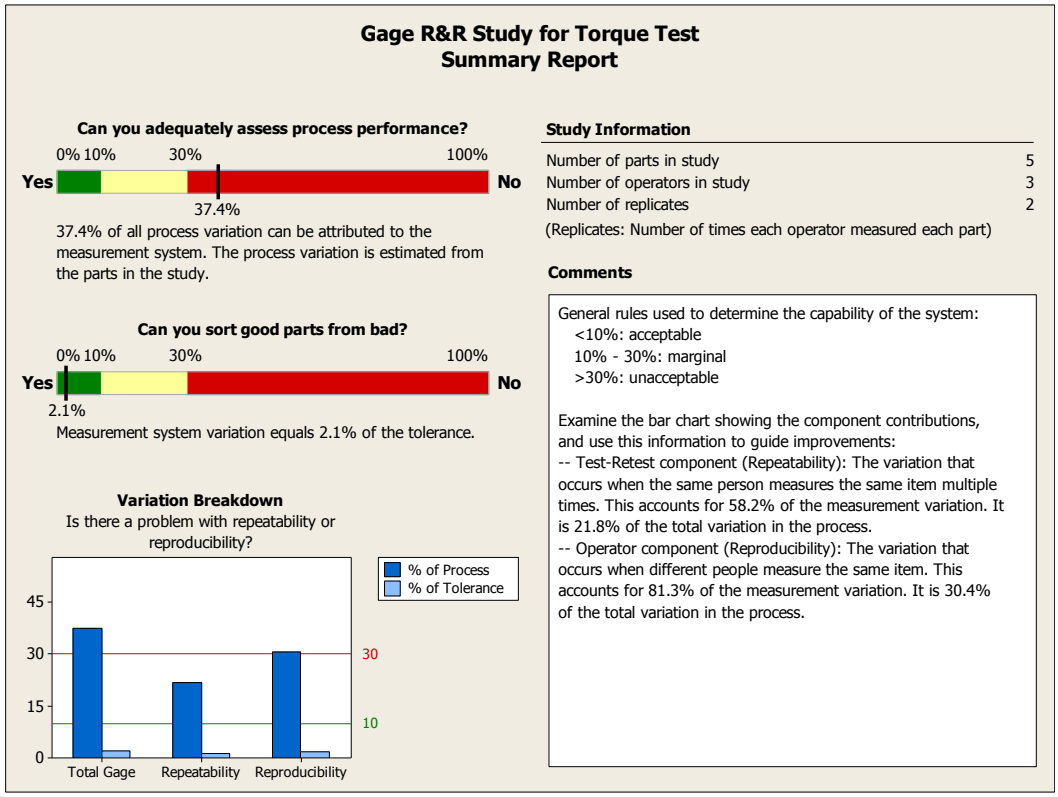

Figure 3.3: Summarized output from a torque test gauge study

The summarized gauge study for the torque test method indicates that 21.8% of the total variation in the process is due to non-repeatability and that 30.4% of the total variation in

the process lies with non-reproducibility, The study also shows that this measurement method has good capability with regard to distinguishing good parts from bad parts.

This assembly can rotate either clockwise or counterclockwise from the viewpoint of the user. As configured, the maximum speed of rotation is 60 RPM since the implanting physician is instructed to keep the rotational speed low during the turning of the coil/helical electrode into the heart muscle. The measurement procedure is to insert a reusable 0.0380 ± 0.000 inch diameter stainless steel wire with a length of 6.00 ± 0.2 inches into a 4.00 ± 0.13 inch plasma-treated tubing sample to form a test assembly. This test assembly is placed in a straight-grooved fixture and then vacuum chucked to fixate the tubing. The wire is then gripped by the jaws on the apparatus and rotated while the friction between it and the tubing sample results in a torque being exerted on the sample while the sample exerts an equal and opposite counter-torque on the wire. The torque is detected by the torque transducer and read out by the test system or torque tester with units of inch-ounces.

The rod is used as long is its straightness is verified. There are two simple methods of verifying the rods straightness. The first method is by rolling the rod on a flat surface and looking for the smoothness of the rolling motion. The second method is to determine if the rod can easily pass through a precision bore pipe. This method is to pass the friction element through a precision bore pipe that is sized just 0.0005” greater in diameter than the diameter of the rod. Figure 3.4 shows a photographic example of this straightness verification method.

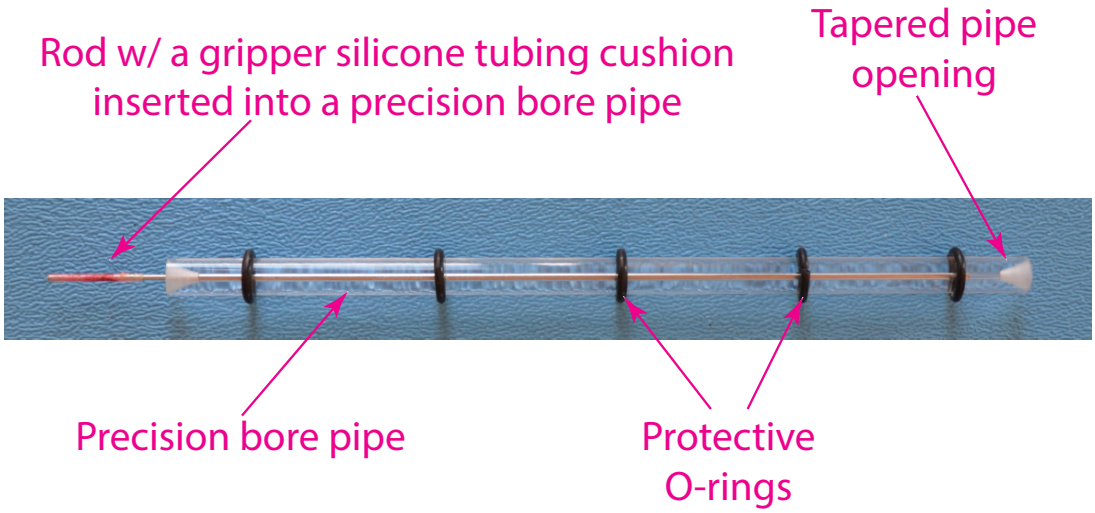

Figure 3.4: A customized method to verify the straightness of the rotatable friction element

The numerous reuses of the rod are based on no discernable changes to the torque test output from tubing treated at conditions known to improve lubricity. Note that prior to the main experiments, the rod has its surface pre-conditioned during what are termed running-in cycles. The running-in behavior of friction is examined in an article by [21]. The running-in of the rod is performed to condition the rod surface with the naturally occurring lubrication that occurs when the silicone-plasma tubing exudes silicone oils that transfer to the rod surface. During running-in cycling, it is empirically observed that the torque values stabilize. Usually, the pattern is seen as decreasing to a stable plateau. More details on running-in behavior and its possible mechanism are given in Chapter 5.

The units of torque reflect the definition of torque as being a cross product of a force vector and a lever-arm vector. The lever arm is defined as the distance between the axis of rotation and the point of application of the force. Since a cross product is taken, the only component of the force vector that contributes to the torque is orthogonal to the lever-arm vector. For this case of a rotating cylinder, the lever arm is simply the radius R of that cylinder's cross-section. The torque T exerted by a force F perpendicular to the lever arm R is described by the formula:

$$T = F \times R \tag{1}$$

4 Mechanics of sliding friction

When two contacting dry surfaces are in relative motion to each other, a friction force F opposes the motion. For a wide range of materials, it has been noted that friction is proportional to the normal force N pressing those two surfaces together. The constant of proportionality is dimensionless and is referred to as the coefficient of kinetic friction, μ_k. The relationship between the normal force N, the friction force F, and the constant of proportionality μ_k is shown in Eq. (2):

$$F = \mu_k N \tag{2}$$

The coefficient of kinetic friction can depend on the chemical composition of the two contacting surfaces, the surface finish or morphology, the temperature, the presence of lubricants or contaminants, as well as several other factors influencing the system. Even given these dependencies, typical ranges for coefficients of kinetic friction for various systems and material combinations can be found in the literature. When evaluating a new system, the typical course of action is to measure the friction force over a wide range of normal forces, sliding velocities, and running-in times in order to establish the linearity of the relationship between the normal force N and the tangential force F, This information is used to identify factors that might limit the accuracy or the applicability of Eq. (2).

5 Force models for friction torque

Two general approaches to generate a friction torque have been investigated in this work. The first approach is to place the cylindrical element between two precisely parallel plates as shown in Figure 5.1.

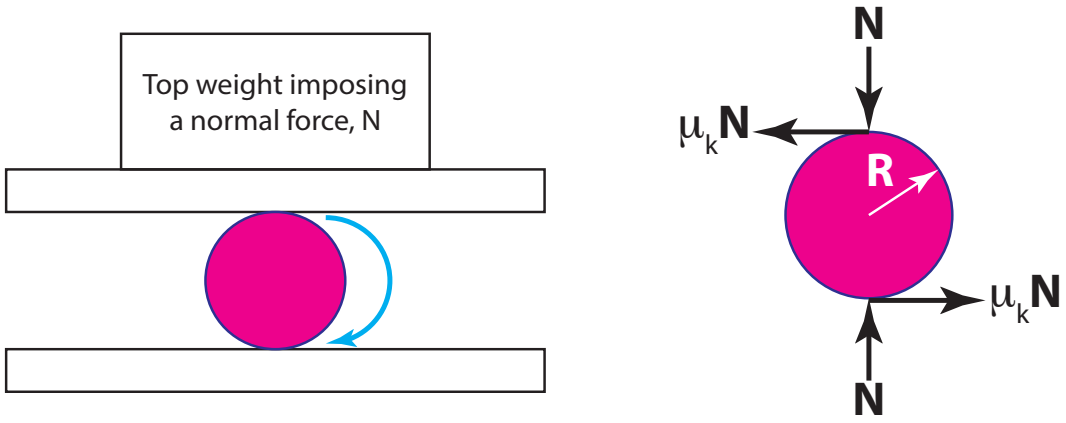

Figure 5.1: Experimental setup showing a cylinder between parallel plates, weight, and the corresponding force diagram

The force model, displayed in Figure 5.1, shows a top weight, which imparts a normal force through the upper plate onto a cylinder that will be rotated. There is an equal and opposite reaction force exerted by the cylinder onto the top plate. Static equilibrium is maintained by the cylinder exerting a normal force on the lower plate, with an equal and opposite reaction force imposed by the lower plate onto the cylinder. The normal forces result in friction torques, and rather than canceling each other, these torques sum together as illustrated by the force diagram in Figure 5.1. As a result, the friction torque T can be expressed as:

$$T = RF = 2R\mu_k N \tag{3}$$

Equation (3) is validated by experimental data in a later section.

An alternative approach to generate friction torque is to bend an elastic cylinder or coil around a stationary semicircular path or track, as depicted in Figure 5.2.

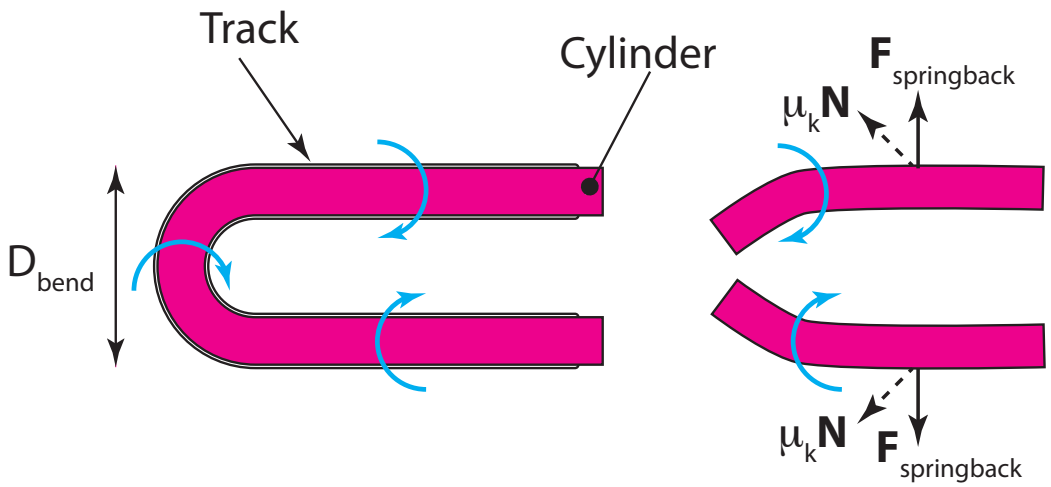

Figure 5.2: Elastic cylinder (coil) imparting a normal force on a track, and a force diagram

The elastic cylinder (here, the elastic cylinder is a nickel alloy coil) imparts a springback force on the track at the beginning and end of the curve. An image of a coil similar to the one used for this study was displayed as Chapter 3, Figure 2.3.

This springback force will, in general, be a function of the bending diameter D_{BEND}. The springback force is responsible for generating a normal force N, as shown in Figure 5.2. The friction torque T experienced as the elastic cylinder is rotated is then expressed by

$$T = RF = 2R\mu_k F_{springback} \tag{4}$$

For this system, the vectors designated as $\mu_k N$ are directed down below the plane of the page. Work to validate Equation (4) is documented in a later section.

6 Torque test methodology

6.1 Calibration

The torque measurement device used for the development of a tubing bore lubricity torque test system is an Interface, Inc. [Scottsdale, Arizona] T11 torque transducer with a range of ±0.005 N-m, a stated combined error of ±0.1% of full scale, and non-repeatability of ±0.02%, The output signal of the transducer is a voltage with a range of ±10 V (positive signals correspond to torques on the transducer which are clockwise from the perspective of the operator). For the majority of the data documented in this report (collected using clockwise motion), the friction torques transmitted by the cylindrical element to the transducer is counterclockwise, resulting in negative torque readings. These readings have generally been reported as absolute values in order to simplify the presentation of data.

By means of a herein-invented deadweight lifting apparatus, shown in Figure 6.1, the accuracy of the calibration of the torque transducer was evaluated.

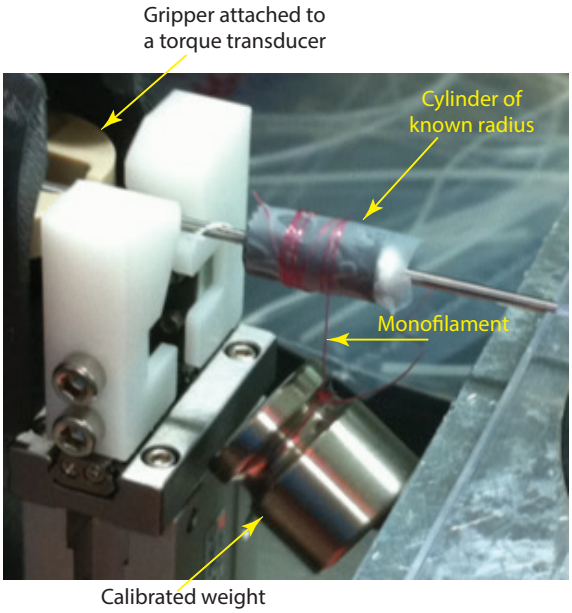

Figure 6.1: Herein created deadweight lifting apparatus used to calibrate the torque transducer

For the calibration procedure, weights of 2, 5, and 10 grams-force were attached to a monofilament fish line and wound around a 0.257-inch diameter shaft programmed to rotate in either the clockwise or counterclockwise directions. The torque indicated by the torque transducer was read from the human-machine interface (HMI) screen of the torque test system and converted to inch-ounces. For each weight and each programmed direction, five independent measurements were recorded. Results are shown in Figure 6.2.

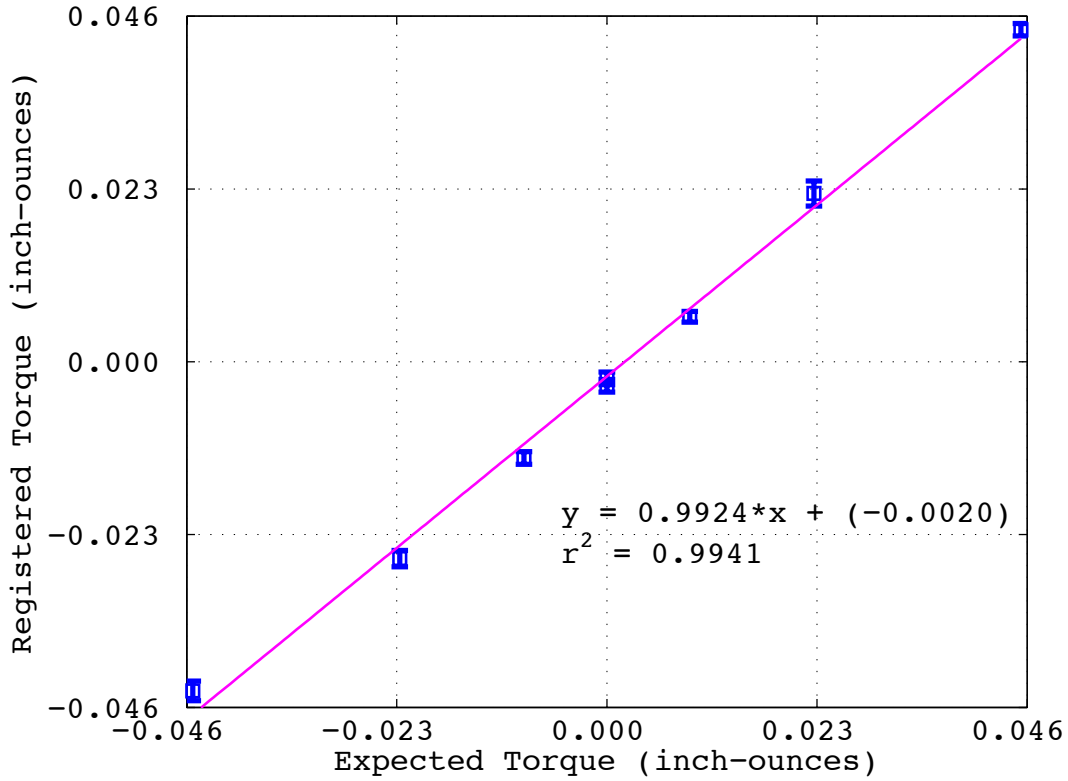

Figure 6.2: Expected versus registered torque

The torque transducer exhibited good repeatability and linearity over the range of torques employed as shown in Figure 6.2. The linear regression generated the following equation

Registered Torque = 0.9924(Expected Torque) - 0.002*

as the line of best fit with a correlation coefficient of 0.9924. This excellent agreement provides mutual support to the underlying theory and to the experimental technique. The slope of the line of best fit was 0.9924, indicating that approximately 1% less torque was measured than expected based on the weight and lever-arm distance used. This slight discrepancy may be due to friction between the non-gripped end of rotating shaft and the supporting groove on the right-hand side of the apparatus seen in Figure 6.1.

An offset of -0.002 inch-ounces was also indicated by the linear regression. Based on these results, the offset was programmed into the Human Machine Interface (HMI) of the torque tester in order to achieve a true zero reading. All data presented in subsequent sections of this report have had the offset correction applied. In addition, a torque of approximately -0.009 inch-ounces is typically observed when the transducer rotates freely in the clockwise direction (without an attached load). This value is also generally subtracted from the acquired torque to give the net torque due to friction between the test sample and rotating rod only.

6.2 Validation of the Force Models

The force model for a rotating cylinder confined between two plates presented in Section 2.3 implies that both the normal force pressing down on the cylinder from above and the reaction force pushing up on the cylinder from below both contribute to friction. This means that there is a factor of two in the torque equation given by Eq. (3), $T = RF = 2R\mu_k N$. To validate the torque force model, the torque required to rotate a 0.036-inch diameter SS304 rod trapped between two SS304 stainless steel plates was measured using 100, 200, and 300 grams-force of top weight. The custom apparatus used to gather these data is shown as Figure 6.3.

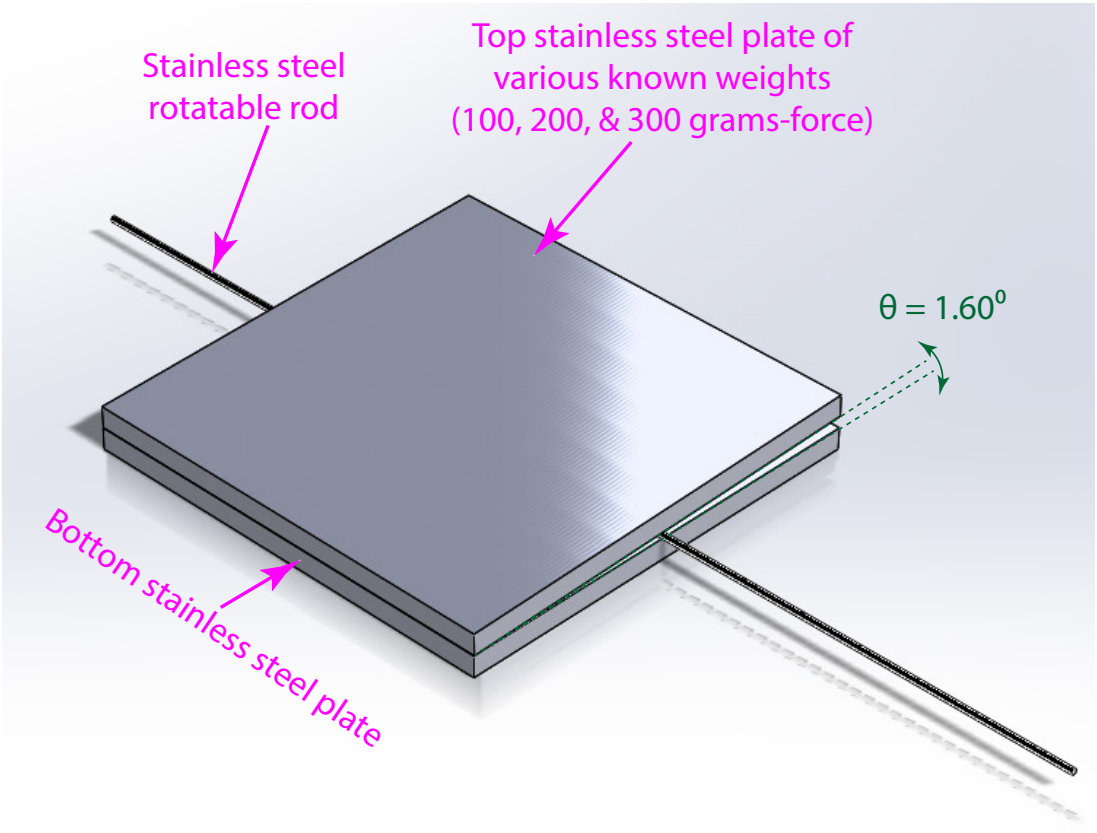

Figure 6.3: Apparatus to measure steel-on-steel torque (stainless steel rod sandwiched between stainless steel plates)

Note that the upper plate was tilted slightly to contact the lower plate on one edge; however, the resolved normal force is so close to the actual weight due to the almost zero angle of tilt that no correction was deemed necessary. One of the free ends of the rotatable rods was clamped to the gripper that is attached to the torque transducer and three test cycles were executed for each setting of top weight. Here, a test cycle is defined as seven revolutions of the rod. A linear regression of the averaged outcome of the three cycles of the torque testing is shown in Figure 6.4.

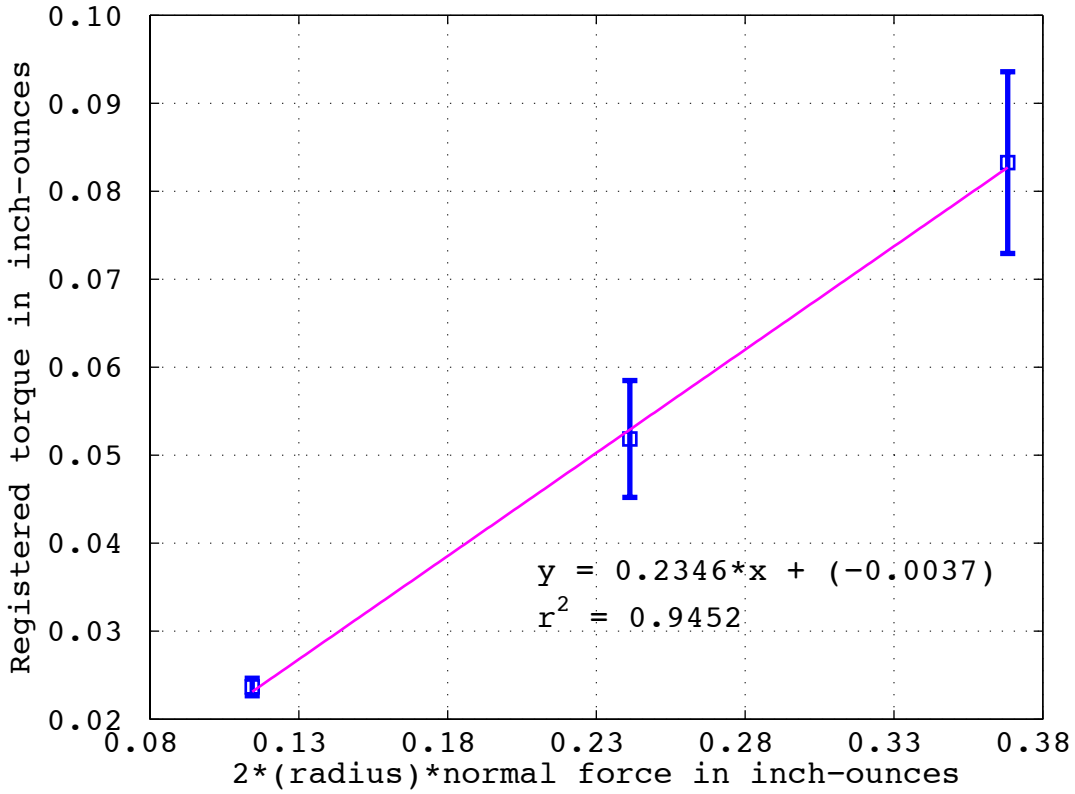

*Figure 6.4: Linear regression fit of torque vs. 2*R*N for steel-on-steel system with error bars*

Note that the slope of the regression fit shown in Figure 6.4 is 0.23 corresponding to the derivative of Eq. (3), $T = RF = 2R\mu_k N$. In other words, $\frac{d(RF)}{d(2RN)} = \mu_k = 0.23$ indicating a steel-on-steel coefficient of friction equal to 0.23 ± 0.05 (the 95% confidence interval of the slope ranges from 0.184 to 0.285).

The doubling of the torque output for a rotating rod trapped by two plates is somewhat counterintuitive. Because of this, an alternative friction test method was performed to validate the torque force friction model. This was accomplished by comparing the friction measured by the torque system to the friction measured by a simpler and more time-honored test method, the sled test, In a sled test, a stainless steel sled is dragged over the sample surface while a load cell measures the tangential force

required to pull the sled. The test described is fundamentally based on methods commonly employed to measure both static and kinetic coefficients of friction between either identical or dissimilar materials, (see for example, ASTM D1894). The sled test apparatus (the fixturing is custom and not off-the-shelf) is shown in Figure 6.5.

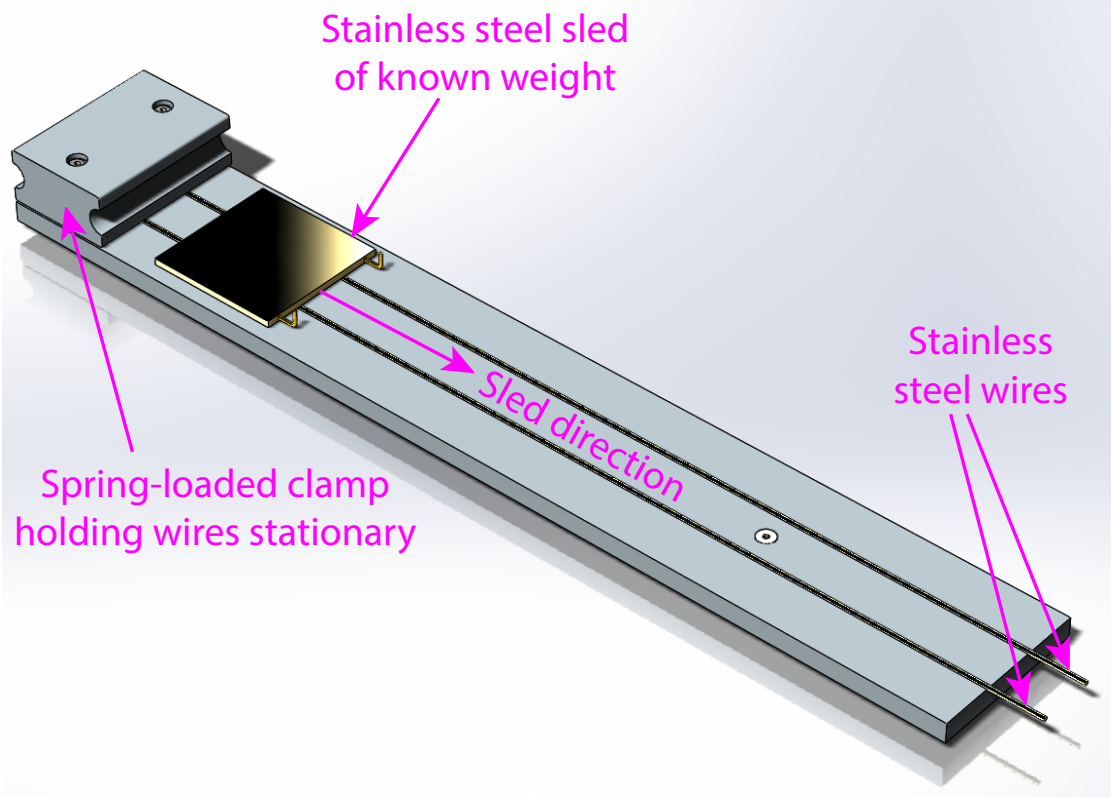

Figure 6.5: A custom sled test apparatus

As depicted, a stainless steel sled of known weight is pulled along on top of stainless steel wires. The stainless steel wires are in parallel grooves and are held stationary using a spring-loaded clamp. The sled is tethered to a load cell (or force transducer) that records the force required to pull the sled for a set amount of time. The data generated do not include the first few seconds of time so as to discard the force required to overcome the static friction.

The normal force for the sled test is simply the weight of the sled pressing down on the sample. This simple linear force system is described by the equation

$$F_{\tan} = \mu_k W_{sled} \tag{5}$$

A linear regression of the averaged outcome of the three cycles of the sled testing is shown in Figure 6.6. Here, F_{tan} is on the y-axis and W_{sled} is on the x-axis.

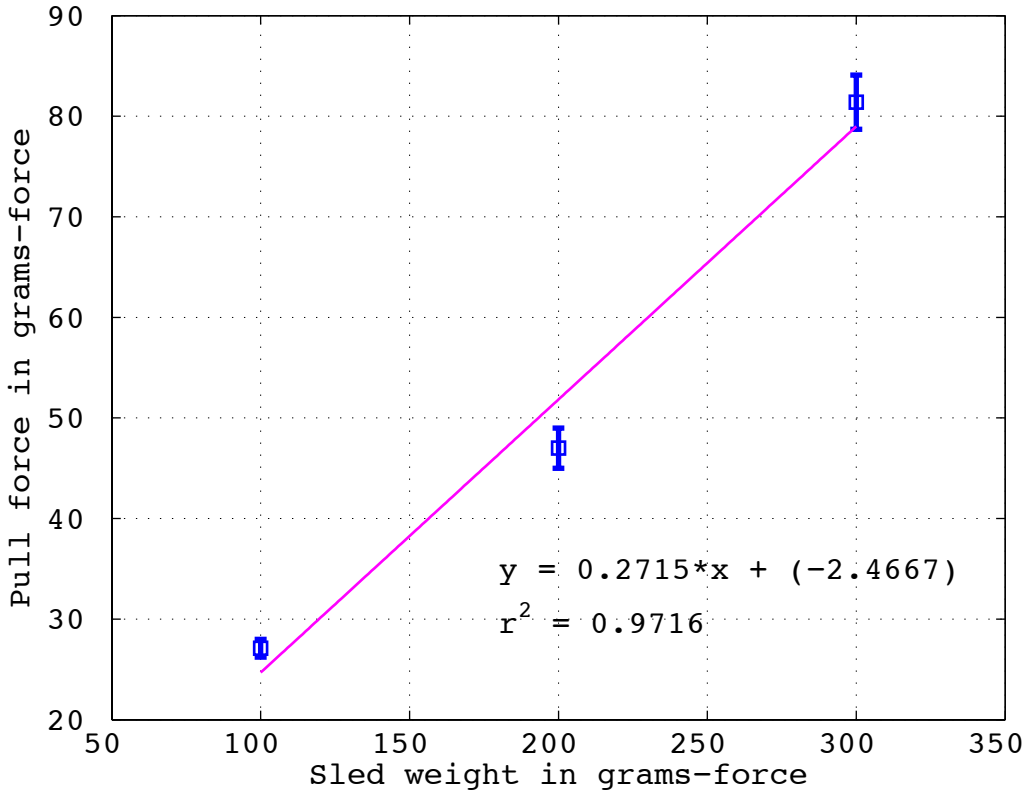

Figure 6.6: Linear regression fit of F_{tan} as a function of F_{normal} for steel-on-steel system with error bars

Note that the slope of the regression fit shown in Figure 6.6 is 0.27 that corresponds to the derivative of Eq. (2), $F = \mu_k N$. In other words, this study indicates a steel-on-steel coefficient of friction equal to 0.27 ± 0.04 (the 95% confidence interval of the slope ranges from 0.230 to 0.313).

It is relevant to compare the extracted coefficients of friction extractions deduced from the data of Figures 6.4 and 6.6 (COFs of 0.23 and 0.27 respectively). These independent coefficient of friction extractions for a steel-on-steel system for each of the two experimental setups differ by only 0.04. This difference is not statistically valid as the 95% confidence intervals do overlap. This work validates the force model as presented by Eq. (3).

6.3 Characterization sample preparation

As a means to create tubing with a wide variety of tubing bore surface lubricities, engineering runs were performed using a reactor that uses hexamethyldisiloxane (HMDSO) and argon plasma, During these research runs, a series of step changes in normalized and dimensionless transport rate, pressure, and pulsed RF power were employed as shown in Table 6.1 and Figure 6.7.

Table 6.1: Normalized input conditions employed to create a range of tubing bore lubricities

Treatment	Normalized Speed	Normalized Pressure	Normalized Power
1	1.25	0.10	0.34
2	1.25	0.10	0.49
3	1.25	0.50	0.49
4	1.25	0.50	0.65
5	1.25	1.25	0.65
6	1.25	1.25	1.00
7	1.00	1.25	1.00
8	0.75	1.25	1.23

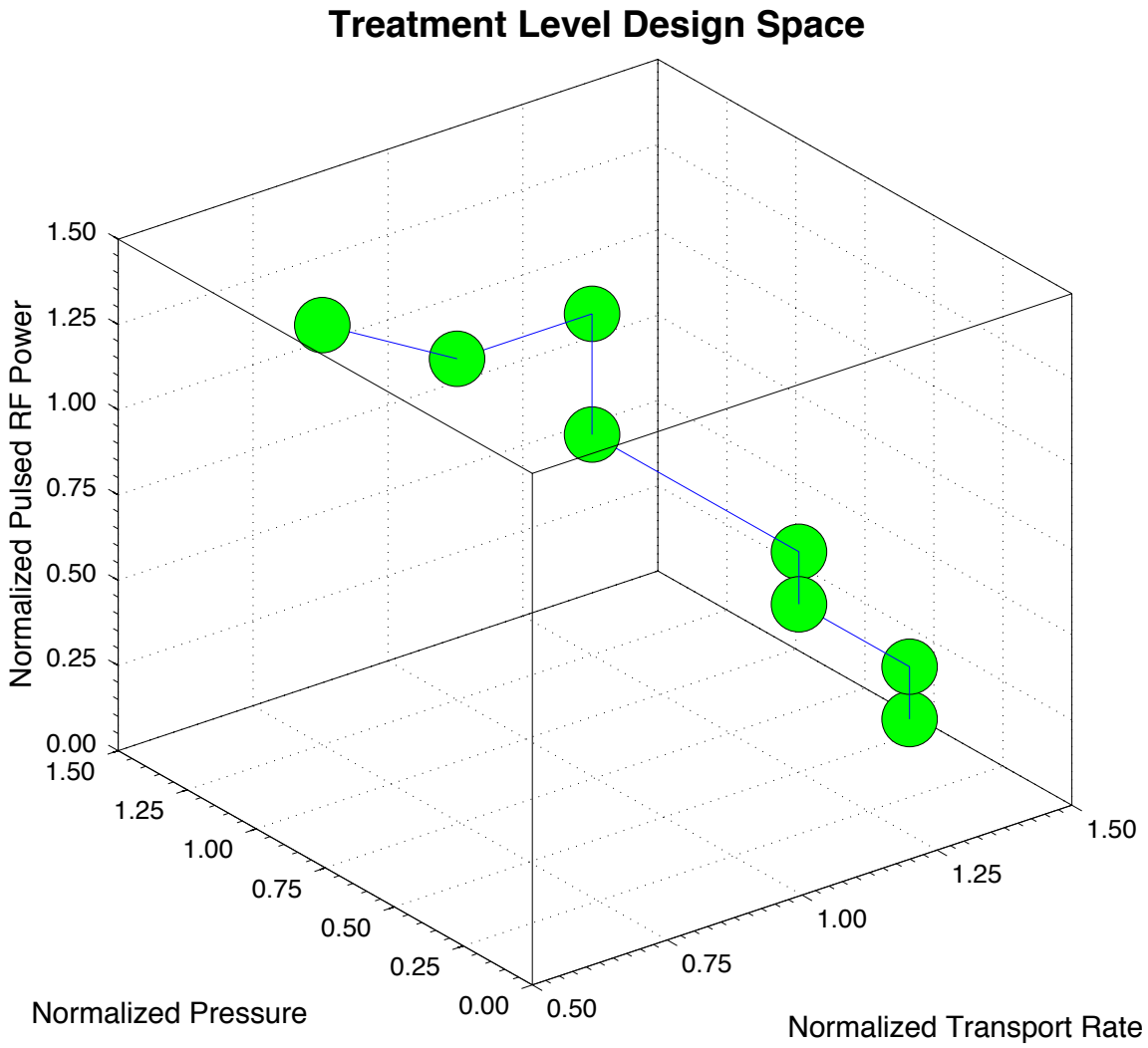

Figure 6.7: Process design space used to create a wide range of tubing bore surface lubricities

Table 6.1 and Figure 6.7 show a total of eight different transport rates, pressure, and power inputs that have been normalized with respect to process settings that historically have produced high quality tubing bore lubricity. Based on personal processing experience, the material exposed to the highest transport rate, lowest saturation pressure, and lowest pulsed RF power is expected to receive the least treatment (i.e., exhibit the highest COF). On the other hand, the material exposed to the lowest transport rate, highest saturation pressure, and highest pulsed RF power is expected to receive the best treatment (i.e., exhibit the lowest COF).

6.4 *Curvilinear torque test characterization*

In an attempt to validate the force model embodied by Eq. (4), some experiments were performed. For convenience, Eq. (4) is repeated below.

$$T = RF = 2R\mu_k F_{springback} \tag{4}$$

As part of the validation effort, the springback forces needed to maintain a 0.036-inch nickel alloy coil in a series of given bend diameters were measured using a force transducer (load cell) connected to a jawed gripper which was mounted on a Thwing-Albert FP-2255 peel tester [West Berlin, New Jersey]. An illustrative experimental setup used to determine the force required to bend the chosen coil to a diameter of 1.5 inches is shown in Figure 6.8.

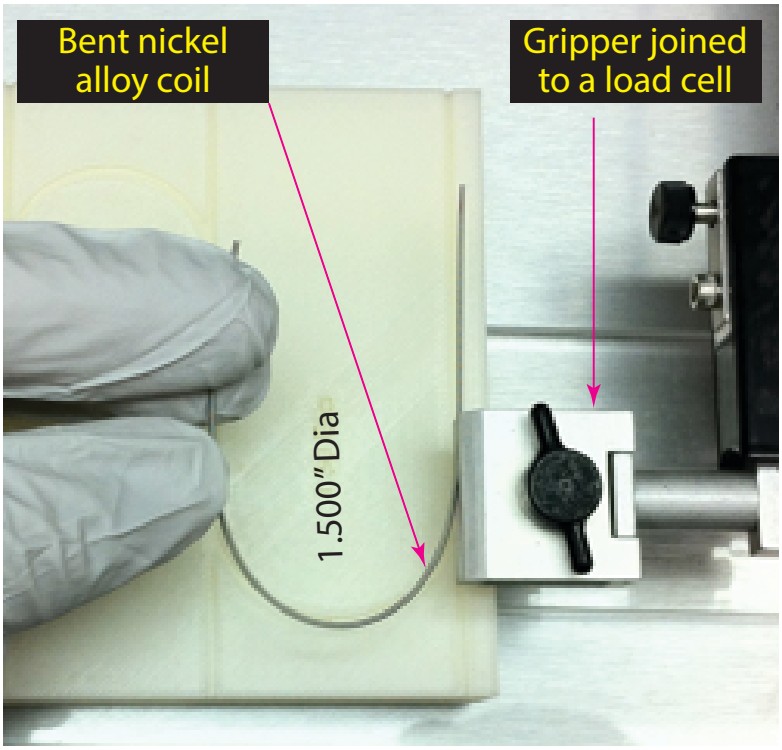

Figure 6.8: Custom apparatus used to determine the force of spring back to bend a nickel alloy coil to a given radius of curvature

Figure 6.8 shows a closed gripper that is attached to a load cell and gripping a small segment of the coil. The method was to drive the gripper holding the coil forward while recording the force at the point that the desired radius of curvature was achieved. This work was repeated over a range of bend diameters of 0.4 to 1.5 inches. The springback force rises with the inverse of the bend diameter, as expected. The data were fairly accurately fit ($R^2 = 0.93$) over an inverse bend diameter range of 0.67-2.67 inches^{-1} using a second-order polynomial curve. The plotted data from the experiments are shown with the second-order polynomial fit in Figure 6.9.

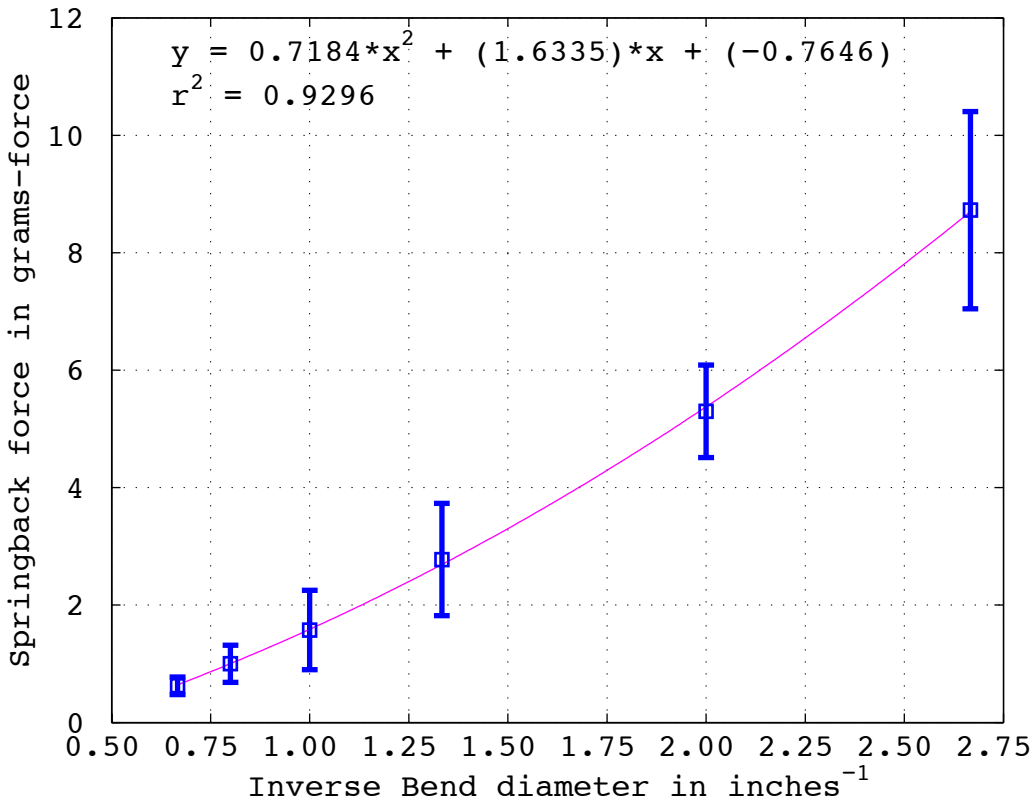

Figure 6.9: A polynomial fit to the springback force as a function of inverse coil bend diameter

An alternative model relating the springback force to the bend diameter can be written as Equation 6:

$$F_{springback} = k_{spring} \cdot (D_{bend})^{-2} \tag{6}$$

Plotting the springback force as a function of the inverse square of the bend diameter enables the extraction of the slope (corresponding to a type spring constant parameter). The plotted data yield a slope of 0.93 as shown in Figure 6.10.

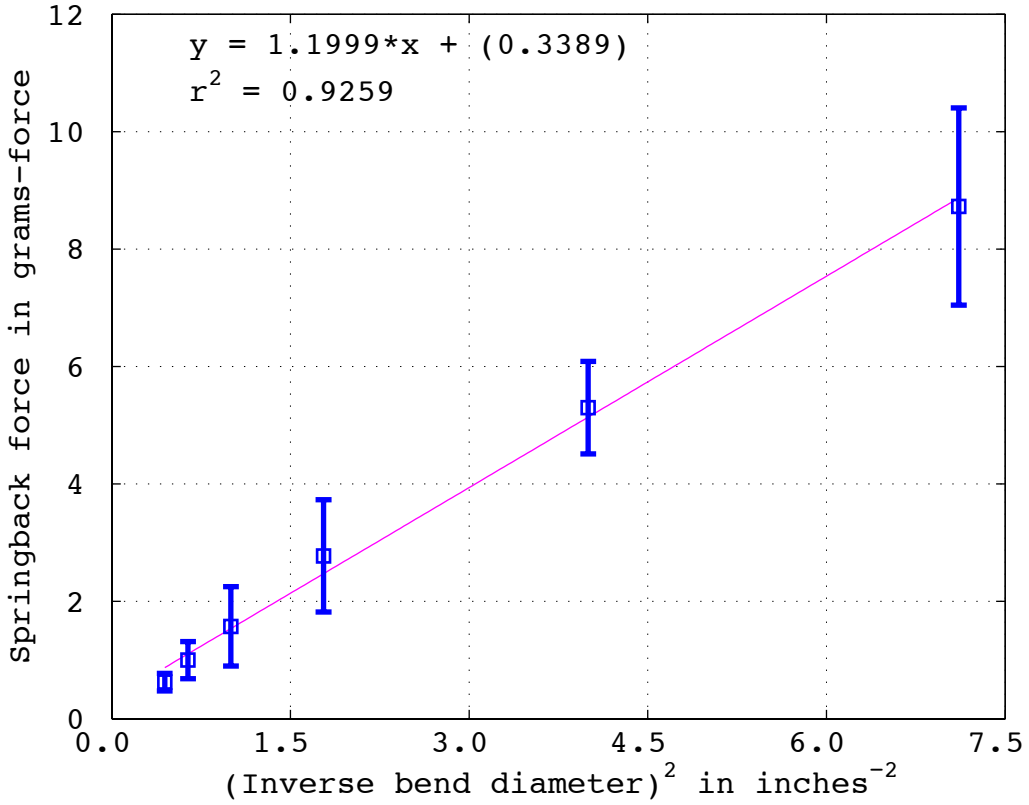

Figure 6.10: A linear fit to the springback force as a function of the inverse-squared coil bend diameter

The slope of the fitted model or k_{spring} shown in Figure 6.10 is seen to be 1.2 grams-force*inches^2 or 0.042 ounce-force*inches^2. With a relationship between bend diameter and the springback force (an inferred horizontally oriented normal force without the influence of the coil weight) in hand, attention was turned to collecting data using an "S-shaped" fixture designed to accommodate a sample under test in an S-shaped grooved track. This work was performed to determine if an S-shaped grooved track fixturing

would perform better than a linear grooved track fixture when measuring friction, The custom fixturing is shown as Figure 6.11.

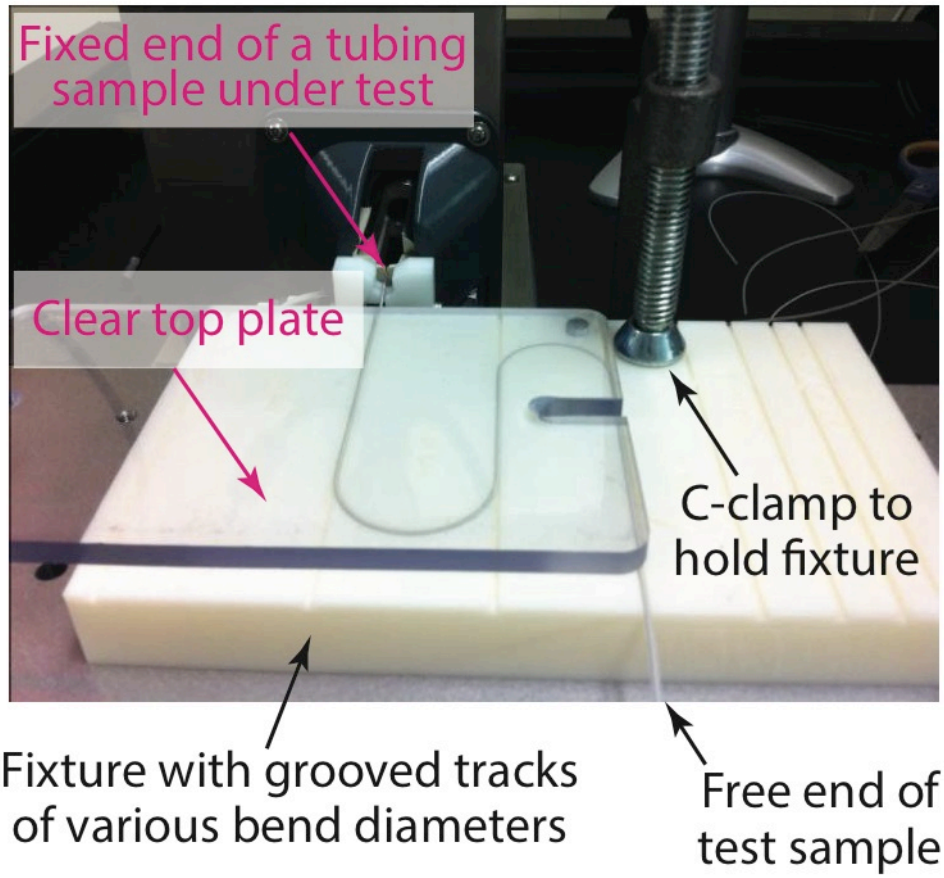

Figure 6.11: A custom test fixture designed to accommodate a plasma-treated sample under test in a grooved track with a freely rotatable coil inserted into the sample

Figure 6.11 shows a white fixture with inlaid S-shaped grooved tracks. The S-shaped grooved tracks form two 180° turns, with each turn having a different radius of curvature. The figure also shows a plasma-treated tubing sample with a 0.036-inch diameter coil (diagram of the coil is shown in Figure 2.3, Chapter 2) inserted into its bore. Jaws that are attached to a torque transducer grip one end of the coil and the other end of the coil is allowed to freely rotate. The tubing is held stationary in the S-shaped groove, and a clear plate has been placed on top of the fixture/test assembly to prevent the sample under test from "jumping out" of the groove. The clear top plate does not impart any force on the rotating coil under normal test conditions and is only there to

assist in the initial test setup. The force model used for the data analysis in this section involves the use of Eq. (4), repeated below.

$$T = RF = 2R\mu_k F_{springback} \tag{4}$$

Substitution of Equation 6 into Equation 4 results in a new relationship, Equation 7.

$$T = RF = 2R\mu_k k_{spring} (D_{bend})^{-2} \tag{7}$$

Since every test setup that used the configuration shown in Figure 6.11 involves an S-shaped grooved track that has two different bend diameters, Equation 7 was slightly modified to account for these different diameters. The modified equation is shown as Equation 8.

$$T = RF = 2R\mu_k k_{spring} \left\{ (D_{bend\_1})^{-2} + (D_{bend\_2})^{-2} \right\} \tag{8}$$

Equation 8 shows D_{bend_1} and D_{bend_2} corresponding to two differently sized bend diameters. Three different configurations of S-shaped bends were employed for each case of using treated and untreated tubing samples. The plotted data with linear fits are shown below in Figure 6.12.

A flaw in the experimental S-bend setup did not augur well for the attainment of results of high accuracy. In preliminary torsion experiments performed in the no-load situation, the registered results displayed a periodic pattern. This it pattern but with different numerical values was also observed for the experiments with load. It is believed that these outcomes can be attributed to an insufficiency in the torque capabilities of the motor.

In view of this finding, the collected data were averaged after excluding the startup and shutdown transients. However, the presented data for the S-bend experiments have to be regarded as qualitative, at most.

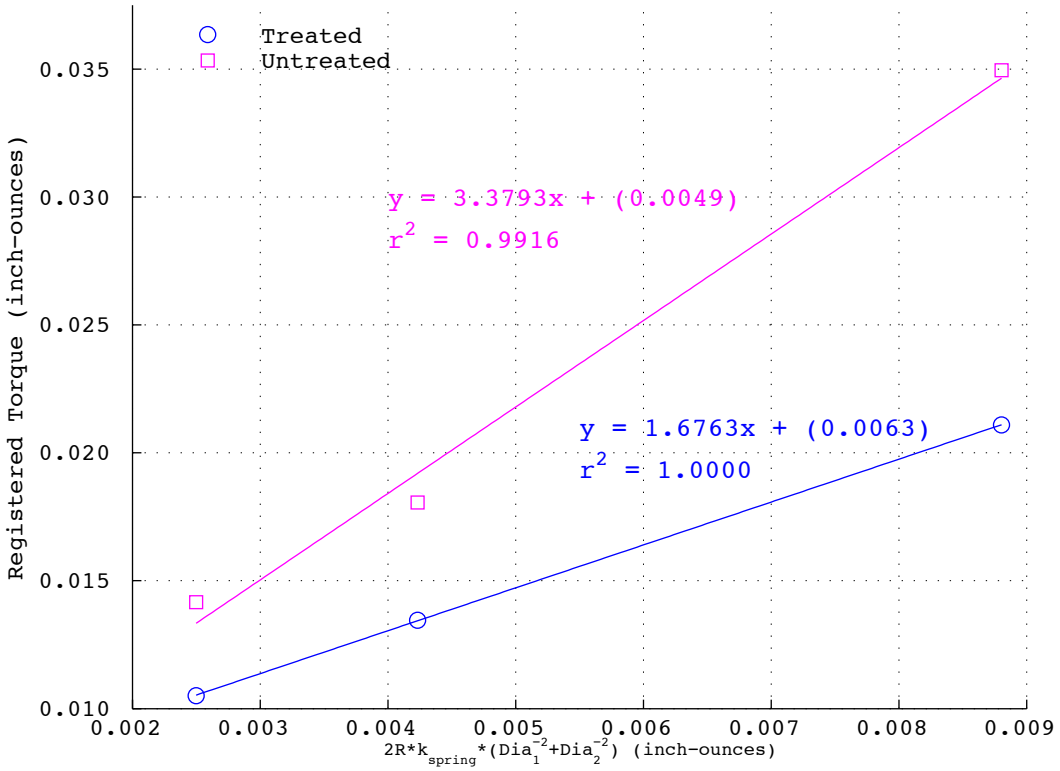

Figure 6.12: Registered torque as a function of the parameter $2RK(D_{bend\_1}+D_{bend\_2})^{-2}$ *with fitted lines for each treatment level*

The results displayed in Figure 6.12 reveal that the torque required to rotate the coil is linearly proportional to the grouping 2RμkFspringback as intimated by Equation 4, Nonetheless, the best-fit coefficients of friction obtained were significantly higher than expected based on past experience with the plasma treated silicone tubing, For this dataset, μ_k was found to be 3.38 for untreated tubing, while a more typical value for the COF between an untreated silicone rubber on metal system ranges between 2.0 and 2.5, Additionally, μ_k was found to be 1.68 for nominally treated tubing, whereas this value is usually considered to lie in the range between 0.3-0.7, In summary, the torque values measured by this technique are considerably greater than can be explained by the

springback force model as presented by Eqn. 4. Based on this work, this method has been deemed unreliable when used to extract the COF from a silicone rubber/metal system.

Sample tubing lengths from each of the eight unique treatment conditions were evaluated by the three previously described methods: the historical U-bend test method (pulling a 0.026-inch diameter nickel alloy coil through the plasma-treated tubing sample), the S-shaped track torque test (using bend diameters of 1.00 and 1.25 inches and rotating a 0.036-inch diameter nickel alloy coil inside the plasma-treated tubing sample). and the linear track torque test (using a 0.035-inch diameter stainless steel rod and a top weight of 291 grams-force rotated inside the plasma-treated tubing sample). The data are presented in Figures 6.13 – 6.15.

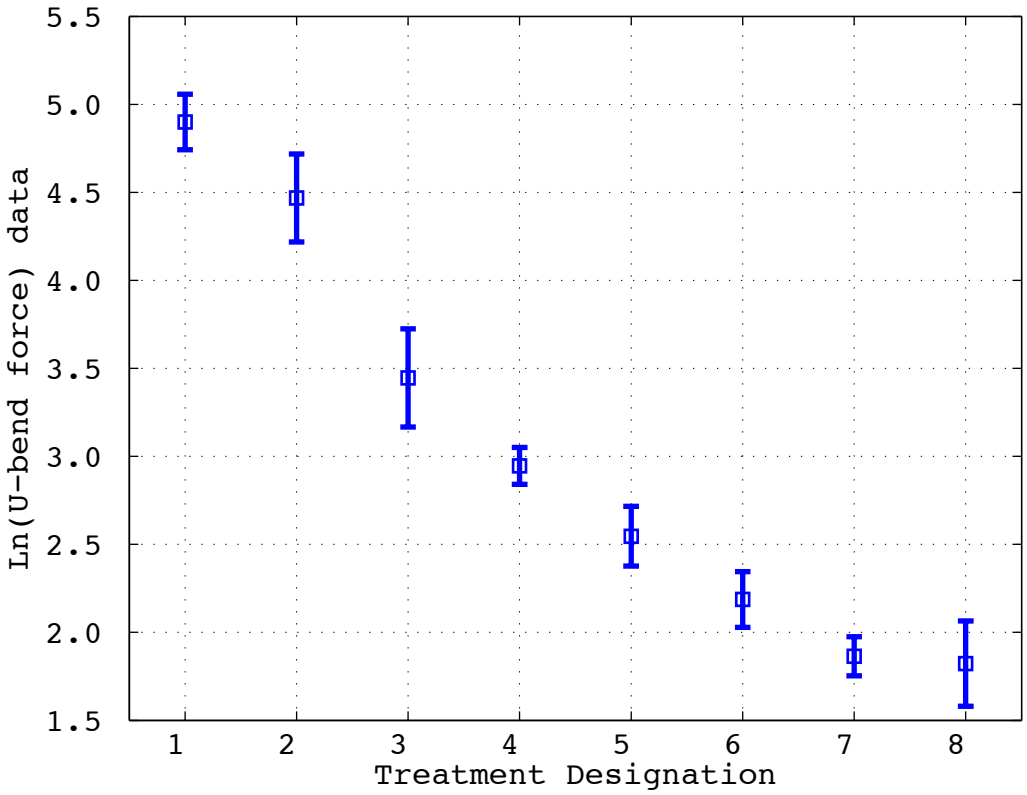

Figure 6.13: U-bend test method pull force data generated for each treatment level

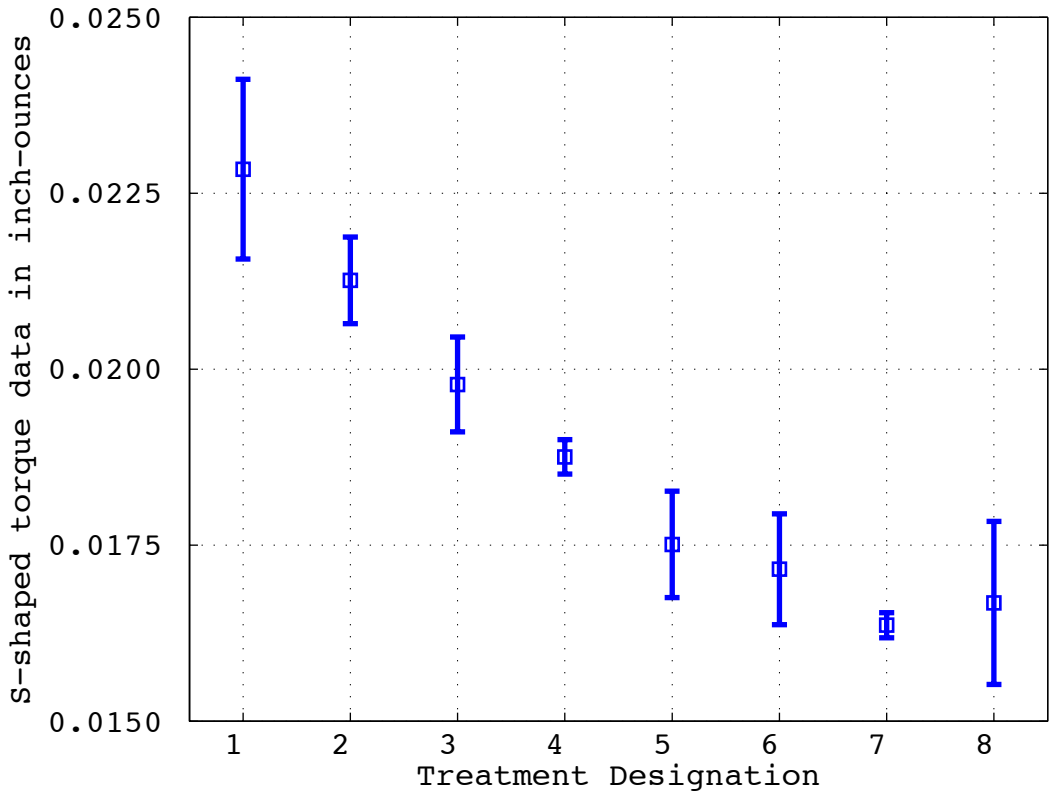

Figure 6.14: S-shaped track test method torque data generated for each treatment level

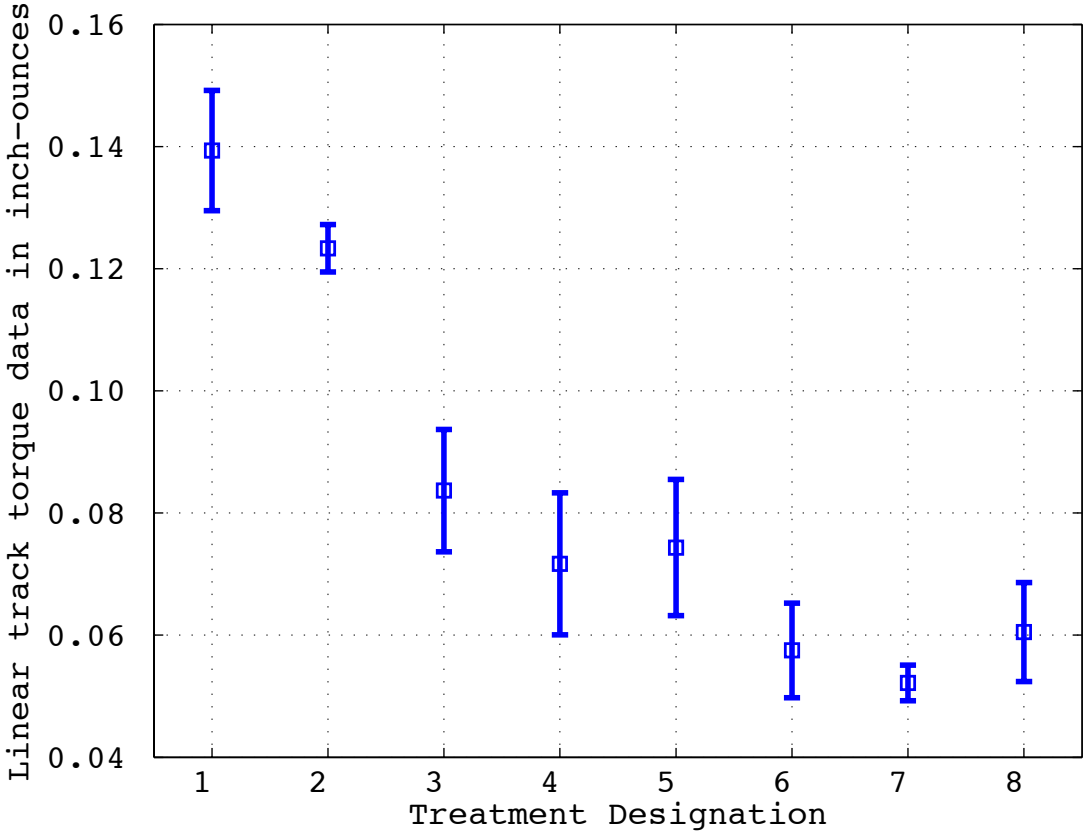

Figure 6.15: Linear track test method torque data generated for each treatment level

As expected, Treatment 1 resulted in the highest test results (highest friction, lowest lubricity) according to all three methods of the test methods, and Treatments 6-8 gave the lowest test results, Clearly, all three methods are capable of distinguishing between various degrees of tubing bore lubricity, Inspection of Figures 6.13 – 6.15 shows that the historical U-bend test method exhibits data of high linearity and reproducibility, with each of the treatment levels clearly distinguished, The S-track data exhibit good linearity although the reproducibility is clearly not as good as that of the U-bend test, The linear track torque test data exhibit less linearity than do the S-track torque test data and similar reproducibility, On the other hand, the linear track torque test data span a much wider range of torque values than do those of the S-track torque test (0.05-0.15 inch-ounces compared to 0.016-0.023 inch-ounces). It is important to note that the torque transducer's full scale is 0.70 inch-ounces. This means that the S-track torque test

generates data between 2.3 to 3.3% of full scale. On the other hand, the linear track torque test generates data between 7.1 to 21.4% of full-scale. Because of the higher dynamic range, the linear track torque test may be more robust to long-term variations in the measurement system than would the S-track torque test. Based on this reasoning and the fact that the test setup is simpler and quicker than the S-track torque test, the linear track torque test method was chosen for further characterization.

6.5 Linear track torque test method characterization

After the linear track torque test method was selected for further characterization, input factors were considered and chosen based on their perceived influence on the torque output, The following factors were chosen for the characterization evaluation:

- Weight used (grams-force) to develop the normal force on the system (range 0 to 291 grams-force applied)
- Diameter of the stainless steel 304 rod (range 0.034 to 0.038 inches)
- Speed of rotation during test (range 0.25 to 1.00 revolutions per second)

The material of fabrication for the rod is to be examined in later sensitivity studies. The surface finish of the rod was not selected for study since there were no readily available examples of rods with variation in their surface conditions. For the first study, a three-factor designed experiment was performed on the least and most treated silicone-tubing samples. The experimental design space is shown in Figure 6.16.

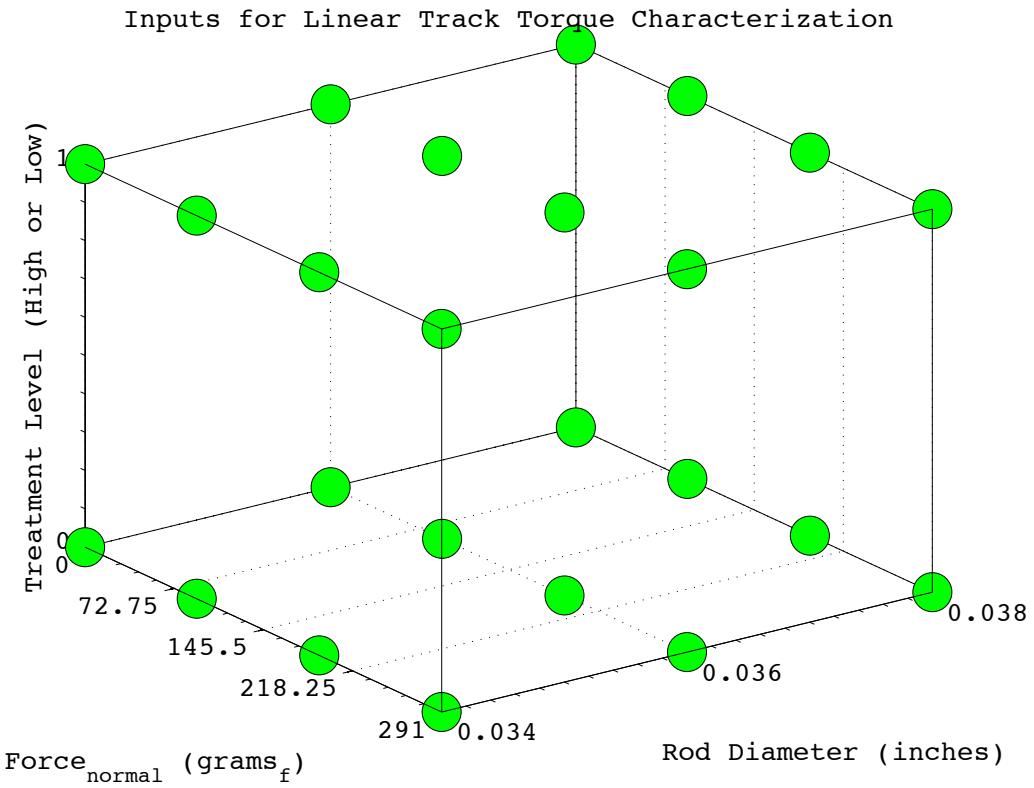

Figure 6.16: Inputs for initial characterization of the linear track torque test method

Response surfaces were created for showing torque as a function of the rod diameter and applied normal force for the extreme treatment conditions. The response surfaces are shown side by side in Figure 6.17 to compare and contrast the torque outputs for these two extreme conditions.

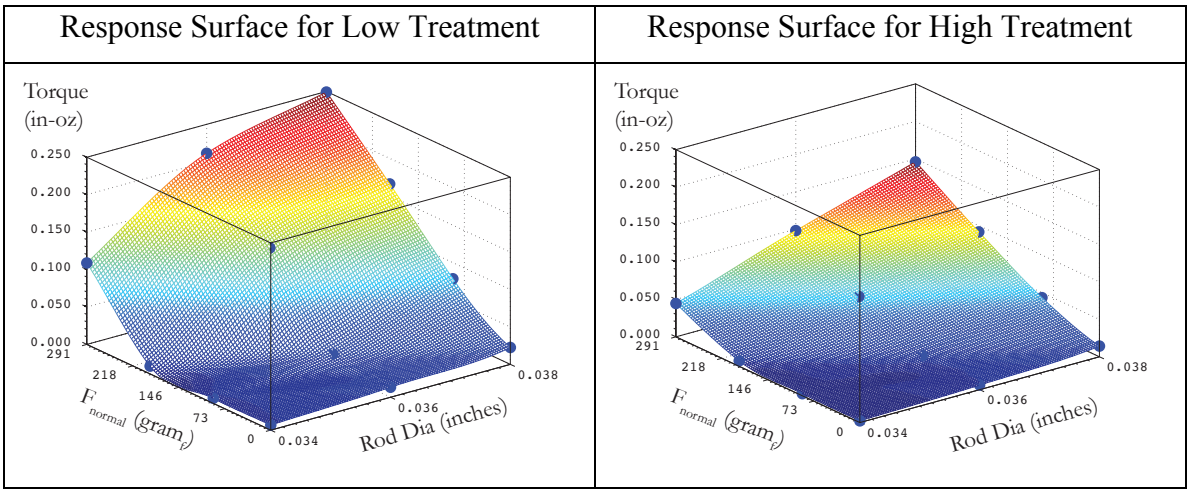

Figure 6.17: Torque response surfaces for low (left) and high (right) surface modifications

The response surfaces shown in Figure 6.17 for the low- and high-surface modification processes clearly reveal that the torque test output is strongly dependent on all three factors studied, Increasing the top weight applied to the tubing generally results in an increased torque output, although the effect is muted for small top weights and smaller rod diameters, In addition, increasing the wire diameter resulted in higher torque test outputs and improved linearity of dependence on the top weight, In all cases, the low-treatment samples showed higher torque outputs than high-treatment samples, although the difference between the two samples varied widely, Overall, the results suggest that rod diameters in the range 0.036-0.038 inches and top weights in the range 91-291 grams-force result in an evaluation method that clearly distinguishes between high and low treatments of the silicone tubing.

7 Summary

Among the methods that have been evaluated in this chapter, the linear groove method has been demonstrated to have the best properties with regard to metrology. Its sensitivity is superior to the historical method and to the S-groove method. The ease of setup, implementation and operator-independence are highly cost effective. Provided the

samples being tested can be compressed with a top weight, the straight groove torque test method can readily be adopted by any situation that requires a quick and sensitive tubing bore lubricity test. A nice feature about this test method is that it generates data that can be used for the extraction of a coefficient of friction.

Chapter 3

A NEW INVENTION TO CHARACTERIZE THE LUBRICITY OF BIOMEDICAL CONDUITS

1 Introduction

The scarcity of suitable methods to determine the lubricity of biomedical conduit tubing bore surfaces motivated the invention of a simple and accurate method to deduce the lubricity outcomes of the conduits following lubricity-increasing processing. The novel method developed during the course of this writer's research may be termed "The Pressure Cuff Friction Test Method", or "The pCuff Method". This pCuff method was inspired by an existing apparatus known as a tail-cuff blood pressure measuring system that is in no way intended for friction measurements, Rather, its function was to determine the blood pressure of mice and/or rats [18]. That apparatus functioned by squeezing down on the rodent's tail with a pressure cuff with a known and regulated pressure while sensing the rat or mice tail's systolic/diastolic blood pressures (also see: SC1000 Single/Dual Blood Pressure Analysis System marketed by Hatteras Instruments, Inc., Cary, North Carolina 27518).

The first version of the herein-invented friction measurement system is displayed in Figure 1.1 in a photographic view.

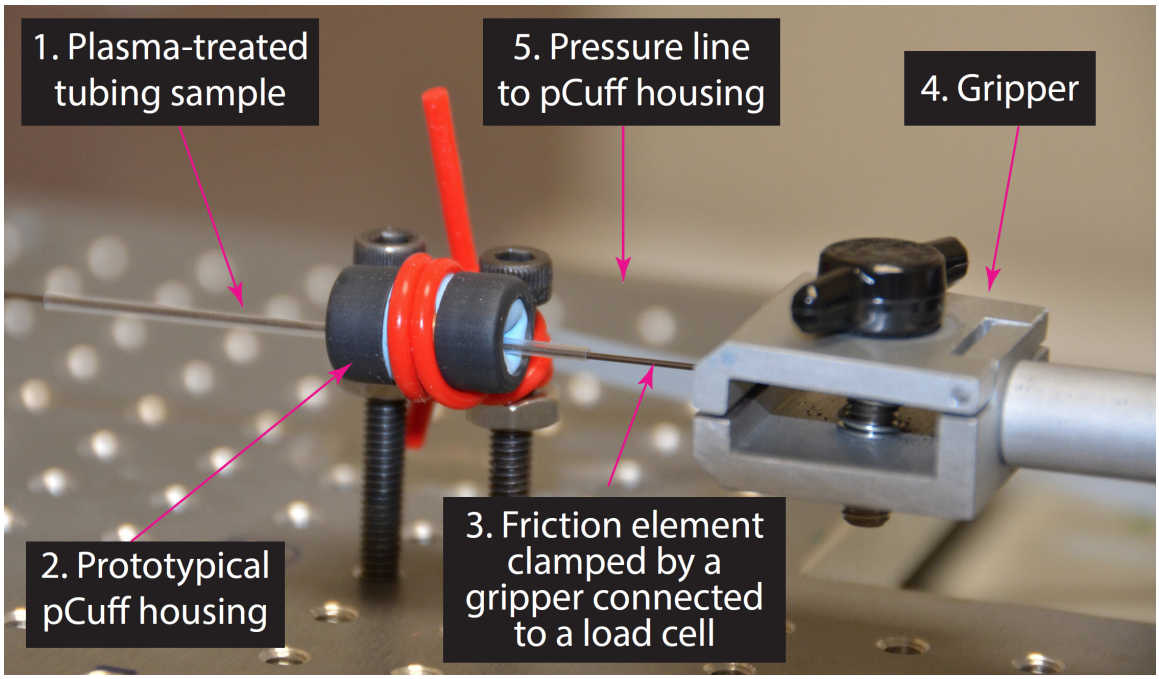

Figure 1.1: Initial version of the friction measurement system

The initial version of the pCuff friction measurement system has some key elements. The key elements are identified as:

1. A plasma-treated tubing sample to be assessed is placed inside the pCuff housing.

2. A prototypical pCuff housing that houses an air-bladder. The air-bladder is inflated to provide a normal force on a friction element that will be pulled through the stationary plasma-treated tubing sample.

3. A friction element or tribo-partner that is pulled through the stationary plasma-treated tubing sample.

4. A gripper that clamps down on the friction element. The gripper is connected to a force registering load cell.

5. A pressure line (out of focus, whitish polypropylene line) to a pressure supply pump. The pressurized line is used to inflate an air-bladder that is part of the pCuff housing.

The new technique relies on knowing the normal force applied to a plasma-treated sample on a sliding friction element and the tangential pulling force required while

translating the sliding element through the stationary sample. With the normal and tangential force known, the coefficient of friction for the system can easily be derived.

Feasibility work using the first version of the friction measuring system indicated that the method was capable of distinguishing varying degrees of plasma-treated tubing bore lubricity. The work also showed that precisely knowing and controlling the area being pressurized and the pressure are both critical in the extraction of accurate coefficients of sliding or kinetic friction.

A refined version of the friction measuring system was designed, fabricated, and used in this research. The details of the new friction system will be developed in this chapter.

2 Force diagram for pressure cuff friction test method

A force diagram showing the system being tested is displayed in Figure 2.1.

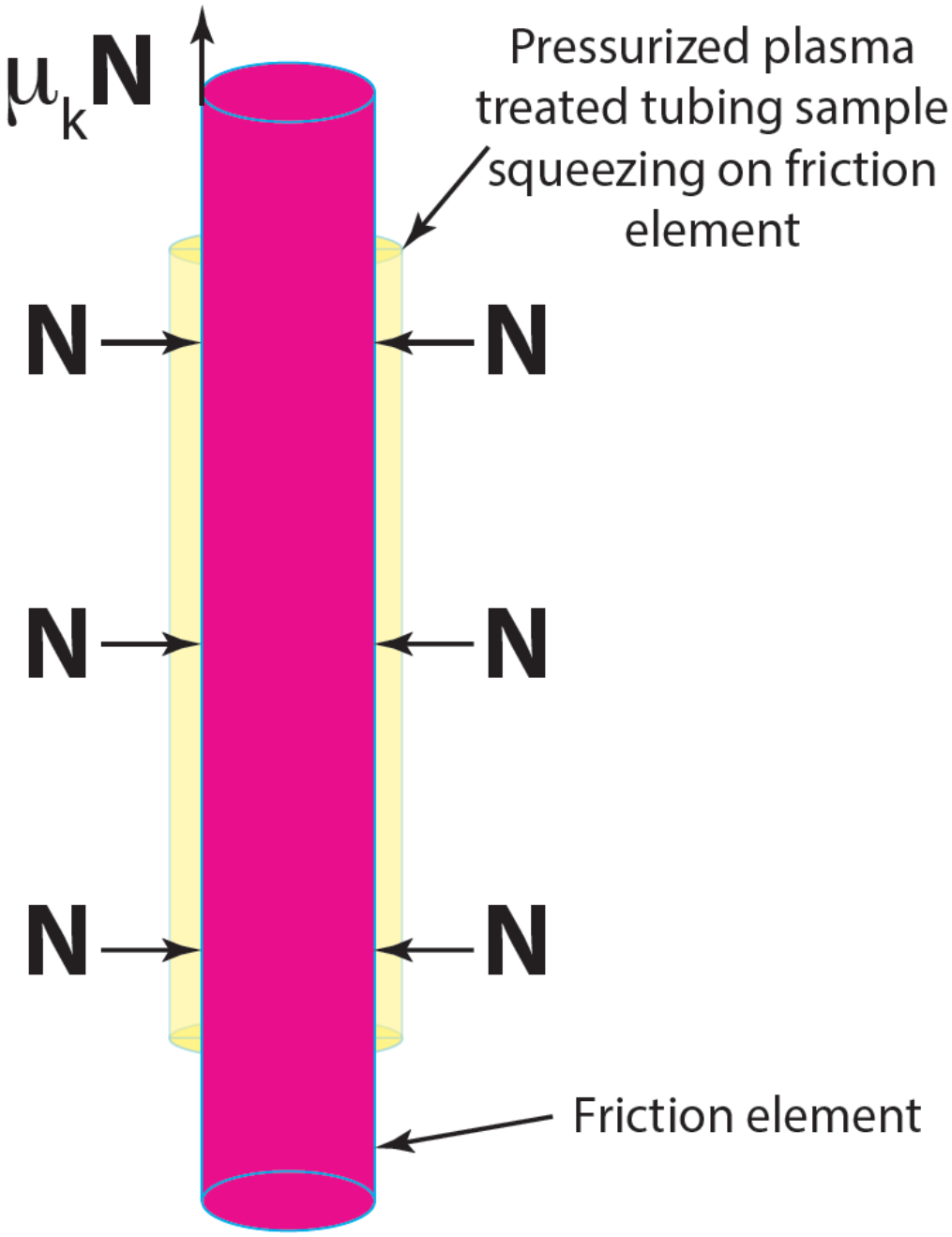

Figure 2.1: Force diagram for the pressure cuff friction test method

Figure 2.1 shows a plasma-treated tubing sample that is pressing down on a friction element. The friction element is pulled axially upward while being gripped with a Jacob's drill chuck that is connected to a calibrated load cell. The tangential force is simply the coefficient of kinetic friction multiplied by the normal force. Pressurizing the tubing sample to a known pressure with a known constant pressurized area sets the normal force.

3 Description of pressure cuff test method components

3.1 Pressure cuff housing, air-bladder, and sample under test

The custom designed and built pressure cuff used for this tribological research consists of several main sub-assemblies to include the housing that fixates the sample under test ("SUT") as shown in Figure 3.1.

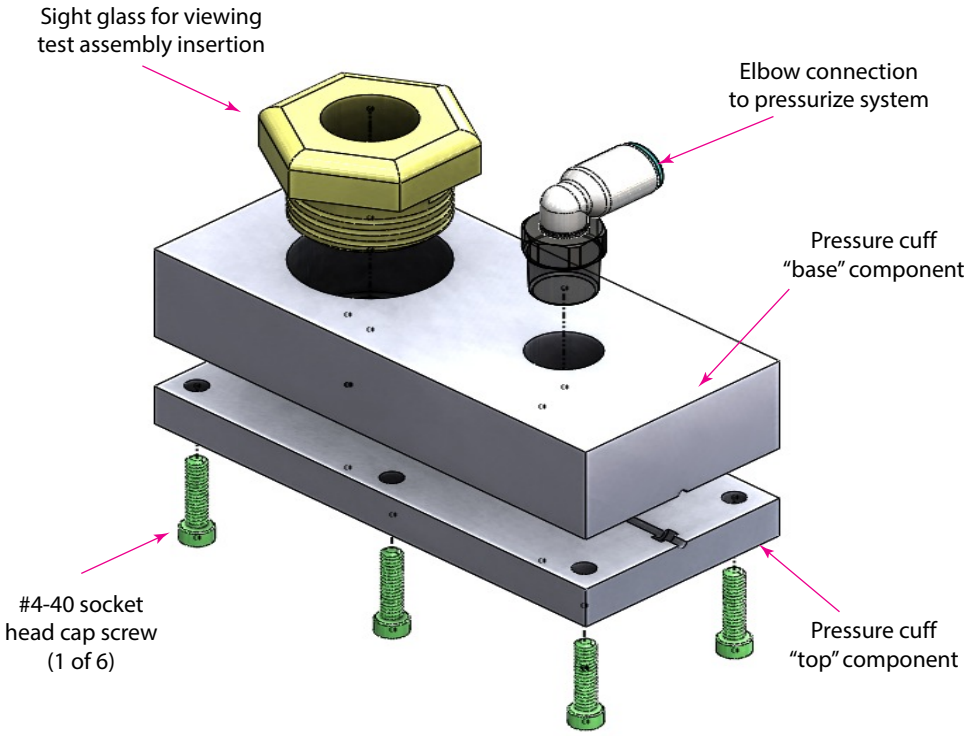

Figure 3.1: Pressure cuff housing used to fixate air-bladder and the test assembly

The pressure cuff housing has grooves in the base and the top that accommodate an air-bladder assembly that, when pressurized, imparts a normal force upon the plasma treated tubing sample that is being assessed. The pressure cuff housing also has two O-ring grooves to improve the pressure isolation of the sample under test. The sample under test is threaded down the axial axes of what is known as an air-bladder assembly. The air-bladder assembly that accommodates the test assembly is held in place by the pCuff housing. The air-bladder assembly is illustrated in Figures 3.2 and 3.3.

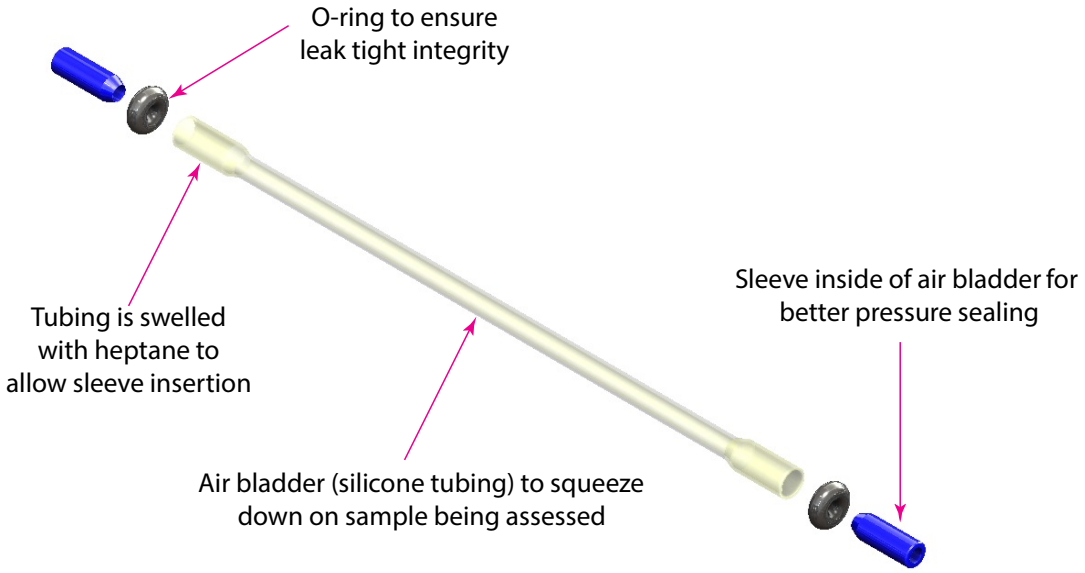

Figure 3.2: Air-bladder assembly designed to hold the sample under test – exploded and color enhanced

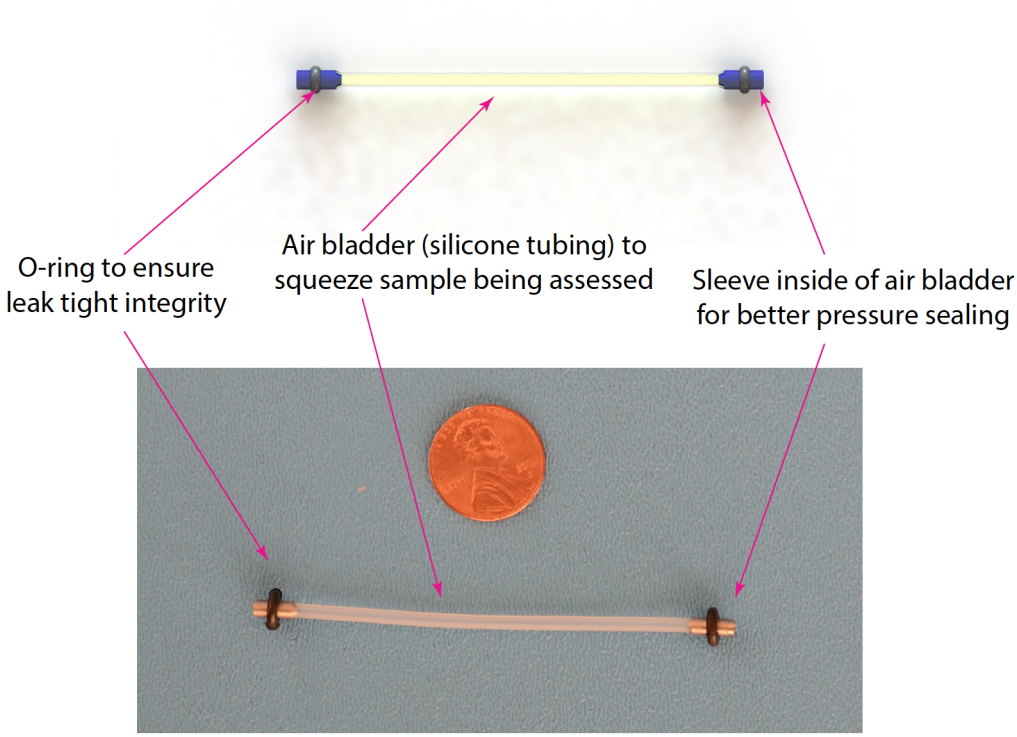

Figure 3.3: Air-bladder assembly designed to hold the sample under test – ready for mounting into pressure cuff housing

The air-bladder assembly incorporates two sleeves inserted into the air-bladder and additionally uses two -006 O-rings that fit into the grooves of the pressure cuff housing. The air-bladder (silicone tubing) is temporarily swollen with heptane on the extreme ends to facilitate the insertion of the stainless steel sleeves. The air-bladder is designed to allow for a plasma treated sample under test to be inserted down its axial axis and to squeeze down on the sample to hold it fast. The sample has a friction element or "tribo-partner" inserted down its axial axis. The friction element is pulled through the stationary tubing using an MTS, Eden Prairie, MN USA 55344, test system with associated software that records the extraction force. The plasma-treated tubing sample to be assessed with a 316 SS 0.0405" diameter 8-inch length stainless steel friction element, and the air-bladder assembly is displayed in Figure 3.4.

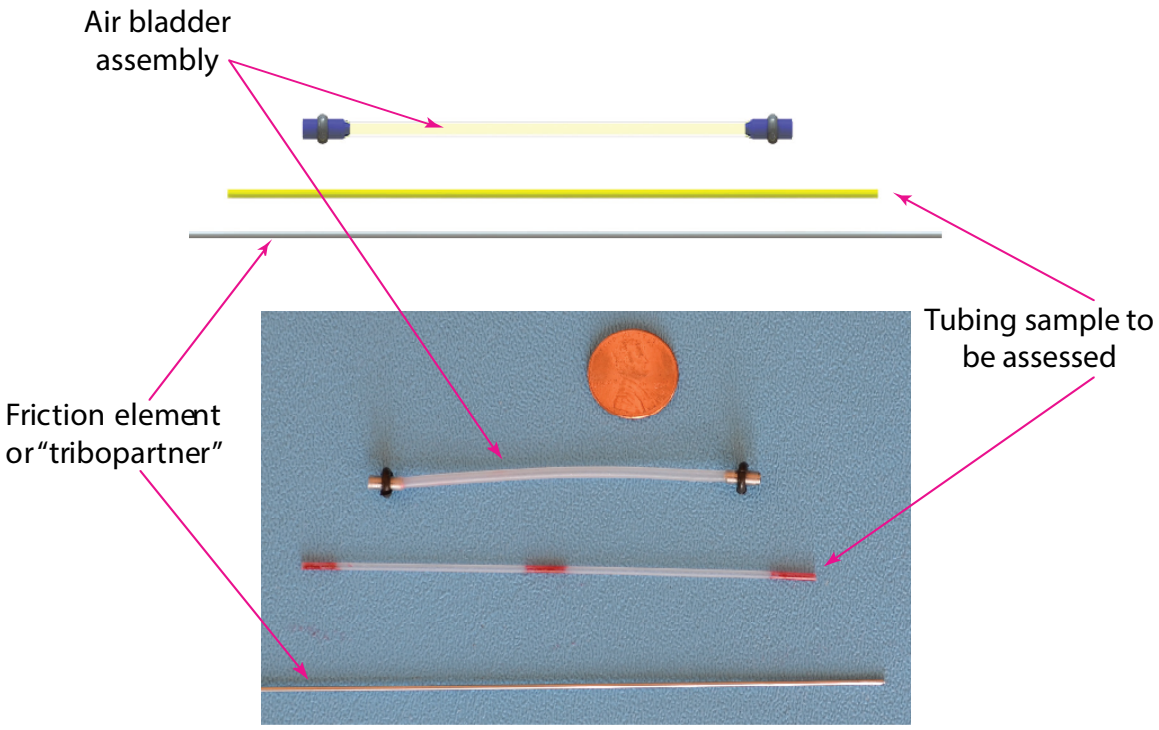

Figure 3.4: Air-bladder assembly, sample to be tested, and friction element

The 0.0405" diameter, 8-inch long friction element (316 stainless steel rod or wire, also referred to as a "tribo-partner") is inserted axially down the tubing sample bore to prepare the sample for test. The fiction element/sample assembly is then inserted into the air-bladder assembly (fixated by pressure cuff housing). A view of the sample, to be tested with the threaded tribo-partner within the air-bladder assembly is shown in Figure 3.5.

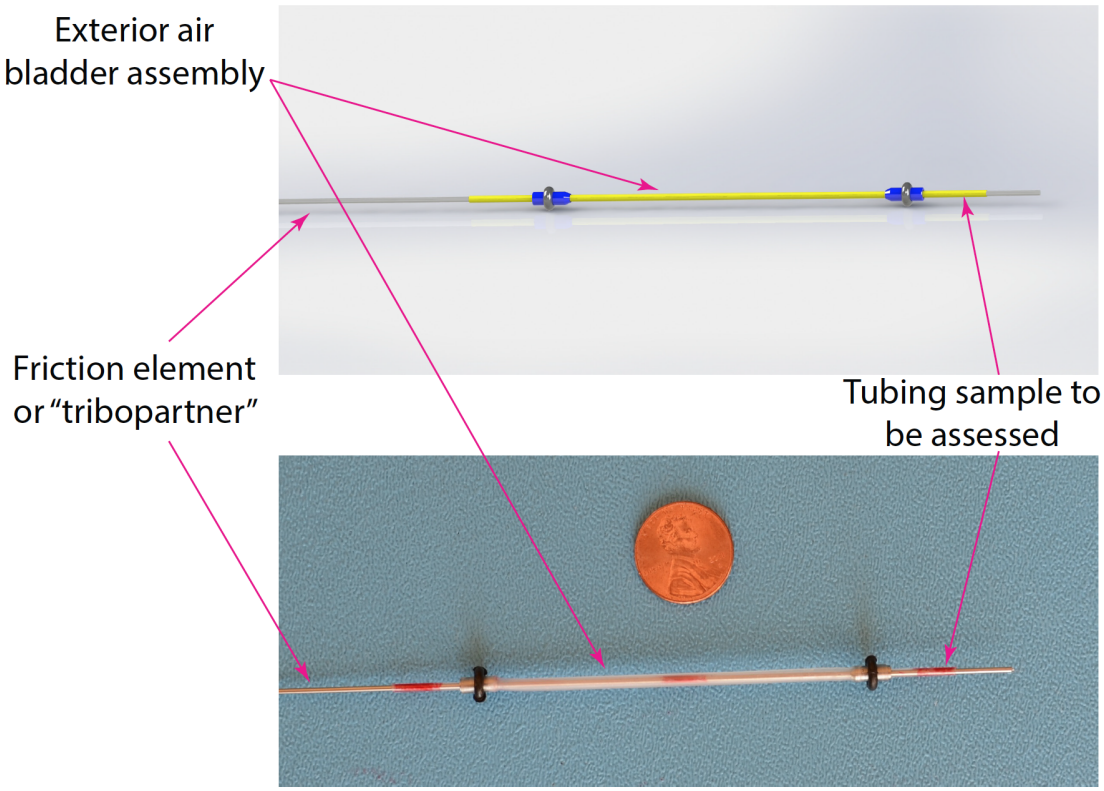

Figure 3.5: Plasma-treated sample prepared for testing with friction element inserted down its axial axis, ready for placement in the air-bladder assembly – color enhanced

The overall assembly with the components labeled is shown from different vantage points in Figure 3.6 and Figure 3.7.

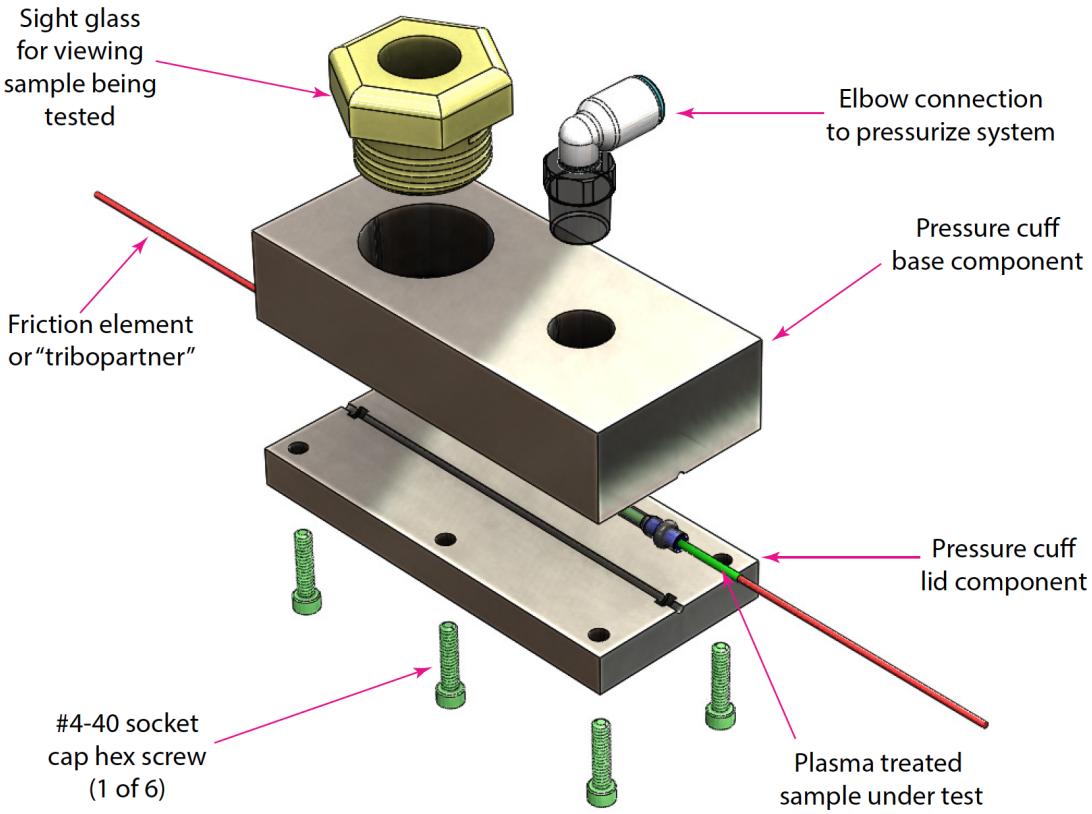

Figure 3.6: Pressure cuff hardware with sample under test – isometric view

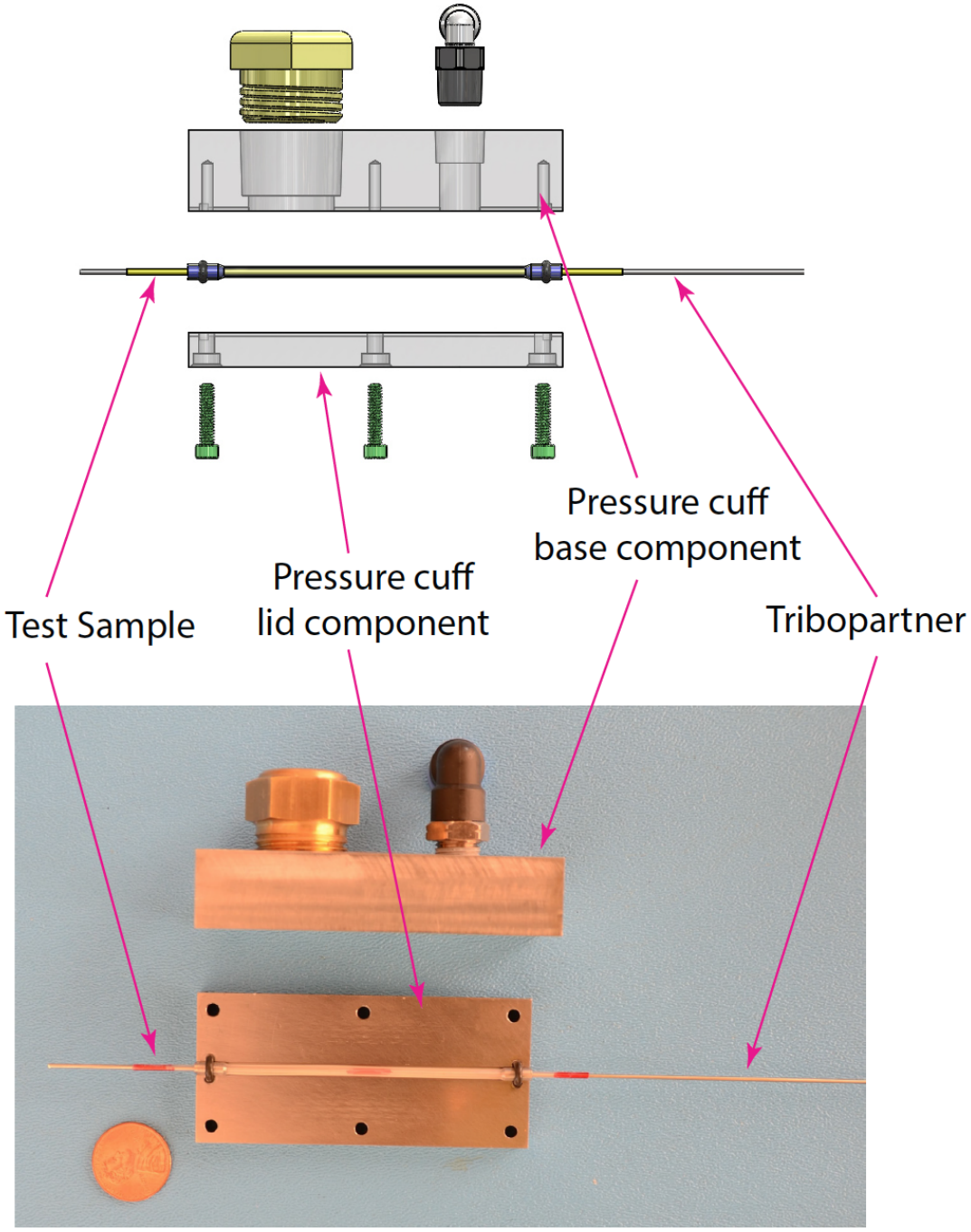

Figure 3.7: Pressure cuff hardware with sample under test – back view

The overall assembly illustrations and images of Figures 3.6 and 3.7 show a sight glass used to facilitate threading the sample under test and the tribo-partner. There is an elbow that is connected to a pressurized hose that is in line with a precision digital

pressure controller. The figures show the semicircular grooves on the base and lid components that accommodate the sample under test. The O-ring grooves are also depicted on the lid component. The lid component is to be secured to the base component with socket cap hex screws.

3.2 Pressure cuff frame

The pressure cuff housing and associated hardware are held vertically with a custom designed and built frame that mates with a MTS test system. The pCuff housing in the frame is illustrated in Figure 3.8 and Figure 3.9.

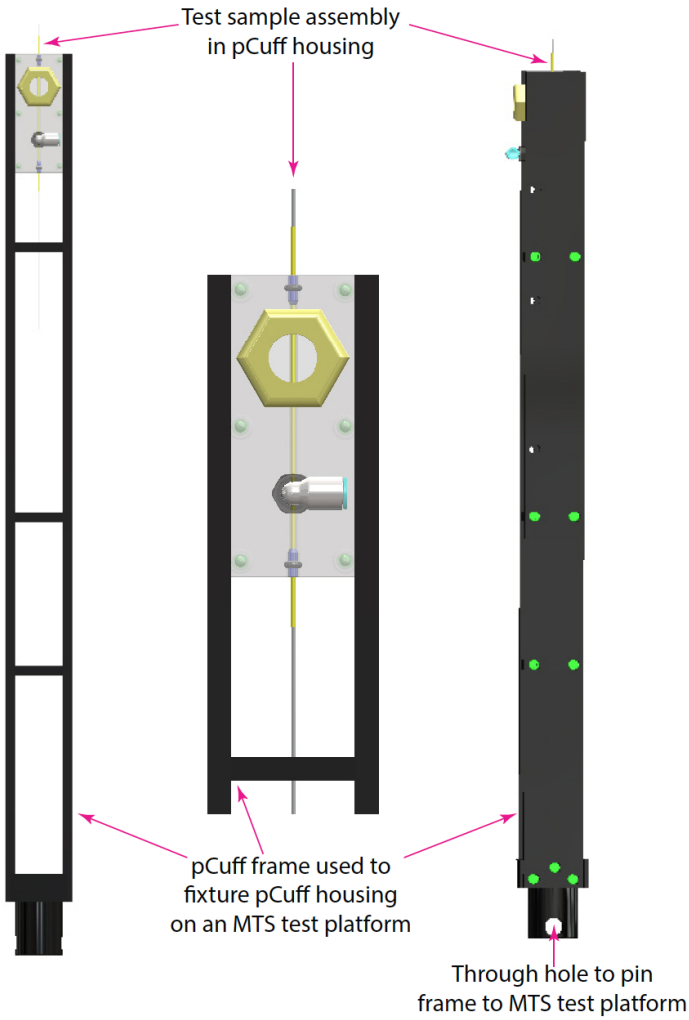

Figure 3.8: Pressure cuff housing held inside of custom frame - drawings

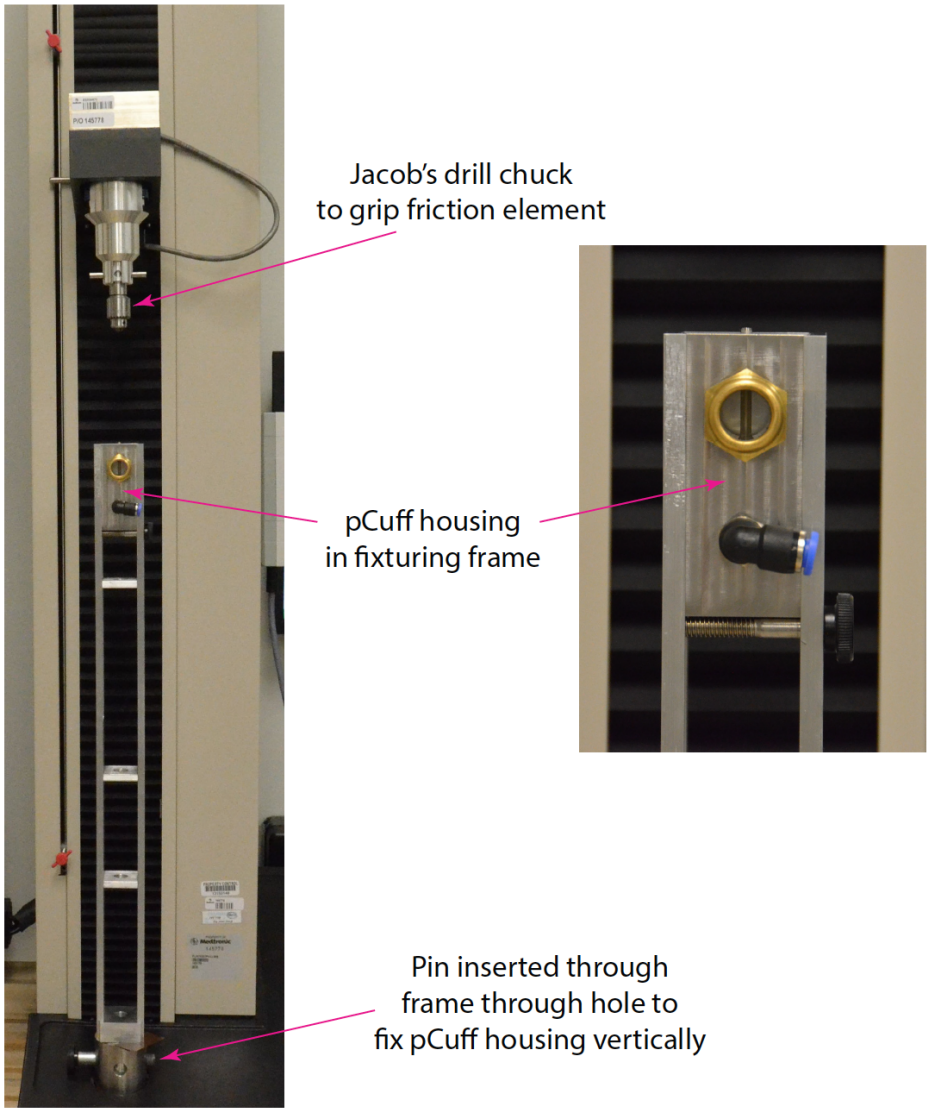

Figure 3.9: Pressure cuff housing held inside of custom frame - images

The pressure cuff frame holds the pressure cuff housing in the X, Y, and Z planes. The frame has three spacers with center holes that allow for varying lengths of friction elements to be used if desired. The base of the pressure cuff frame has a through hole to accommodate a pin that connects the frame to the MTS test system. Figure 3.9 shows the

Jacob's drill chuck that is connected to a calibrated 50 Newton load cell or force transducer.

3.3 Pressure cuff pressure control system

The pressure cuff friction test method is critically dependent on precise pressure control as the combination of the pressure and the area under test set the normal force applied to the friction element. The pressure control system is shown in Figure 3.10.

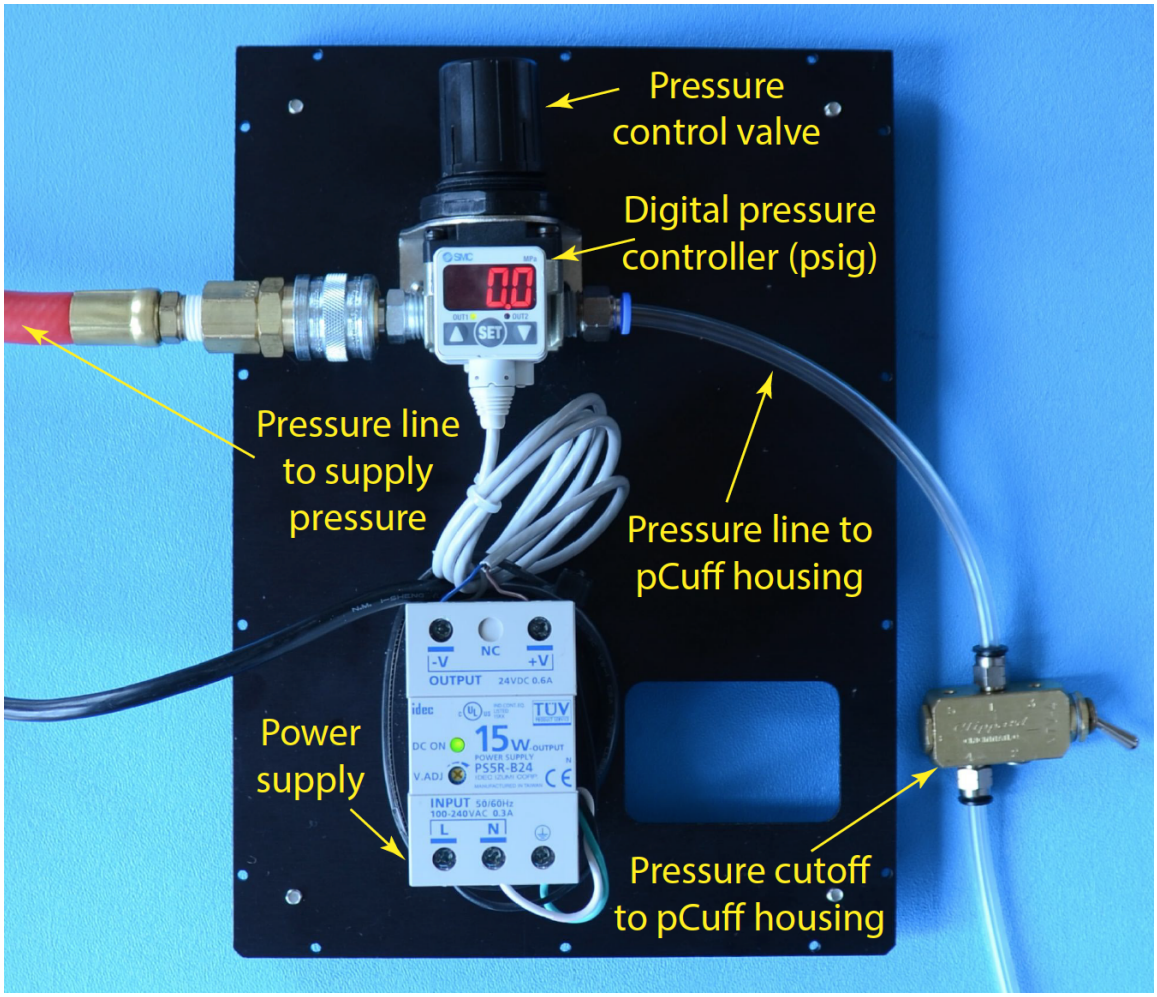

Figure 3.10: Pressure cuff pressure control system

The pressure control system is comprised of six main elements. Central to the control

system is the digital pressure controller. This pressure controller is a high precision digital pressure switch series ISE40, SMC Corporation of America, Noblesville, Indiana 46060, The stated set pressure resolution is 0.1 psi with a repeatability of ± 0.2% of full scale (145 psi). The high precision digital pressure switch uses the power supply for its power. The system also has a pressure control valve used to set the pressure supplied to the pCuff housing unit. The pressure control system is supplied with pressure (≤ 90 psig) by a red pressure line. The control system is outfitted with a pressure cutoff switch to the pCuff housing that enables rapid sample turn around times.

3.4 Pressure cuff measurement system

Friction tests were carried out on a MTS Synergie 200 apparatus equipped with a calibrated 50 N cell with an accuracy of 0.01%. The test system has software specifically designed for the acquisition of displacement versus force measurements. This software; TestWorks® 4, was programmed to pull the friction element at a rate of 0.5 inches per minute for a displacement distance of 0.5 inches. The pull rate and the distance were determined to give output in a short period of testing time while not sacrificing accuracy. The software displays the displacement versus force data in real time and additionally stores those data for later engineering review. An image of the test system is shown in Figure 3.11.

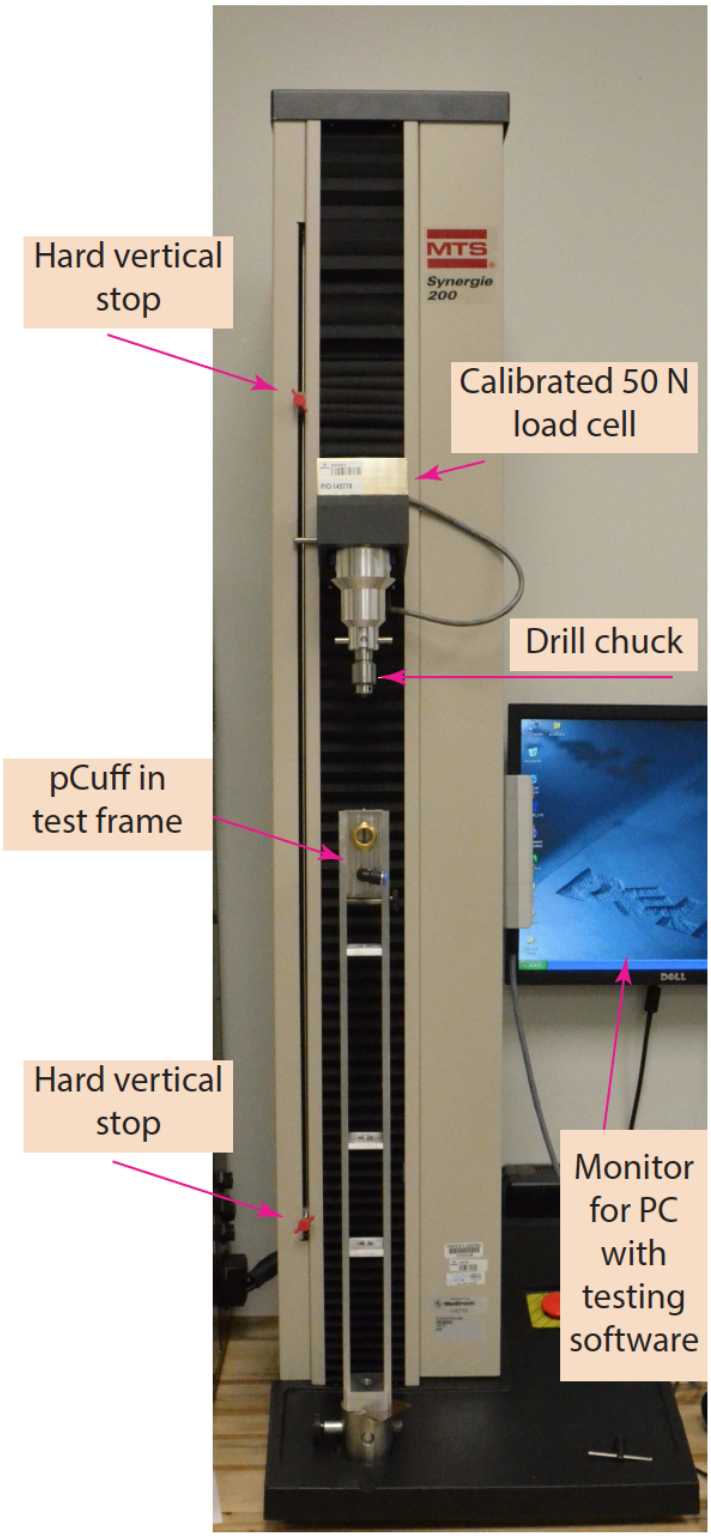

Figure 3.11: MTS Synergie 200 test system used for friction testing

The test apparatus has features that allow for rapid sample test turn around times. The features include a solid fixed in space test frame and a pressure cutoff switch to rapidly depressurize the system for new sample loading. The newly invented test apparatus can be used by anyone interested in determining the tubing bore lubricity of biomedical conduits or any other tubing that can be compressed.

4 The pressure cuff test method procedure

The procedure developed to test tubing bore lubricity is as follows:

1. Verify that the 50 N load cell is on the MTS test system and is within the calibration time window
2. Turn on the computer that has the TestWorks® 4 software and select the test method, "pCuff"
3. Mount the pCuff housing frame onto the MTS Synergie 200 test system and pin it to the test system base
4. Mount the Jacob's drill chuck to the test system and pin it into place
5. Power up the digital pressure control switch by plugging the system into a 110 VAC electrical outlet
6. Connect the supply air line to the pressure control system
7. Set the desired pressure using the digital pressure controller valve with the pressure cutoff switch off
8. While wearing latex or nitrile gloves, clean the friction element with heptane and lint-free cloth and allow to air dry.
9. While wearing latex or nitrile gloves, thread the friction element or tribo-partner down the axial center of the plasma-treated tubing sample
10. Insert the test sample assembly (sample and friction element) down the pCuff housing tunnel

11. Turn on the pressure cutoff switch to pressurize the pCuff housing (this secures the test sample assembly in place)

12. Adjust the digital pressure switch to the desired pressure set point

13. Place the pCuff housing with the test sample assembly into the pCuff frame and secure it with the thumbscrew bolt

14. Lower the Jacob's drill chuck down to the friction element and tighten the friction element in place

15. Zero out the load cell and the crosshead location

16. Start the test routine

17. After the test routine has been completed, cancel the cycle and reverse the loading procedure

18. If there are more samples to test, repeat steps 9 through 17

5 Summary

A newly invented test instrument has been constructed and detailed. The pressure cuff friction test method is both simple and rapid with test times from setup to setup of less than 2 minutes. The invention can be used for any tubing that is compressible with air-bladder and housing modifications.

Chapter 4

EXPERIMENTAL RESULTS FROM THE NEW FRICTION MEASURING SYSTEM

1 Introduction

After the design for the newly invented friction measurement system was completed, the customized components were fabricated. The system was then exercised and fine-tuned with regard to data extraction rates and displacements that delivered reliable friction measurement data. After the input parameters were set, the zero-force pressure offset was determined. This offset will be defined as the pressure set point that compresses the air-bladder and sample under test to the point where a normal force is just starting to be applied to the friction element. Once the zero-force pressure offset was determined, post-processing of the experimental data could be performed to extract the coefficient of kinetic friction. Subsequently, the system was employed to distinguish varying degrees of tubing-bore lubricity. The results from the experiments using the pCuff friction measuring apparatus are presented in this chapter with the conclusion that the new tribometer is an effective method to measure the bore lubricity of biomedical conduits.

Of major importance to the fidelity of the final results is ensuring that the effect of the air-bladder structural properties is fully resolved by the zero-force pressure offset. This issue can be dealt with if the zero-force pressure offset is determined before any set of measurements is to be made. The requirement that this offset be determined

must be imposed regardless if a previously used bladder is reused or if the bladder is changed as elected by the researcher. the S-shaped track torque test (using bend diameters of 1.00 and 1.25 inches and rotating a 0.036-inch diameter nickel alloy coil inside the plasma-treated tubing sample),

2 Zero-force pressure

To determine the pressure at which normal force is just starting to be imparted to the friction element, multiple measurements were made at pressure set points of 7, 11, and 15 psig. Figure 2.1 shows the measurements for these three pressure set points.

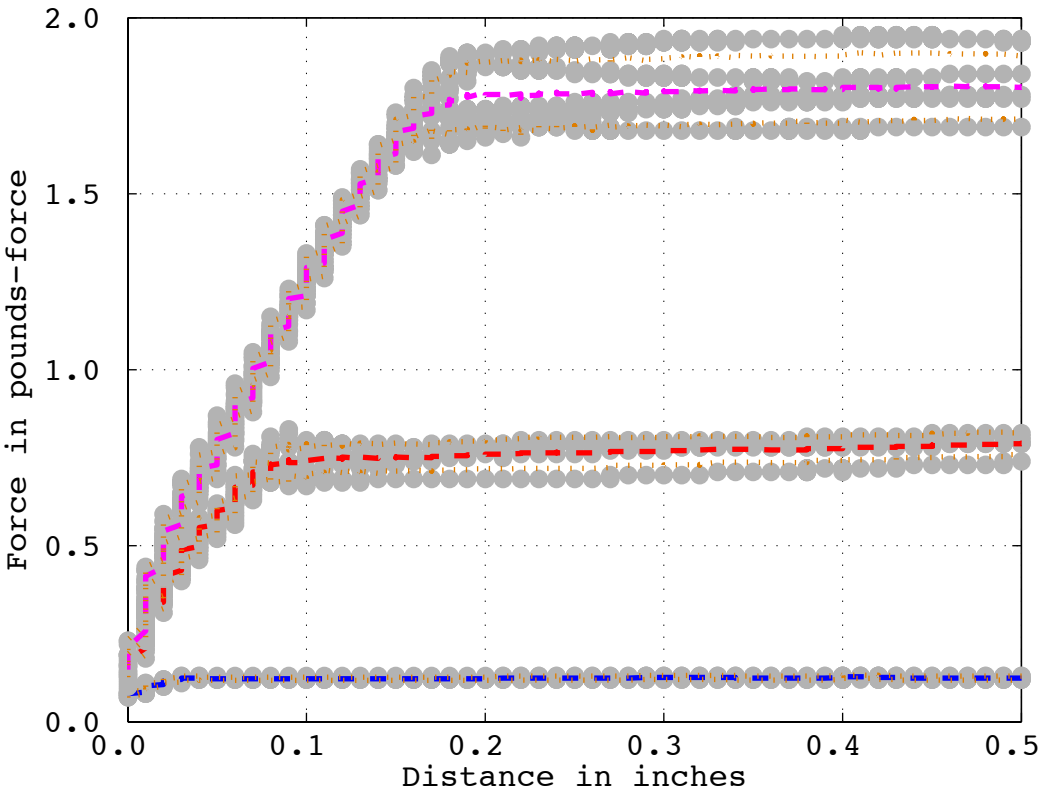

Figure 2.1: Distance versus force curves for five well-treated plasma samples at pressure set points of 7, 11, and 15 psig - dashed curve is the average of the data

The dashed curves of Figure 2.1 show the pull force as a function of the distance pulled for each of the pressure set points. The least force corresponds to the data collected at 7 psig lowest curve, the middle force corresponds to the data collected at 11 psig middle curve, and the most force corresponds to the data collected at 15 psig highest curve. The test protocol was to pull the friction element at a rate of 0.5 inches per minute for one minute. The data display a start-up pattern during which the force increases with pull distance, After the pull distance exceeds a few tenths of an inch, depending on the value of the set point pressure, the force data become more or less independent of distance, During the start-up period, static friction effects are still existent, but these effects disappear when the force no longer depends on distance. The attainment of constant-force operation occurs at longer pull distances as the pressure set point value increases.

The force data extracted from the constant-force operating region of the foregoing graphs have been plotted as a function of the pressure set point in Figure 2.2. A linear fit was applied to the data as shown in the figure, The straight line was extrapolated to the zero-force intercept.

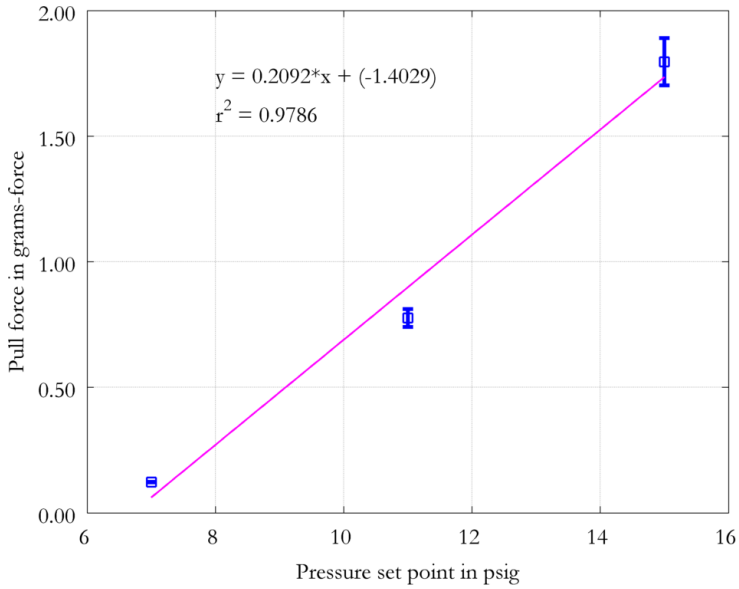

Figure 2.2: Pull force as a function of set point pressure

The intercept on the pressure-set-point axis was found to be 6.7 psig. This tare value was subsequently subtracted from the pressure setting to arrive at the actual force imparted to the friction element.

3 Pressure cuff sensitivity capability

As a means to assess the sensitivity of the test method in discerning various levels of plasma treatment, material taken from different treatment levels was evaluated. The material came from four different and purposefully modified plasma treatment levels. For these experiments, the pressure set point was 15 psig, and the pull rate was set to 0.5 inches per minute for a total of two minutes. Box plots of the data taken from the plateau region of the force vs. displacement curves show that the test method can definitively discriminate among varying degrees of plasma treatment. Figure 3.1 shows the box-plotted data with some statistics from each treatment level.

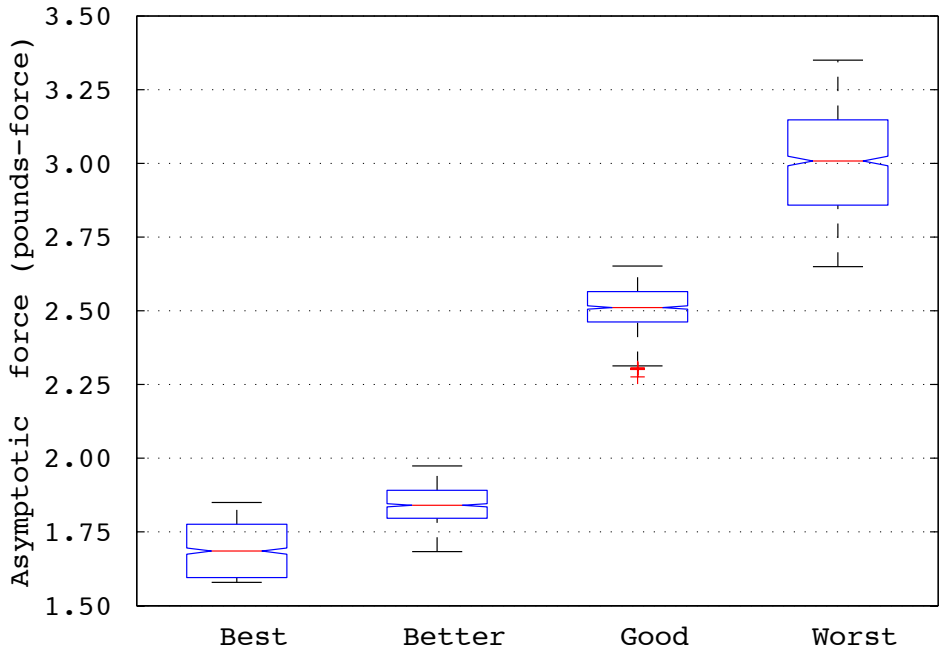

Figure 3.1: Box plot showing the discriminatory capability of the new friction test method

The box-plotted data on the far left of the plot are taken from material treated at the "Best," condition, which is the current plasma-treatment process. The "Better", "Good," and "Worst" treatment material correspond to Sections #5, #3, and #2 previously described in Chapter 2.

4 Extraction of sliding coefficients of friction from pressure cuff measurements

To illustrate the method of coefficient-of-friction (COF) extraction from the information collected by the pressure cuff, the data from the four populations of plasma-treated tubing shown in Figure 3.1 will be used. By use of the previously determined zero-force pressure of 6.7 psig, the applied pressure to the friction element is 8.3 psig for all cases. The area being pressurized is simply the diameter of the friction element (0.0405 inches) multiplied by π and by the length of the compression zone (2.47 inches). The normal force imparted to the friction element is the pressurized area (0.314 in^2) times the applied pressure (8.3 psi). The computed normal force is, therefore, 2.61 pounds-force, and the tangential force averages change with plasma-treatment level and are taken directly from the MTS test system's software. The coefficient of kinetic friction for this system is defined as the ratio of the tangential force to the normal force. Table 4.1 shows the needed inputs and final extracted COFs for each treatment level.

Table 4.1: Extracted coefficients of friction for various plasma-treatment levels of sample tubing

Treatment (category)	Normal force (pounds-force)	Tangential force (pounds-force)	Coefficient of friction (dimensionless)
Worst	2.61	3.59	1.40
Good		2.64	1.01
Better		1.98	0.76
Best		1.73	0.67

The data shown in Table 4.1 confirm that variation in plasma treatment levels are easily discriminated using the newly invented pressure cuff tribometer.

5 Summary

This tribometer has been proven effective and is a viable method of measuring lubricity for viscoelastic biomedical conduits. The fact that coefficients of friction can be extracted from the pressure cuff data makes the information more valuable and more standardized than having merely comparative pull force resistance numbers from various lubricity tests.

Chapter 5

RUNNING-IN BEHAVIOR OF INTERNALLY PLASMA-TREATED SILICONE TUBING

1 Introduction

Plasma treatment that modifies silicone-tubing surfaces is used to reduce tackiness both on the inner and outer surfaces. For the inner surfaces, several test methods used to measure the effectiveness of the treatment have been described in Chapter 2. The historical "U-bend" test data exhibit test-order sequence effects, with early measurements in the sequence tending to be higher and more variable while later measurements tend to be more stable, lower in force values, and more consistent. This behavior can be referred to "running-in." Surface analyses presented in the present chapter suggest that the nickel alloy friction-sensing element used in the measurement is being conditioned by picking up a very thin layer of silicon-rich material from the tubing during use in earlier tests. Note that the nickel alloy friction-sensing element is a coil similar to the one shown in Chapter 2, Figure 2.3. A different method of promoting conditioning of the friction elements that was explored was to store the friction elements inside treated tubing when not in use. Once friction elements are conditioned, variation in the measurement outputs due to the coil and test operator are reduced while the test retains its sensitivity. This behavior is also discussed in this chapter. Here, the running-in effect is documented for the new measurement system, and countermeasures are described and implemented. Recommended countermeasures going forward are storing the friction elements in

treated tubing when not being used for testing and verifying the conditioned state of the friction elements before beginning a test session. The storage method for the friction elements is to insert the elements into plasma-treated tubing with little clearance (on the order of 0.007 in.) between the outside diameter of the friction element and the inside diameter of the treated tubing. This close proximity between the surface of the friction element and the surface of the tubing would allow for easy transfer of the silicon-rich material.

2 Empirical evidence of running-in behavior

Tube-bore lubricity data collected from samples taken from tubing conditioned during six routine batch runs to produce tubing to be used in actual products. Data from these samples were plotted according to test sequence order. The data show that the force (directly related to friction) displays a transient effect. The initial measurements tended to be higher and more variable while the later measurements stabilized and plateaued out. The Z-score (a method to normalize the force values from run to run) of an observation Z_i is defined as

$$Z_i = \frac{X_i - \bar{X}}{s} \tag{1}$$

Equation (1) symbols X_i, $\bar{X}$, and s denote an individual data point, the sample mean, and the sample standard deviation respectively. In other words, data is given in units of how many standard deviations it is from the mean [19]. Figure 2.1 is a plot showing the force Z-score arranged according to the test sequence. The figure consists of six graphs, each of which relates to samples taken from a single batch production run of approximately 2500 feet. From each production batch, 14 never-before-tested samples were extracted and each sample was measured with regard to the resistance force (using the U-bend test method).

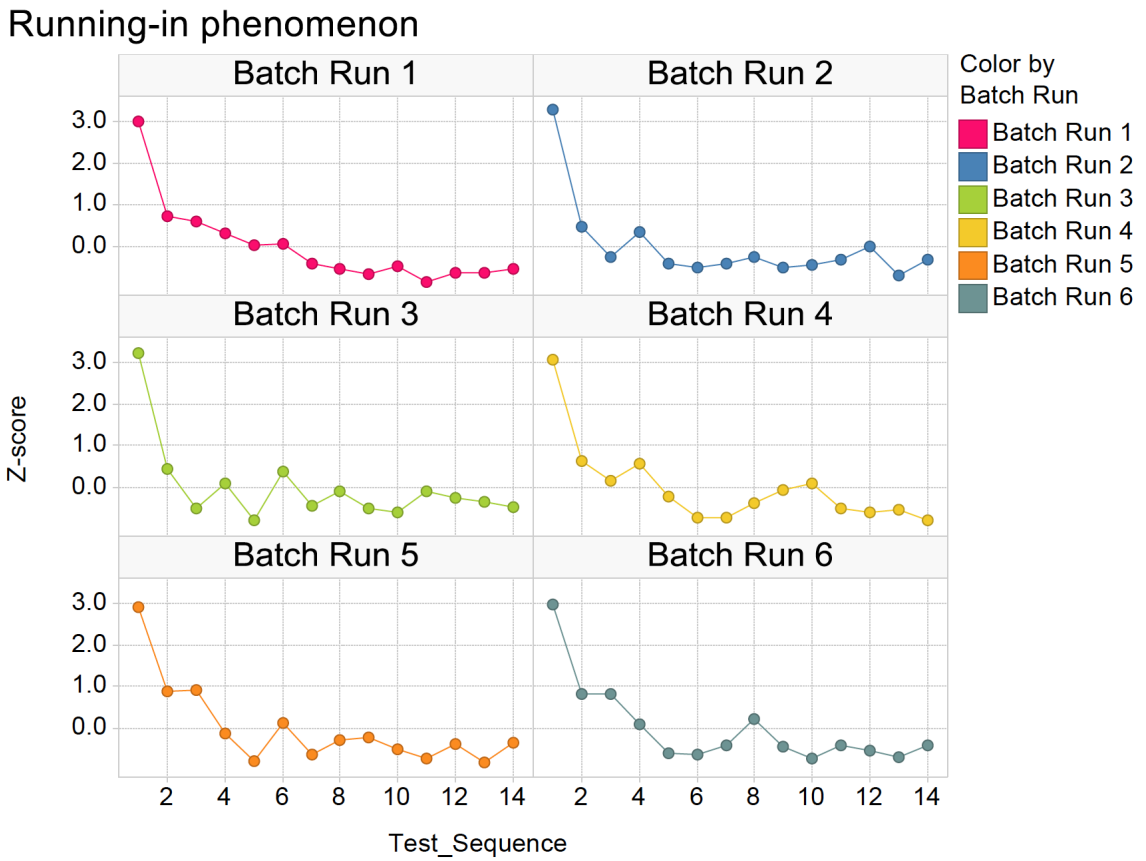

Figure 2.1: Tubing bore lubricity data arranged by test sequence order

The data correspond to three different test operators, indicating that the results are not test-operator-dependent behavior. The data have a generally downward trend until after 7 to 11 tests have been performed, at which point the force required to pull the coil through the plasma-treated silicone tubing sample plateaus out.

3 Reproducibility of running-in behavior

The just-displayed friction running-in effect can be shown to be reproducible. Two friction elements were used for the validation experiment. One of the friction elements came from pristine, “never-before-used” coil stock, and in contrast, the other one had been extensively used for lubricity testing. Plasma-treated tubing from two processing runs with identical input parameters was used. Tubing samples from each of

the two process runs were cut to length and randomized, with the goal to have the participating tubing be equivalent across the runs, or at least randomly distributed to eliminate sample selection as a significant factor. A single test operator performed all of the friction measurements. This was done such that any unique effects due to the performance of single test operator would show up in the global data set. Finally, 10 measurements were made with each of the friction elements, with randomized test-order sequencing using commercial statistical software, Minitab. Each measurement was performed on silicone tubing that was freshly cut from the processing run (never before tested). The results extracted from the U-bend tests are shown in Figure 3.1.

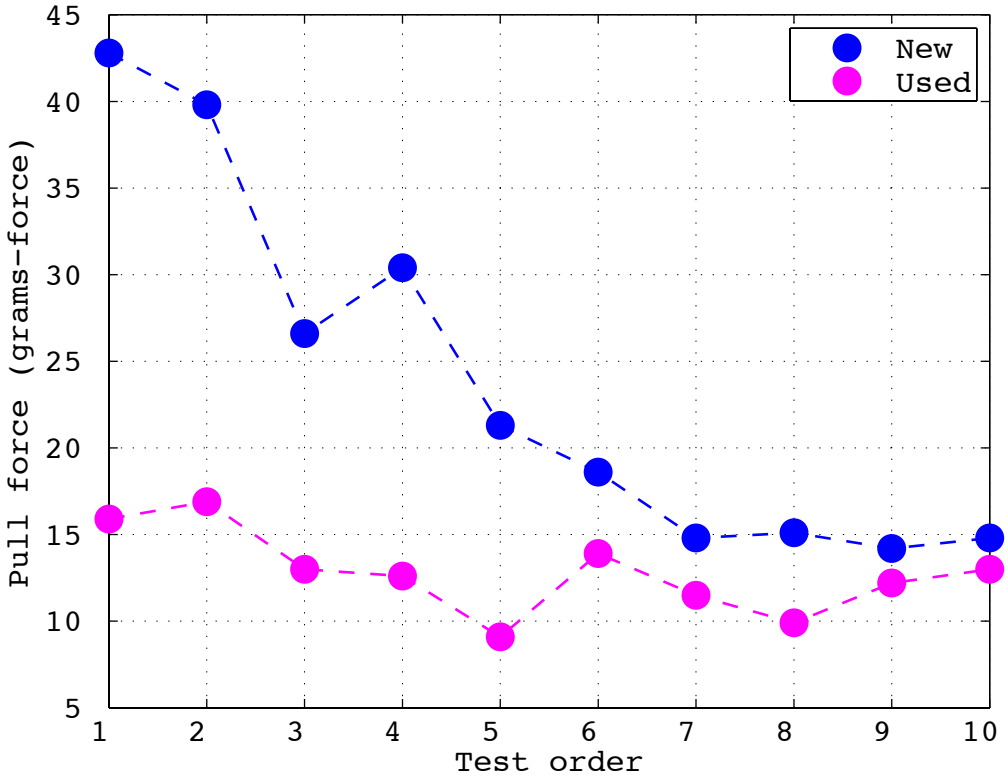

Figure 3.1: Test results contrasting a new and a used friction element

The data associated with the new coil of Figure 3.1 exhibit marked test-order sequence effects, with early measurements in the sequence showing resistance forces in excess of 40 grams-force and steeply dropping with test sequence order. The new coil

resistance data drop down to approximately 14 grams-force after the sixth test and stabilize at that value. Note that the data range for resistance forces gathered using the new coil is 14 to 43 grams-force. In contrast, the coil that had been used extensively prior to the test data collection showed much less variability in the resistance force (ranging from 9 to 17 grams-force) and stabilized after the second test.

The data shown in Figure 3.1 reinforce the point that the condition of a pristine, "never-before-used" friction element changes (top curve) with repetitive use and eventually stabilizes while a friction element that had been extensively used does not show nearly as much variation (bottom curve). For the new friction element, the pull forces are generally higher and more variable for the initial tests, while after some use, the values become lower and more stable. This finding suggests that there is something affecting a new pristine measurement coil after repeated usage. The end result is a coil that has become conditioned. The outcome shows that this conditioning is necessary to get stable and reproducible tribological test results. It is speculated that the surface chemistry of the measurement coil changes until it reaches an equilibrium state.

The running-in behavior and the conditioning of the friction element are not necessarily a single event; rather, the running-in behavior can recur. To illustrate this point, friction elements that had been used and then left idle for more than two days were employed in testing samples from the same sources as those tested for the data of Figure 3.1. As a basis of comparison, the recently used and conditioned (not idled) friction element was employed. Pull force data from the experiment are presented as Figure 3.2.

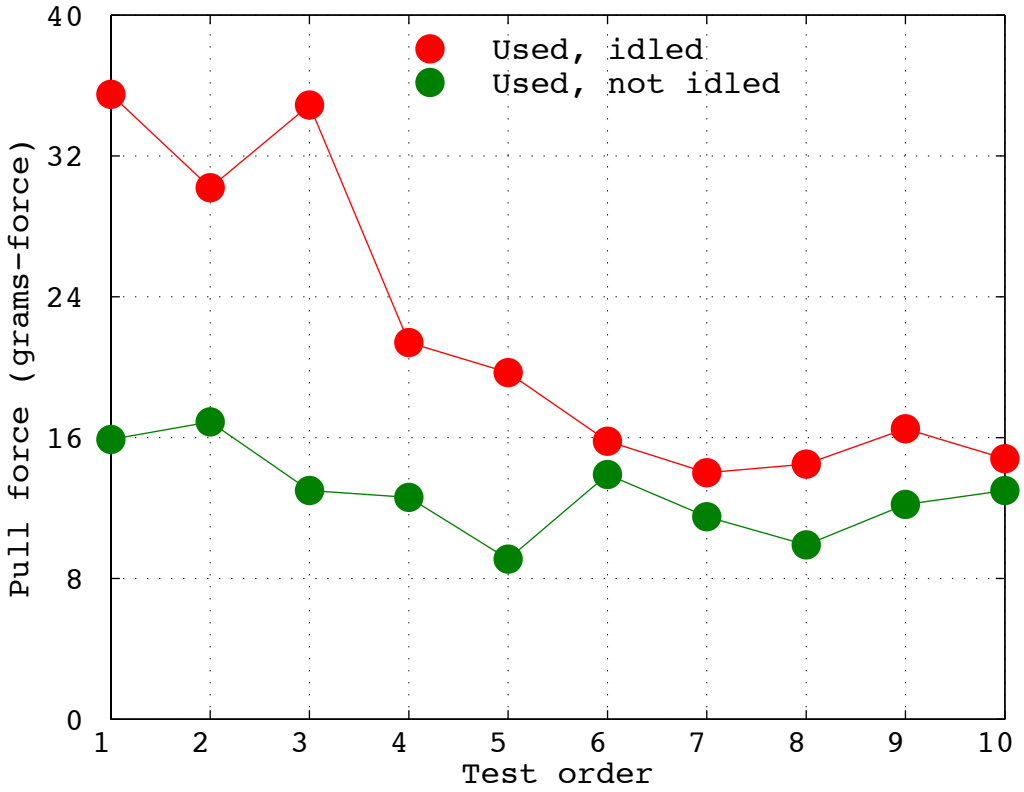

Figure 3.2: Test results showing the contrast between a used and idled friction element versus a used and not idled (conditioned) friction element

The data of Figure 3.2 show that coil can become "un-conditioned", as the used but left idle coils are still subject to this effect (top curve), though apparently to a lesser degree than with a new pristine, "never-before-used" coil (bottom curve). The conjecture is that a thin layer of silicon-rich material is being transferred to the coil as it passes through the tubing and coats the friction element. Further, this coating is needed to stabilize the interaction between the nickel alloy coil and the silicone rubber surfaces and result in more repeatable testing outputs.

4 Diagnostics

To better understand the mechanism of the running-in effect shown in the previous

two sections, surface analysis measurements were made on the coils or friction elements. Two surface analysis techniques were used for this work: X-ray Photoelectron Spectroscopy (XPS), also known as Electron Spectroscopy for Chemical Analysis (ESCA), and Time of Flight Secondary Ion Mass Spectrometry (TOF-SIMS). The results from the first technique (XPS) will be presented first, followed by the results from the second technique (TOF-SIMS).

A survey spectrum to characterize all elements present (except hydrogen) is first acquired from each sample. The spectra are used to obtain quantitative surface composition by integrating the areas under the photoelectron peaks and applying empirical sensitivity factors. High-resolution spectra can also be acquired for elements identified in the survey spectra. The high-resolution scans can reveal binding energy shifts, which often contain useful chemical information. The depth of analysis of this technique is on the order of 75Å.

Coils that had three different histories were used for the surface analyses. The coils used for this study are made from a nickel alloy, are unifilar in construction, and are nominally 0.036 inches in diameter. The three histories of the submitted coils are as follows: (a) a brand new, pristine, “never-before-used” coil, (b) a coil that was exercised through multiple testing cycles, (c) and a brand new pristine coil that was stored for a week in plasma-treated tubing but had never been used for friction testing. For convenience, the (a) coil will be designated as “pristine”; the (b) coil will be referred to as “exercised”; and the (c) coil will be identified as “stored”. The XPS spectra from the three coil samples are shown in Figure 4.1, and the data for the important to the material transfer hypothesis marker elements of carbon, oxygen, and silicon from the XPS analysis are listed in Table 4.1.

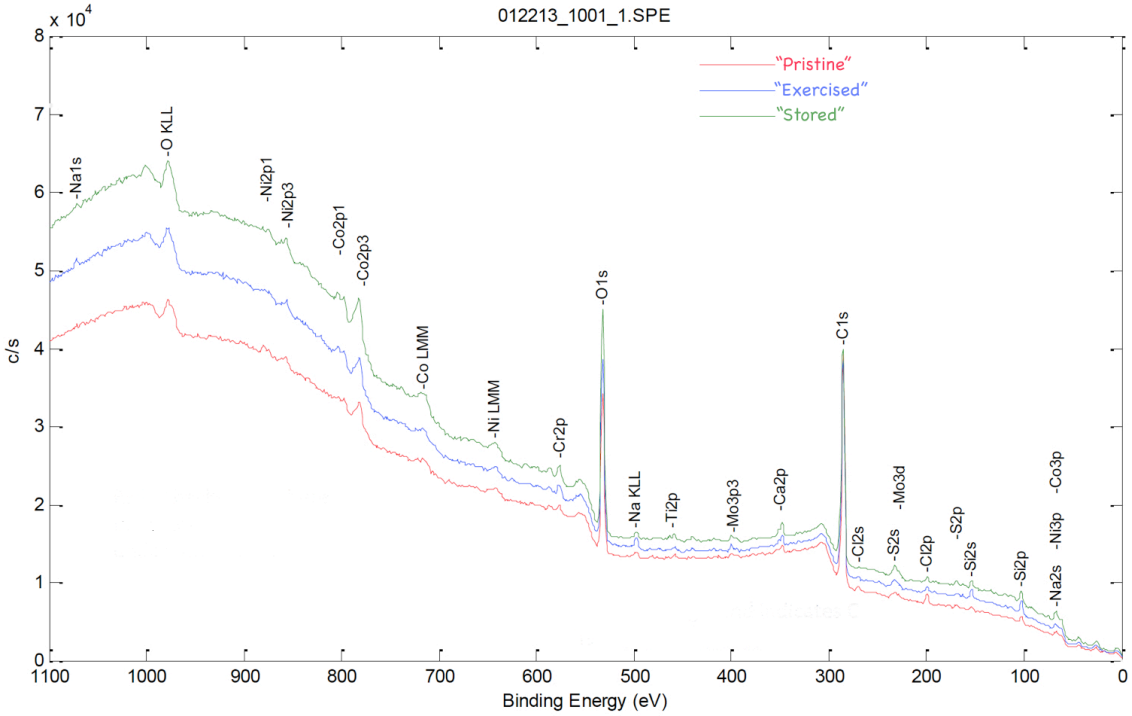

Figure 4.1: XPS spectra from the coil samples

Table 4.1: Part 1 - The surface chemistry for the pristine coil as measured by XPS

Coil category	Atomic weight % of carbon	Atomic weight % of oxygen	Atomic weight % of silicon
"Pristine" coil	71.2	22.2	2.0
	69.5	23.5	1.9
	66.4	25.6	2.2
	65.8	26.5	2.2
	64.9	26.8	2.1
Average	**67.6**	**24.9**	**2.1**
Standard Deviation	**2.7**	**2.0**	**0.1**

Table 4.1: Part 2 - The surface chemistry for the exercised coil as measured by XPS

Coil category	Atomic weight % of carbon	Atomic weight % of oxygen	Atomic weight % of silicon
"Exercised" coil	66.3	24.9	3.4
	65.8	25.5	3.5
	64.1	27.2	3.6
	65.8	25.5	3.6
	65.4	26.0	3.8
Average	**65.5**	**25.8**	**3.6**
Standard Deviation	**0.8**	**0.9**	**0.2**

Table 4.1: Part 3 - The surface chemistry for the stored coil as measured by XPS

Coil category	Atomic weight % of carbon	Atomic weight % of oxygen	Atomic weight % of silicon
"Stored" coil	62.1	28.1	3.0
	61.0	29.1	3.1
	60.4	29.8	3.2
	59.1	30.5	4.0
	59.8	29.9	3.3
Average	**60.5**	**29.5**	**3.3**
Standard Deviation	**1.1**	**0.9**	**0.4**

The information conveyed in Figure 4.1 and reinforced by Table 4.1 contains a great amount of information. The high atomic weight percentages of carbon indicate that all samples are largely masked by carbonaceous material, implying that there is some foreign material at the surface. This could be due to the plastic bags in which they are contained or from previous manufacturing or handling steps. From the standpoint of the present significance, it is the silicon data that are of major significance. For the silicon, a one-way ANOVA evaluation was performed for each of the coils with regard to the respective atomic weight percentages of the marker elements. For the pristine, exercised, and stored, the atomic weight percentages were 2.2, 3.6 and 3.3 respectively. The

importance of this outcome is that the silicon content is the major factor in causing the running-in phenomenon.

Table 4.2: One-way ANOVA summary for silicon from the XPS studies and direction of the difference

Coil	Silicon
"A", pristine	Low
"B", exercised	
"C", stored	

ANOVA specifically illustrates that the there is a large difference is for the silicon level in the exercised and stored samples relative to the pristine sample. Of most interest for this study is the lower level of silicon found in the pristine sample relative to both the stored and the exercised sample.

The one-way ANOVA test indicates that the amount of Si measured at the surface is statistically significantly different at the 99% confidence level. The practical significance of this mean shift can be recognized when it is envisioned what a monolayer of silicone oil would look like from the perspective of XPS. It can be shown that for a homogenous material, approximately 10% of the non-scattered photoelectrons come from the top monolayer of atoms. The coil samples have a significant amount of carbon on them which can be roughly approximated as a homogenous organic material. This would mean that 10% of the non-scattered photoelectrons are coming from the top monolayer of atoms. Discounting hydrogen (not seen using XPS), the theoretical composition of silicone is 50 at% C, 25 at% O, and 25 at% Si. If silicon were used as the unique marker for silicone oil, then a continuous monolayer of silicone oil would result in approximately a 2.5 at% silicon level (10% of non-scattered photoelectrons from top monolayer of atoms times 25 at% Si = 2.5 at% silicon). The new coil has silicon levels below this and, furthermore, there is no guarantee that the atomic silicon seen on the pristine coils is even

silicone related as it had never touched silicone tubing. By looking at the box plot of Figure 4.2, it is obvious that the pristine coil data set is lower than the other two coils.

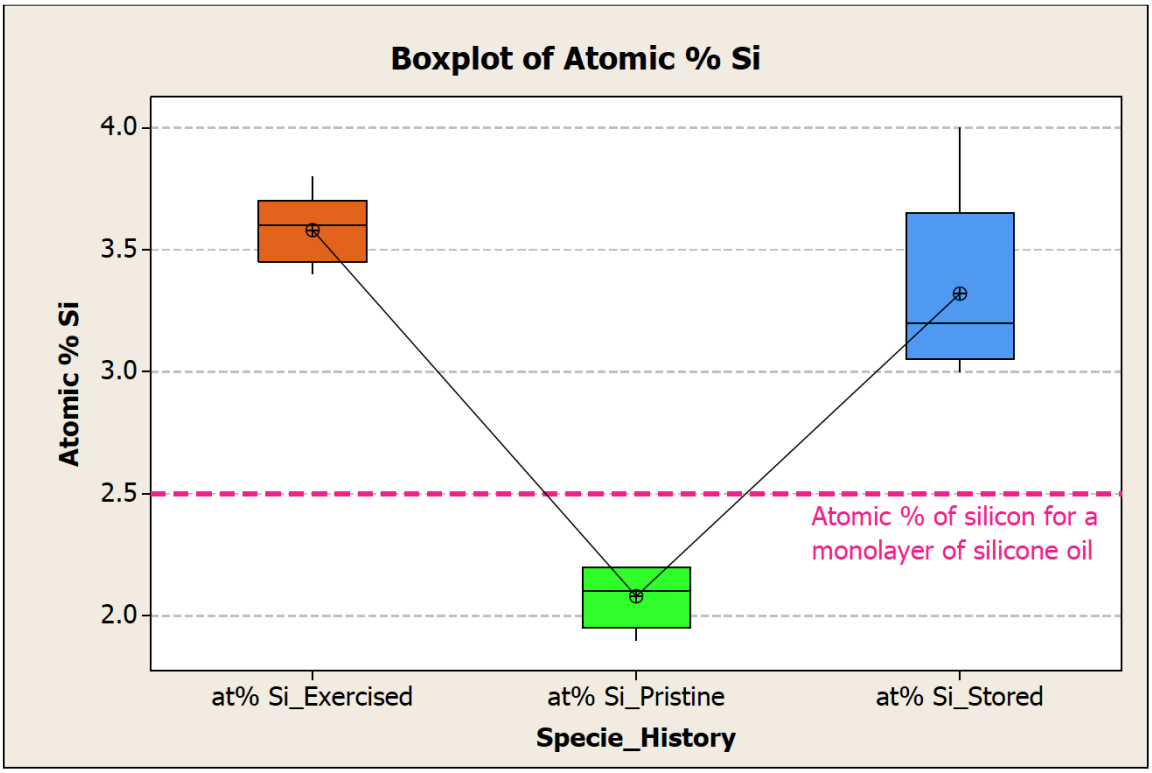

Figure 4.2: Box plot of atomic % silicon as measured by XPS for each coil sample with the atomic percentage of silicon for a theoretical monolayer of silicone oil shown as a dashed line

The Figure 4.2 shows a box plot of the atomic percent of silicon measured at the surface of each coil, using the five data points shown in Table 4.1. To highlight the silicon atomic weight percentage differences between the different coils, a theoretical monolayer at% silicon level has been overlaid on the plot. The box plot clearly shows that the two coils that had been exposed to plasma-treated tubing have at% Si levels above this theoretical monolayer threshold. This can indicate at least two things: (a) the increase in Si due to exposure to the tubing likely means that silicone-like species have been transferred to the coil and (b) the levels seen are sufficient to create a full monolayer. It is worth noting that the XPS data are consistent with a full layer, but it is not conclusive because it is not possible to tell the difference in this case between a

continuous layer and material coalesced in islands.

A corroboration of the foregoing findings is provided by Time-of-Flight Secondary Ion Mass Spectrometry (TOF-SIMS). In this methodology, an ion beam is used to probe the sample surface, and secondary ions from the sample itself are measured. The time-of-flight analyzer allows the mass of the secondary ions to be detected, from which elemental and molecular information can be determined. The primary ion beam flux is limited so that only the uppermost monolayer (~20Å sample depth) of the sample is probed. TOF-SIMS uses a pulsed primary ion beam is used which generates secondary species. The majority of the species emitted are neutral; however, a small percentage comes off as either a positive or negative secondary ion. These secondary ions are then conveyed to an analyzer by a high voltage potential, and their mass is determined by measuring their time-of-flight from the sample to the detector. The mass spectrum and secondary ion images can then be used to obtain compositional information [20].

The qualitative results from the TOF-SIMS analysis are complementary to the foregoing XPS data interpretation and are seen in Table 4.3. In this table, the designations S, M, W, and VW mean that the signal was Strong, Medium, Weak, or Very Weak.

Table 4.3: TOF-SIMS surface chemistry output with silicon, polydimethylsiloxane (PDMS), and low molecular weight (MW) hydrocarbons

TOF-SIMS analysis	**Pristine**	**Exercised**	**Stored**
Si	W	M	S
PDMS (73, 147, 207 etc.)	VW	VW	W
Low MW hydrocarbons	VW	W	W

It is worth mentioning that TOF-SIMS is not a quantitative technique, but it is still appropriate to compare relative peak intensities for similar samples. For the data shown in Table 4.3, the TOF-SIMS signals for Si, polydimethylsiloxane (PDMS, the constituent polymeric backbone of silicone), and low molecular weight hydrocarbons are weak to very weak for the pristine coil that had not been exposed to tubing. For the coil that was stored in tubing, the intensity of both those signals increased, indicating that more silicone oil was on this sample as compared to the pristine coil. The exercised coil saw a

more moderate increase in the Si signal and not a remarkable increase in PDMS signal compared to the new coil. This finding may be consistent with the behavior seen during testing; that is, that an idle coil still needs to be reconditioned before it gives stable results. However, the needed reconditioning is less than for the idle coil. PDMS is known to be highly mobile, as it is observed with TOF-SIMS as a contaminant on a large number of historical samples. It is likely that the PDMS that is on the outer surface of the coils would migrate over time to the inside of the coils and to the container in which the coils are stored, resulting in surfaces with lower PDMS concentrations. This may explain the reconditioning effect as the tubing re-supplies the PDMS that had migrated away from the outer surface of the coil.

5 Pre-conditioning of a coil

The foregoing analyses indicate that there is an opportunity to reduce the variability in the friction results. There are several benefits of doing this, including increased reliability on determining the acceptance or rejection of plasma-treated tubing for tubing bore lubricity. This increased reliability would apply to an entire portfolio of plasma-treated silicone tubing products. As a method of increasing the testing reliability, the concept of housing the coils inside the bore of plasma-treated tubing was investigated. Using this storage method helps to pre-condition the friction elements and reduces test time as it reduces the actual conditioning time. To quantitate the efficacy of this approach, plasma-treated material was again cut and randomized for U-bend testing. The test sequence order was randomized as well. Three coils were utilized for the experiment. The first coil was a new, pristine, never-before-used one. The second coil was an exercised and conditioned coil (i.e., it had been used). The third and final coil started as a new, pristine coil; however, this coil was inserted into a length of plasma-treated tubing for a number of days prior to its use.

The output from the pristine, never-before-used coil showed running-in effects and did not stabilize until after at least 17 test cycles as seen the upper tier of Figure 5.1. A

moving range chart is displayed in the lower part. The figure shows the changing nature of the resistance force readouts with observation order. An I-MR chart is an Individuals chart and Moving Range chart in the same graph window. The Individuals chart is drawn in the upper half of the screen; the Moving Range chart in the lower half. Seeing both charts together allows tracking of both the process level and process variation at the same time, as well as detect the presence of special causes [21]. The pristine coil used to test silicone tubing generated erratic readings until about 17 test cycles. The mean for the testing was 22.8 grams-force and the moving range average was 7.9 grams-force.

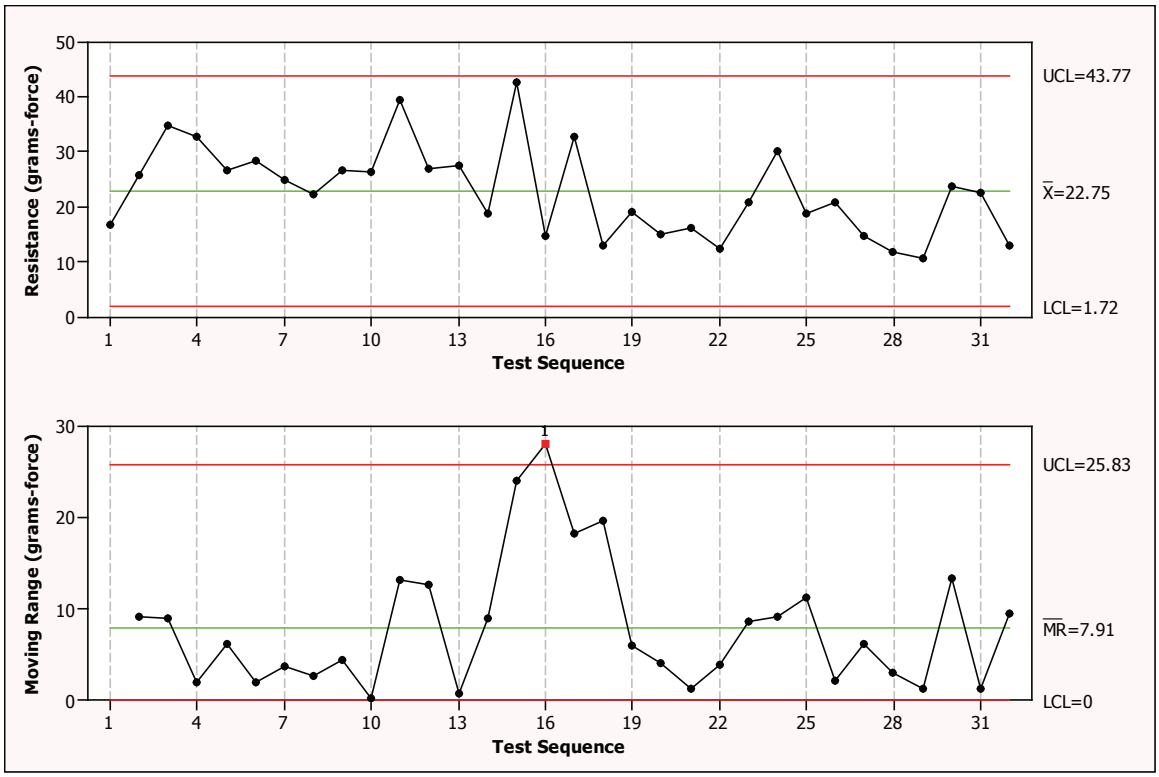

Figure 5.1: Individual Moving-Range plots for changing resistance force as gathered by using a new, pristine friction element

To contrast the data of Figure 5.1, the conditioned and the stored coil results are exhibited in Figures 5.2 and 5.3. The exercised and conditioned coil generated relatively consistent measurements almost immediately, and the data are seen to range much less than the data shown in Figure 5.1. A separate I-MR plot of the resistance data by test

sequence for the exercised and conditioned coil is shown in Figure 5.2. The exercised and conditioned coil used to measure the resistance force of plasma-treated tubing appears very repeatable with a low moving range. The mean value for the testing was 14.0 grams-force with a moving range average of 3.3 grams-force.

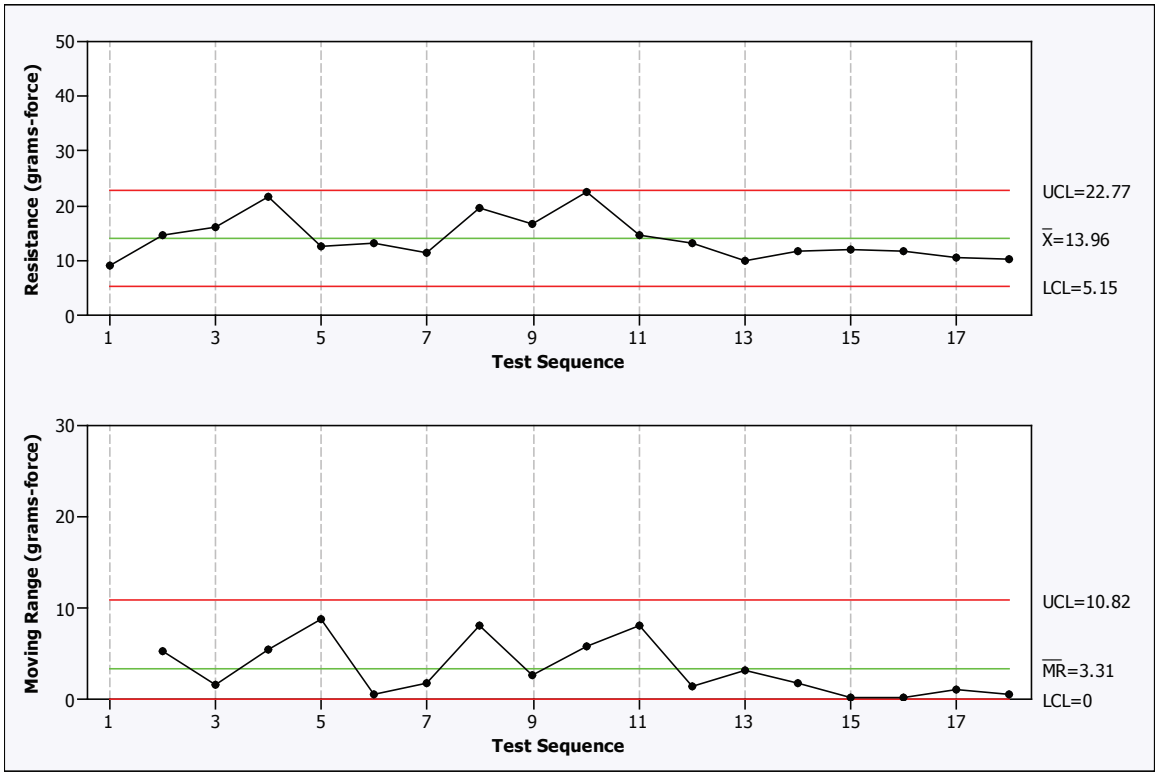

Figure 5.2: Individual Moving-Range plots for fairly stable resistance forces as gathered by using an exercised, conditioned coil

Similar to the exercised and conditioned coil, the "stored in plasma-treated tubing bore" coil generated relatively consistent measurements almost immediately. An I-MR plot of the resistance data by test sequence for the stored in tubing coil is shown in Figure 5.3. The stored in tubing coil used to measure the resistance force of plasma-treated tubing also appears very repeatable with a low moving range. The mean value for the testing was 15.0 grams-force with a moving range average of 2.9 grams-force.

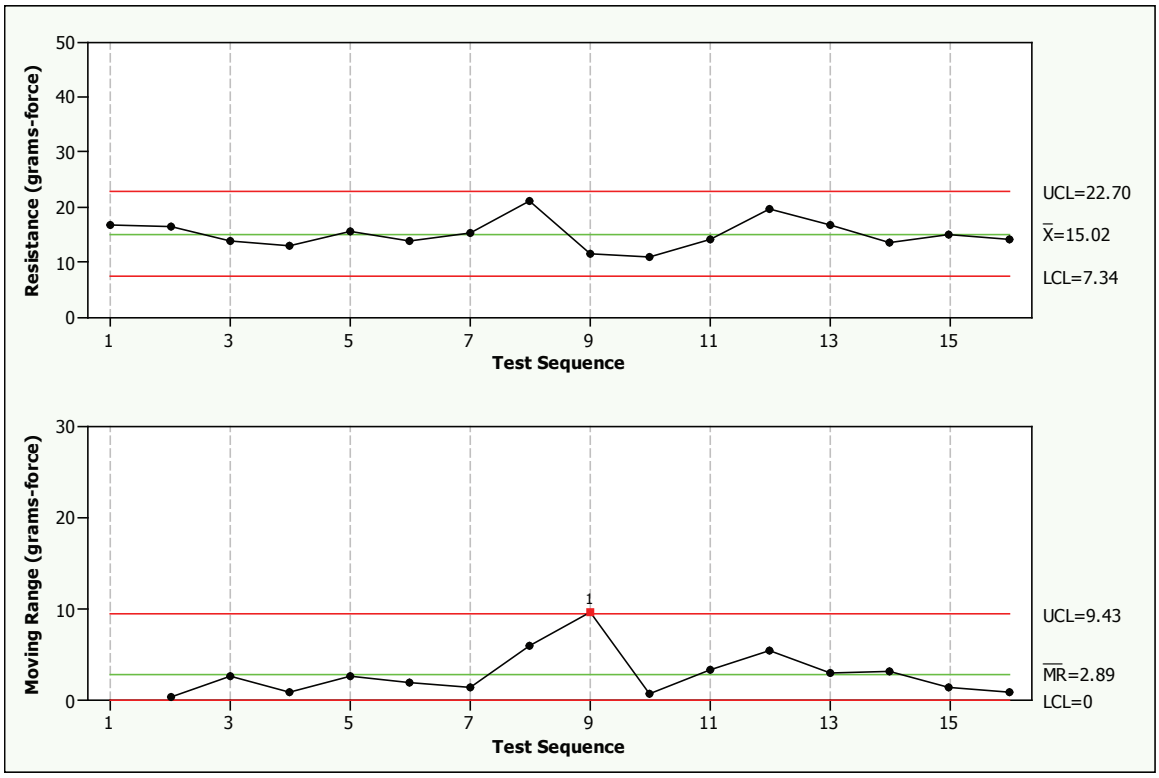

Figure 5.3: Individual Moving-Range plots for fairly stable resistance forces as gathered by using a coil that had been stored in plasma-treated tubing

The data presented in this section point to the efficacy of storing the coils inside of plasma-treated tubing. This type of storage could keep the coils in a pre-conditioned state and would minimize the running-in effects and lead to more stable resistance measurements.

6 Discussion

The running-in phenomenon, crucial to the measurement of the lubricity of biomedical transporting tubing, has now been understood and methodology devised for eliminating the uncertainty. The phenomenon can be understood in the framework of the plasma-treated tubing transferring material to the coils, with low molecular weight silicone oil containing PDMS constituents as the most likely species. This PDMS would act as a lubricant in the system, enabling consistent and repeatable behavior. This

lubricant does not degrade the sensitivity of the test; rather, it is an essential and inevitable feature of the test. The measurement coil will necessarily take up this material during use. This understanding is applicable to measurements that are made with media using conditioned coils. It is important that the conditioning is maintained prior to friction evaluation. Data suggest that a possible method of accelerating the conditioning of the coils is storing them in treated tubing. It is recommended that the test coils be stored inside the bore of plasma-treated tubing and that the degree of conditioning be verified before beginning lubricity measurements.

Chapter 6

CONCLUDING REMARKS AND DISCUSSION

1 Introduction

This final chapter summarizes the accomplishments of the thesis. The motivating need for the research is the enhancement of biomedical therapeutic devices, but the outcomes have a broader utility in applications where lubricity is an issue, Available techniques of tube-bore lubricity assessment techniques are reviewed and critically evaluated. Intrinsic flaws in these techniques are revealed by in-depth diagnostics. In particular, running-in behavior, a major flaw, is carefully documented and methods to eliminate it altogether are developed, A major outcome of the work is the invention and implementation of a new tribometer having manifold applications.

2 Summary

Chapter 1 highlights the goals of the research activity and the great importance of beneficial tribological coatings for biomedical conduits. The chapter sets forth methods of friction reduction on biomedical conduit surfaces and explains the need for a tribometer to gauge the degree of that reduction, A plasma treatment process that modifies silicone rubber tubing on both the tubing exterior and tubing bore surfaces is described in detail. Key plasma treatment process inputs are reviewed. Chapter 1 goes on to shed light on different friction-reducing coating characteristics and some important methods of friction characterization. As macroscale friction

characterization is central to this work, different methods of measuring friction on tubing exterior and tubing bore surfaces are reviewed. There is little in the literature regarding tubing bore surface friction characterization; however, three methods were identified: (a) the 360° pull test method, (b) a torque tribology test, and (c) a reciprocating balloon test method. All of these methods found in the literature were comparative in nature and none of them enables the determination of the coefficient of friction. This chapter contains some discussion on nanoscale coating characterization instruments used for morphological and elemental surveys and concludes with how surface coatings can be evaluated.

Chapter 2 reinforces the requirement for lubricious biomedical conduits and goes into depth regarding a well-established venerable tubing-bore lubricity test method, the U-bend method, The shortcomings of that method are quantitatively documented. A new method to evaluate tubing bore lubricity, the straight-groove torque test method, is introduced, described, and implemented. The nature of the underlying physical process for the traditional and new methods are majorly different from each other. The U-bend test is used to collect pull-force resistance data, and the straight-groove torque test is used to measure torque resistance. A gauge study demonstrated that the U-bend test does a poor job of assessing process performance and cannot be used to sort good parts from bad parts. Contrasting to this, a gauge study of the straight-groove torque test indicated that this method is superior to the U-bend test both for assessing process performance and for sorting good parts from bad parts. In this chapter, force models for a straight- (or linear-) grooved torque test and a tight-bend radius (or curvilinear-) grooved torque test are developed and evaluated. A means of selection of an appropriate diameter and material for the friction element was developed using sensitivity data. Overall, the linear-grooved torque test was found to be superior to both the venerable U-bend method and the curvilinear-grooved torque test when considering ease of setup, implementation, gauge studies, sensitivity, and operator-independence.

Chapter 3 focuses on a new invention used to characterize the lubricity of biomedical conduits. The method uses a pressure cuff or air-bladder to compress a plasma-treated silicone tubing sample onto a friction element. The invention sets up a metal sliding-friction element/silicone tubing system. The tubing is stationary while the friction element that has been inserted into the tubing bore is pulled. The tubing is held stationary with a known and regulated pressure, which allows the user to infer the normal force pressing on the sliding component. The pull force (tangential force) is registered and recorded using a commercial pull-test frame. Knowing the normal and tangential forces means that the coefficient of friction for the system can be extracted using this instrument. The key components are described in depth in this chapter, and the procedure to use the instrument is documented.

Chapter 4 documents the experimental results performed using the pressure cuff friction tester. One of the first tasks was to determine the zero-force pressure imparted by the air-bladder to the friction element. A series of repetitive measurements at three different pressure set points using well-treated silicone tubing were performed and evaluated. These data were smoothed by averaging, plotted, and fitted to a linear model relating the pressure set point to the pull force. The linear regression line was then extrapolated to the zero-force pressure point. With the zero-pressure set point in hand, it becomes a simple exercise to extract the pressure force on the sliding friction-sensing element. Another series of experiments using varying degrees of plasma-treated silicone tubing was then performed to assess sensitivity and to calculate the average coefficient of friction for the different samples. Since coefficient of friction information for the system being evaluated can be obtained using this method, the information is more standardized and easier to compare to other lubricity test methods.

Chapter 5 explores the running-in behavior observed during biomedical conduit friction assessment. Empirical evidence of the running-in phenomenon is documented and a hypothesis regarding its source is set forth. The theme of the hypothesis is that

material related to the constituents of silicone rubber is taken up by the friction element (coil, in this case) over several test cycles and thereby alters the system until it stabilizes. Subsequently, the coil becomes equilibrated with the chemical makeup of its environment, and this is why the resistance force stabilizes.

To test the hypothesis, coils with three different histories were submitted for elemental analyses. The three histories of the submitted coils were as follows: (a) a brand-new, pristine, "never-before-used" coil, (b) a coil that was exercised through multiple testing cycles, (c) and a brand-new pristine coil that was stored for a week in plasma-treated tubing but had never been used for friction testing. The elemental surveys revealed that a coil that had never been exposed to silicone-tubing friction testing (a) had a statistically significant less amount of silicon on it compared to coils (b) and (c). Follow-up work was completed using coils with similar histories. The results of this undertaking showed that pristine coils displayed markedly more running-in phenomenon when compared to either an exercised coil or a stored-in-silicone tubing coil,

3 Refinements to biomedical conduit lubricity evaluation

Considering the straight-groove torque test method, future work would perfect the 3-D alignment of the friction element, the groove, and the center of the gripper jaws. Additionally, automation of the top weight placement (perhaps by using small-scale pneumatic pistons) would reduce any operator variation in that placement. It is recommended that roughness evaluations of the friction element surface and the silicone tubing be performed. This could be accomplished using relatively simple techniques such as scanning white-light interferometry that doesn't require a great deal of expertise or ancillary equipment.

Regarding improvements to the pressure cuff evaluation, opportunities for improvement include making certain there is impeccable vertical alignment of the

friction element and pressure cuff housing. Additionally, more absolute verification of the pressure cuff's friction element straightness using the method depicted in Chapter 2, Figure 3.4, is suggested. Similar to the straight-groove refinement, roughness evaluations of the friction element surface and the silicone tubing should be performed. Gauge studies are also of value to determine the operator-to-operator variation.

To reduce the variability in the running-in behavior, storing friction elements inside of plasma-treated tubing has proven effective. The housing of the friction elements inside of tubing coupled with conditioning test cycles on stored and "not-under-evaluation" plasma-treated tubing greatly reduces test data variability.

Bibliography

[1] Stannett, V. "The transport of gases in synthetic polymeric membranes—an historic perspective." *Journal of Membrane Science* 3.2 (1978): 97-115.

[2] Van Amerongen, Gerrit Jan. "The permeability of different rubbers to gases and its relation to diffusivity and solubility." *Journal of Applied Physics* 17.11 (1946): 972-985.

[3] Norton, Francis J. "Permeation of gases through solids." *Journal of Applied Physics* 28.1 (1957): 34-39.

[4] Barrer, R. M., and Eric K. Rideal. "Permeation, diffusion and solution of gases in organic polymers." *Transactions of the Faraday Society* 35 (1939): 628-643.

[5] Czichos, Horst, Tetsuya Saiato, and L. Leslie R. Smith, eds. *Springer handbook of materials measurement methods.* Springer, 2006.

[6] Flaconneche, B., J. Martin, and M. H. Klopffer. "Transport properties of gases in polymers: experimental methods." *Oil & Gas Science and Technology* 56.3 (2001): 245-259.

[7] Lai, Ngoc Anh, Martin Wendland, and Johann Fischer. "Description of linear siloxanes with PC-SAFT equation." *Fluid Phase Equilibria* 283.1 (2009): 22-30.

[8] Scott, D. W., et al. "HEXAMETHYLDISILOXANE: CHEMICAL THERMODYNAMIC PROPERTIES AND INTERNAL ROTATION ABOUT THE SILOXANE LINKAGE1." *The Journal of Physical Chemistry* 65.8 (1961): 1320-1326.

[9] Jones, B. H., and P. B. Mellor. "Plastic flow and instability behaviour of thin-walled cylinders subjected to constant-ratio tensile stress." *The Journal of Strain Analysis for Engineering Design* 2.1 (1967): 62-72.

[10] Reiner, Marcus. "Elasticity beyond the elastic limit." *American Journal of Mathematics* 70.2 (1948): 433-446.

[11] Love, Augustus Edward Hough. *A treatise on the mathematical theory of elasticity.* Cambridge University Press, 2013.

[12] Stewart, Mark T., et al. "Medical electrical lead having controlled texture

surface and method of making same." U.S. Patent No. 6,263,249. 17 Jul. 2001.

[13] Bhushan, Bharat. Principles and applications of tribology. John Wiley & Sons, 2013.

[14] Blau, Peter J. *Friction science and technology: from concepts to applications.* CRC Press, 2010.

[15] Onishi, Makoto, Kenichi Shimura, and Naoki Ishii. "Medical instruments that exhibit surface lubricity when wetted." U.S. Patent No. 5,670,558. 23 Sep. 1997.

[16] McLaughlin, J. A., et al. "Properties of diamond like carbon thin film coatings on stainless steel medical guidewires." Diamond and related materials 5.3 (1996): 486-491.

[17] Doan, Phong D. "Rotatable pin, screw-in pacing and sensing lead having Teflon-coated conductor coil." U.S. Patent No. 5,425,755. 20 Jun. 1995.

[18] Feng, Minjie, et al. "Validation of volume–pressure recording tail-cuff blood pressure measurements." *American journal of hypertension* 21.12 (2008): 1288-1291.

[19] Nist, N. I. S. T. (2006). SEMATECH e-handbook of statistical methods.

[20] Sodhi, R. N. (2004). Time-of-flight secondary ion mass spectrometry (TOF-SIMS):—versatility in chemical and imaging surface analysis. Analyst, 129(6), 483-487.

[21] Minitab, I. (2010). Minitab 16 Statistical Software.